

On methodology and application of smoothed particle hydrodynamics in fluid, solid and biomechanics

Fei Xu^{1,2*}, Jiayi Wang¹, Yang Yang^{1,2}, Lu Wang³, Zhen Dai¹, and Ruiqi Han¹

¹ School of Aeronautics, Northwestern Polytechnical University, Xi'an 710072, China;

² Institute for Computational Mechanics and Its Applications, Northwestern Polytechnical University, Xi'an 710072, China;

³ School of Architecture and Engineering, Chang'an University, Xi'an 710064, China

Received October 13, 2022; accepted November 10, 2022; published online January 18, 2023

Smoothed particle hydrodynamics (SPH), as one of the earliest meshfree methods, has broad prospects in modeling a wide range of problems in engineering and science, including extremely large deformation problems such as explosion and high velocity impact. This paper aims to provide a comprehensive overview on the recent advances of SPH method in the fields of fluid, solid, and biomechanics. First, the theory of SPH is described, and improved algorithms of SPH with high accuracy are summarized, such as the finite particle method (FPM). Techniques used in SPH method for simulating fluid, solid and biomechanics problems are discussed. The δ -SPH method and Godunov SPH (GSPH) based on the Riemann model are described for handling instability issues in fluid dynamics. Next, the interface contact algorithm for fluid-structure interaction is also discussed. The common algorithms for improving the tensile instability and the framework of total Lagrangian SPH are examined for challenging tasks in solid mechanics. In terms of biomechanics, the governing equations and the coupling forces based on SPH method are exemplified. Then, various typical engineering applications and recent advances are elaborated. The application of fluid mainly depicts the interaction between fluid and rigid body as well as elastomer, while some complicated fluid-structure interaction ocean engineering problems are also presented. In the aspect of solid dynamics, galaxy, geotechnical mechanics, explosion and impact, and additive manufacturing are summarized. Furthermore, the recent advancements of SPH method in biomechanics, such as hemodynamically and gut health, are discussed in general. In addition, to overcome the limitations of computational efficiency and computational scale, the multiscale adaptive resolution, the parallel algorithm and the automated mesh generation are addressed. The development of SPH software in China and abroad is also summarized. Finally, the challenging task of SPH method in the future is summarized. In future research work, the establishment of multi-scale coupled SPH model and deep learning technology in solid and biodynamics will be the focus of expanding the engineering applications of SPH methods.

Smoothed particle hydrodynamics, High-accuracy algorithms, Solid mechanics, Biomechanics, Computational efficiency

Citation: F. Xu, J. Wang, Y. Yang, L. Wang, Z. Dai, and R. Han, On methodology and application of smoothed particle hydrodynamics in fluid, solid and biomechanics, *Acta Mech. Sin.* **39**, 722185 (2023), <https://doi.org/10.1007/s10409-022-22185-x>

1. Introduction

Particle methods have been widely developed for decades as an effective tool for the resolution of practical and complicated problems in engineering and science, covering the fields of manufacturing, aerospace, car, and energy pro-

duction industries as well as ocean and coastal engineering, environmental and physical phenomena, and bio-applications among others. Although mesh-based numerical methods have achieved great success, mesh distortion limits the application to many complicated problems, such as dealing with free surfaces, deformation boundaries, and moving interfaces. Considering the typical weakness of grid-based numerical models, meshfree methods have been a major research focus. The smoothed particle hydrodynamics

*Corresponding author. E-mail address: xufei@nwpu.edu.cn (Fei Xu)
Executive Editor: Guowei He

(SPH) method, as the earliest meshfree method, is first proposed in 1977 to solve astrophysical problems in three-dimensional (3D) open space. In 2005, Monaghan [1] systematically reviewed the theory and application of SPH and summarized its merits and demerits. After several decades of development, SPH method has been successfully used in various fields [2-6]. There are several literatures about the application of SPH method in fluid and solid mechanics.

SPH has special advantages in simulating complex fluid due to its ability to naturally trace the free surface and moving boundaries. In 1994, Monaghan [7] first applied the SPH method to a hydrodynamic problem. The first and widely referenced book on SPH is written by Liu et al. [8], providing systematic descriptions on theory, formulation and applications to hydrodynamic problems including high-velocity impact (HVI), penetration, explosion, and water mitigation systems. Since then, the SPH method has been widely applied in the numerical simulation of fluid mechanics. Recently, Liu et al. [2,9] summarized fluid-structure interaction (FSI) problems and compared the differences between the pure SPH framework and the coupling approaches of SPH with other grid-based methods. The unique capability of SPH framework in modeling FSI problems is illustrated by describing numerical simulation applications of wave dynamics, such as dam breaking, water entry, and sloshing phenomena with fluid-solid interaction. In 2019, Ye et al. [10] reviewed the latest research on SPH in the simulation of complex fluid flows. The dissipative particle dynamics approach is coupled to simulate complex fluid at multi-scale, which not only includes microstructural information of complex fluid but also eliminates the construction of the constitutive model used in the macroscopic approach, providing a new perspective for the simulation of complex fluid.

More than a decade after SPH is proposed, it is also attractive in modeling solid mechanics. In 1991, SPH is extended to treat the dynamic response of solids by Libersky et al. [11], and the method has found many new and interesting applications [12-15]. In 2003, Liu et al. [8] concluded applications of the SPH method to solid dynamics, such as penetrations and explosion. The advantages of the adaptive SPH method in such problems are also demonstrated. Recent advances in 2021 for the ballistic penetrating impact on thin structures by the SPH method are summarized by Meng et al. [4]. The article analyzes the common limitations such as tensile instability, boundary inaccuracy, time consumption, and interface contact, in simulating HVI problems, and indicates that the special characteristics of the solid would be the large deformation with various material constitutive laws including damage and crack propagation compatible with SPH formulas. Huang et al. [16] summarized the application progress of the SPH method in the large deformation and failure of geomaterials in geo-disasters. This article reviews some effective solutions to describe the interaction between

different geological materials, including the coupling of multiphase flow in dam breaks, the interface of water and underwater landslide material, solid-water-air bubble interactions in seepage failure. The development potential of the SPH method in the problem of geological is demonstrated.

Much of the early interest in biomechanics is sparked in the 1960s and involved the study of the structure and function of biological systems such as humans, animals, plants, organs, and cells by mechanical or mechanical methods [17]. Here, we divide complex biological systems into three categories: fluid, solid, and other problems. Toma et al. [18] reviewed the application of the SPH method to FSI problems and reviewed its applicability in use. Zhang et al. [19] summarized the research work on the simulation and modeling of biological systems such as soft matter, cells, and biological soft and hard tissues and organs. This indicates that the SPH method has become an ideal approach to studying the emerging area of computational biomechanics.

Although the SPH method has achieved great advancements in hydrodynamics in recent years, the SPH formulation for solid objects is not comprehensive enough. In this paper, we present a comprehensive review of the research progress on the SPH method and its applications in various fields including FSI, solids, and biology. This paper is organized as follows: the basic SPH methodology and the limitations are briefly reported in Sect. 2, and the development of high accuracy algorithms, especially the research status and evolution of the reproducing kernel particle method (RKPM) and improved finite particle method (FPM) algorithm are also summarized. The improved algorithms of δ -SPH and high accuracy of the Riemann Godunov SPH (GSPh) are emphasized for the application of SPH method in multiphase flow. The common algorithms for improving tensile instability and the framework of total Lagrangian SPH are emphasized to solve the challenging tasks of SPH methods in solid mechanics. The common contact approaches are mainly introduced for complex FSI problems. The biomechanical aspect is exemplified by the governing equations for biologically relevant problems and the introduction of their interaction SPH formulations.

In Sect. 3, the widespread application of SPH method in fluid, solid and biomechanics is reviewed. The fluid aspect mainly describes the interaction between fluid and rigid body as well as elastomer, such as sloshing flows, the aircraft tire spray, and the interaction between ocean structures and waves. The development in the application of SPH method in solid mechanics is discussed in terms of various areas such as galaxy evolution, geotechnical mechanics, explosion and impact, and additive manufacturing (AM). Furthermore, the recent advancements of SPH method in biomechanics are discussed with examples of hemodynamically, gut health, and plant growth. In Sect. 4, the technical strategies to adapt to large-scale and efficient

computation such as the multiscale adaptive resolution, the parallel algorithm and the automated mesh generation and the development of commercial software based on SPH method are presented.

2. Theoretical study of SPH

2.1 Basic concept of the SPH method

As a typical meshless method, the essence of the SPH method is to discretize the physical field into a series of particles with physical information such as mass, density, velocity, acceleration and other physical information. The SPH method interpolates the approximation of a continuous function $f(\mathbf{x})$ based on the following integral form [8,20]:

$$f(\mathbf{x}) = \int f(\mathbf{x}') W(\mathbf{x} - \mathbf{x}') d\mathbf{x}', \quad (1)$$

where $f(\mathbf{x})$ is the function value at position, and $W(\mathbf{x} - \mathbf{x}')$ is the kernel function. When $|\mathbf{x} - \mathbf{x}'| \geq \zeta h$, the kernel is effectively zero where ζ is constant and h is the smoothing length.

2.1.1 Particle approximation

When dividing the physical field into a set of mass particles, particle j has mass m_j , density ρ_j and position \mathbf{x}_j . The value of $f(\mathbf{x})$ at particle j is represented by $f(\mathbf{x}_j)$. It can be written in the summation interpolant at particle i :

$$f(\mathbf{x}_i) = \sum_{j=1}^N f(\mathbf{x}_j) W_{ij} V_j, \quad (2)$$

where $W_{ij} = W(\mathbf{x}_i - \mathbf{x}_j)$, $V_j = m_j / \rho_j$ indicates the volume of particle j . N is the number of particles within the supported domain of particle i .

If kernel function W is a differentiable function, then the derivative of $f(\mathbf{x})$ at particle i can be given by

$$\nabla \cdot f(\mathbf{x}_i) = \sum_{j=1}^N f(\mathbf{x}_j) \nabla_i W_{ij} V_j. \quad (3)$$

2.1.2 The kernel function

The kernel function is extremely important for the SPH

method. It not only determines the accuracy and consistency of the kernel approximation and particle approximation, but also affects the computational efficiency and stability of the SPH method. The following commonly used kernel functions are listed, where $r = |\mathbf{x}_i - \mathbf{x}_j| / h$, and the value of the coefficient α_d is determined by kernel normalization. Wendland:

$$W(r) = \alpha_d \left(1 - \frac{r}{2}\right)^4 (2r + 1), \quad 0 \leq r \leq 2. \quad (4)$$

Cubic B-spline:

$$W(r) = \alpha_d \begin{cases} \frac{2}{3} - r^2 + \frac{1}{2}r^3, & 0 \leq r < 1, \\ \frac{1}{6}(2-r)^3, & 1 < r \leq 2. \end{cases} \quad (5)$$

Gaussian:

$$W(r) = \alpha_d e^{-r^2}. \quad (6)$$

Quintic-spline:

$$W(r) = \alpha_d \begin{cases} (3-r)^5 - 6(2-r)^5 + 15(1-r)^5, & 0 \leq r < 1, \\ (3-r)^5 - 6(2-r)^5, & 1 \leq r < 2, \\ (3-r)^5, & 2 \leq r \leq 3. \end{cases} \quad (7)$$

The values of α_d in different dimensions are shown in Table 1.

Figure 1a-c shows kernel functions, its first derivative and its second derivative curves. All kernel function curves demonstrate a monotonically decreasing trend with the increasing r , which conforms to the physical law that the closer to the particle i , the greater influence on particle i . The Wendland kernel and the cubic B-spline kernel show large peak values with small support fields. The Gaussian kernel and the Quintic-spline kernel function have a larger truncation radius, which would increase the computational cost.

Table 1 Kernel function coefficient α_d

Kernel function	Two-dimension	Three-dimension
Wendland	$7/(4\pi h^2)$	$21/(16\pi h^3)$
Cubic B-spline	$15/(7\pi h^2)$	$3/(2\pi h^3)$
Gaussian	$1/(\pi h^2)$	$1/(\pi^{3/2} h^3)$
Quintic-spline	$7/(478\pi h^2)$	$3/(359\pi h^3)$

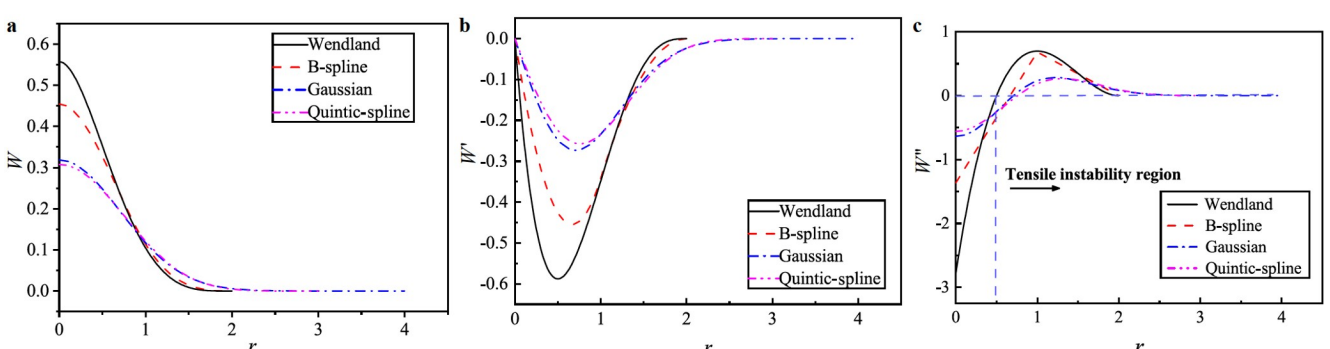


Figure 1 Curves of several kernel functions and their first derivative and second derivative. **a** Curves of different kernel functions; **b, c** first derivative and second derivative curves for different kernel functions.

The trends of four kernel functions are similar. The first derivative of the kernel function decreases and then increases with the increasing r , and the minimum value is obtained in the range of $r = 0.5\text{--}1.0$. The second derivative increases from negative to positive and then decreases to zero. Swegle et al. [21] determined the instability conditions with the Von Neumann stability analysis:

$$W''\sigma > 0. \quad (8)$$

This indicates that the cause of the instability is the incompatible stress σ and the second derivative of kernel function. The region with $W'' < 0$ is the compressive instability region and the region with $W'' > 0$ is the tensile instability region. From Fig. 1c, the region of the tensile instability is larger than that of the compressive instability. Therefore, the tensile instability is more noteworthy in SPH method.

2.1.3 High-accuracy SPH algorithms

From the above analysis, it can be seen that the computational accuracy of numerical simulation depends on the numerical stability to a certain extent, which plays a crucial role in the accuracy of simulation results. Therefore, the high-accuracy SPH algorithm that improves calculation accuracy by constructing a new calculation scheme through mathematical derivation, is a common requirement for the fluid and solid. Despite the essential instability condition, particle inconsistency is the main reason leading to the poor accuracy of SPH [22]. It has been found in research that the particle consistency of SPH could be improved by raising the consistency of kernel function. Lancaster and Salkauskas [23] extended the standard least squares scheme and proposed the moving least square (MLS), which has fine mathematical theory support and high calculation accuracy. However, it is prone to form ill-conditioned or singular equations, leading to computation crash. Dilts [24,25] developed SPH methods based on MLS approximations and extensively studied the issue of local conservation properties. The RKPM proposed by Liu et al. [26–28] is another classical method, in which they constructed kernel functions of arbitrarily high-order consistency by a family of window functions. However, RKPM consumes extra computing resources on the construction of smooth function in the calculation process, and there are strict requirements for the singularity of the matrix constructed by smooth function, which will lead to some limitations in practical application. Sun et al. [29] proposed a non-oscillation weighted reconstruction RKPM using essentially non-oscillatory (ENO) and weighted ENO (WENO), and proved that it could retain high convergence speed and accuracy when local physical discontinuity regions occur in the model with minor numerical oscillation. To eliminate the adverse effects of the different kernel functions on computational accuracy, the

radial basis function (RBF) is introduced into RKPM, and the radial basis reproducing kernel particle method (RRKPM) is proposed by Liu et al. [30]. Ma et al. [31] introduced the normal derivative of RBF into RKPM and proposed a Hermite-type RKPM. This method is applied to elastic mechanics problems, and its advantages and development potential in terms of accuracy and convergence rate are tested. Researchers have been studying the improved algorithms based on the RKPM and MLS frameworks. It is the final objective to retain high accuracy and decrease the computational disadvantages of these improved algorithms [32–34].

The second typical branch of modifications to improve the particle consistency of SPH is based on the Taylor theory. The earliest method is the classical corrective smoothed particle method (CSPM) proposed by Chen et al. [35] in 2000. This algorithm is derived based on Taylor expansion, and its function estimate is as follows, which constructs an equivalent kernel function always satisfying the unity condition in the problem domain. As a result, the calculation accuracy is an order of magnitude higher.

$$f(x_i) = \frac{\int_Q f(x) W(x) dx}{\int_Q W(x) dx} = \int_Q f(x) \left[\frac{W(x)}{\int_Q W(x) dx} \right] dx. \quad (9)$$

As a typical algorithm extending to a discontinuous problem, Liu et al. [36] proposed a more direct SPH improvement algorithm handling one-dimensional (1D) discontinuous interface-discontinuous smoothed particle hydrodynamics (DSPH) in 2005 based on the CSPM framework, which fixes the kernel function consistency in discontinuous regions and improves the interface defects. In 2012, Xu et al. [37] proposed the multi-DSPH method to higher dimensions by solving the difficulties of determining feature points at interface for complex geometric. Although the CSPM and DSPH increase the accuracy by improving the kernel consistency, these methods may introduce the errors of derivative calculation to high-order and induce error propagation. In the meantime, they have a strong dependence on smoothing length and regularity of the particle distribution.

In 2005, Zhang et al. [38] and Liu et al. [39] creatively transformed the numerical iteration scheme for solving higher order derivatives into the calculation of the derivatives simultaneously through linear equations, which is an important improvement for CSPM from the basic computational scheme and in essence improves the accuracy at the interface or the boundary region. The method is called FPM, and CSPM can be considered as its degradation form in nature with just one equation. The basic particle approximation equation in 1D is expressed as Eq. (10), where $W(x_j)$ and $W_x(x_j)$ are the kernel function and its derivative at particle j , $f(x_j)$ and $f_x(x_j)$ are the field function and its derivative

at particle j , and Δd_j is the particle spacing of particle j .

$$\begin{aligned} & \left[\begin{array}{cc} \sum_{j=1}^N W(x_j) \Delta d_j & \sum_{j=1}^N (x_j - x_i) W(x_j) \Delta d_j \\ \sum_{j=1}^N W_x(x_j) \Delta d_j & \sum_{j=1}^N (x_j - x_i) W_x(x_j) \Delta d_j \end{array} \right] \begin{bmatrix} f(x_i) \\ f_x(x_i) \end{bmatrix} \\ & = \begin{bmatrix} \sum_{j=1}^N f(x_j) W(x_j) \Delta d_j \\ \sum_{j=1}^N f(x_j) W_x(x_j) \Delta d_j \end{bmatrix}. \end{aligned} \quad (10)$$

Research and developments on FPM have been ongoing in recent years and can be roughly divided into two types, including the improvement to its basic matrix scheme and the improvement to extend its applicability. The first type could seem to be an essential improvement. In 2016, without any simplified assumptions on the basic equation of FPM, Yang et al. [40] proposed a new FPM calculation framework through matrix decomposition, which is shown in Eqs. (11) and (12). It can be clearly found that the kernel function information, the particle distribution information and the function information are decoupled. Based on this framework, by limiting the number of selected points in the support domain, an improved specified FPM algorithm-specified FPM (SFPM) is suggested based on this new framework, which can greatly improve computational efficiency and ameliorate the potential computational instability of FPM method. Furthermore, the applicability of SFPM is improved. Wang et al. [41] proposed a DSFPM algorithm by combining SFPM and DSPH in order to further improve the computational efficiency and stability of discontinuous problems. Wang et al. [42] proposed a higher order modified SFPM algorithm (H-SFPM) based on SFPM and it is successfully applied in 3D problems. In 2021, the idea from SFPM is introduced into total Lagrangian SPH (TL-SPH) method by Wang et al. [20], and showed the adaptation and stability results for the elastic rubber collision and the crack propagation with extreme boundary. In addition, the other generalized improved algorithm (named GFPM) and its applicability improvements, which have no extra limit on the number of particles in the support domain have been studied.

$$\begin{aligned} & \left[\begin{array}{cc} \sum_{j=1}^N W(x_j) \Delta d_j & \sum_{j=1}^N (x_j - x_i) W(x_j) \Delta d_j \\ \sum_{j=1}^N W_x(x_j) \Delta d_j & \sum_{j=1}^N (x_j - x_i) W_x(x_j) \Delta d_j \end{array} \right] \begin{bmatrix} \Delta d_1 & \Delta d_1(x_1 - x_i) \\ \Delta d_2 & \Delta d_2(x_2 - x_i) \\ \vdots & \vdots \\ \Delta d_N & \Delta d_N(x_N - x_i) \end{bmatrix} \\ & = \begin{bmatrix} W(x_1) & W(x_2) & \cdots & W(x_N) \\ W_x(x_1) & W_x(x_2) & \cdots & W_x(x_N) \end{bmatrix} \end{aligned} \quad (11)$$

$$\begin{aligned} & \left[\begin{array}{c} \sum_{j=1}^N f(x_j) W(x_j) \Delta d_j \\ \sum_{j=1}^N f(x_j) W_x(x_j) \Delta d_j \end{array} \right] \\ & = \begin{bmatrix} W(x_1) & W(x_2) & \cdots & W(x_N) \\ W_x(x_1) & W_x(x_2) & \cdots & W_x(x_N) \end{bmatrix} \begin{bmatrix} \Delta d_1 f(x_1) \\ \Delta d_2 f(x_2) \\ \vdots \\ \Delta d_N f(x_N) \end{bmatrix}. \end{aligned} \quad (12)$$

In our opinion, the second type could be subdivided into the improvements to algorithm applicability and improvements suitable for some physical models. For algorithm applicability, Yan and Xu [43] extended FPM to discontinuous case based on the idea of DSPH, and proposed an improved method, named RDSPH. Chen et al. [44] suggested an updated Lagrangian formulation with Lagrangian kernels for the FPM method, which is effective in eliminating tension instability. Asprone et al. [45] suggested a modified FPM (MFPM), in which the second order basic equations are deformed so that the values of function and derivatives can be directly used to calculate the next step. In the MFPM, since the approximate process is ignored, second order derivative is improved. Afterward, by introducing RKPM into MFPM computing framework, Asprone et al. [46] proposed a novel second order modified FPM method and systematically discussed the calculation error. Nasar et al. [47] suggested an arbitrarily high-order extension of FPM, where the complexity of the consistency correction and the required computations are reduced using simplified versions of the smoothing kernel derivatives. For the physical models, Zhang et al. [48] suggested the decoupled FPM (DFPM) algorithm under a simplified assumption of the diagonally dominant matrices in FPM fundamental equation and applied it to simulate incompressible flow problem. Following the idea of DFPM, Achim et al. [49] suggested a semi-decoupled FPM (SDFPM) by normalizing the kernel using a Shepard factor, which could obtain a comparable precision to the FPM at a lower computational cost. In addition, coupling algorithm is also a common strategy to improve the applicability for physical models. Liu et al. [50] suggested an efficient numeric approach coupling SPH with FPM for FSI problems. Huang et al. [51, 52] suggested the combining of FPM and δ -SPH and realized the interaction between regular waves and rigid plate, and a hybrid approach by coupling the finite difference method (FDM) with FPM to simulate viscous incompressible flows. Zhang et al. [53] suggested a novel approach by coupling the edge-based smoothed finite element method (S-FEM) and DFPM to implement the modeling of FSI problems with elastic structures.

The logical relationship of the mentioned improved methods for FPM is shown in Fig. 2.

2.2 Technical methods of SPH in various fields

2.2.1 Technical methods for fluid

The fluid is usually assumed to be weakly compressible viscous fluid, the governing equations for the fluid in a moving Lagrangian referential can be defined as

$$\begin{cases} \frac{d\rho_i}{dt} = \rho_i \sum_j \frac{m_j}{\rho_j} (\mathbf{v}_i - \mathbf{v}_j) \cdot \nabla_i W_{ij}, \\ \frac{d\mathbf{v}_i}{dt} = - \sum_j m_j \left(\frac{P_i + P_j}{\rho_i \rho_j} \right) \nabla_i W_{ij} + \mathbf{F}_V + \mathbf{F}_B + \mathbf{F}_S, \end{cases} \quad (13)$$

where ρ , P , and \mathbf{v} stand for the density, pressure and velocity, respectively. \mathbf{F}_V , \mathbf{F}_B , and \mathbf{F}_S represent the viscous forces, body force and surface tension.

In order to calculate the pressure in the momentum equation, the state equation is described:

$$P = \frac{\rho_0 c_0^2}{\gamma} \left[\left(\frac{\rho}{\rho_0} \right)^\gamma - 1 \right], \quad (14)$$

where ρ_0 is the reference density. c_0 and γ are the speed of sound and state constant.

Studies on theoretical issues related to SPH have also been continuously carried out, including studies on the effects of model parameters [54], and techniques handling non-reflection boundaries [55,56], modeling of surface tension [57], and formulation of GSPH for energetic materials, where the Riemann solver is integrated into the traditional SPH algorithm to eliminate artificial viscosity [58]. However, the SPH method also has some defects when resolving the fluid problem. The error caused by the SPH interpolation and the tensile instability will lead to the nonphysical fluctuations in the pressure field, even resulting in the particle clumping or void regions. To solve these problems, re-

searchers have made many improvements.

In 2003, Colagrossi and Landrini [59] overcame the pressure noise problem of the SPH method in hydrodynamic problems through density filtration, and introduced XSPH technology in the velocity update to maintain the consistency of particle mass, density and volume. Since then, the SPH method can not only calculate the basic morphology of fluid, but also accurately obtain the internal force. Recently, the incompressible SPH (ISPH) method proposed by Shao et al. [60] has also developed rapidly. This method can obtain a stable pressure field by solving Poisson equation. Xu et al. [61] developed a shifting approach in the ISPH method for homogenized particle distribution. Lind et al. [62] extended this approach to simulate free surface flow with a surface-identification algorithm. Adami et al. [63] proposed a transport-velocity formulation to address particle clumping and void-region problems in weakly-compressible SPH simulation of flow at high Reynolds number, which introduced a velocity correction term in the time integration.

Here, two methods are emphasized, which are effective and more commonly used at present. One is the δ -SPH [64] method, which introduces a density dissipation term in the continuity equation and a viscosity term in the momentum equation. The other one is GSPH based on the Riemann model between two particles. Then, we introduce δ -SPH and GSPH methods in more detail.

(1) δ -SPH method

The δ -SPH model is a widely used method to simulate hydrodynamic problems in different engineering areas [65-67]. δ -SPH is first proposed for the purpose of removing the spurious high-frequency oscillations appearing inside the pressure field, and the Navier-Stokes equations for a weakly-compressible media are discretized using the δ -SPH model in which the diffusive terms have been added to both the continuity and momentum equations. The δ -SPH scheme writes:

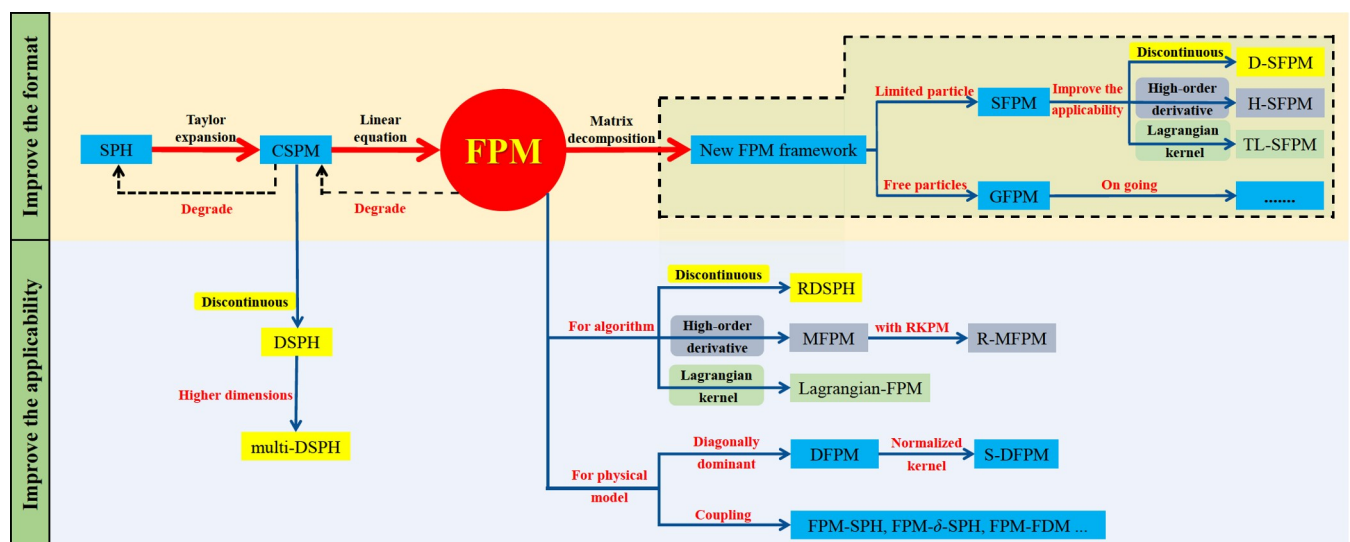


Figure 2 The logical relationship of the mentioned improved methods for FPM.

$$\left\{ \begin{array}{l} \frac{d\rho_i}{dt} = -\rho_i \sum_j (\mathbf{v}_j - \mathbf{v}_i) \cdot \nabla_i W_{ij} V_j \\ \quad + \left(\delta h c_0 \sum_j \Psi_{ij} \cdot \nabla_i W_{ij} V_j \right)_{\delta\text{-SPH}}, \\ \frac{d\mathbf{v}}{dt} = -\frac{1}{\rho_i} \sum_j (P_j + P_i) \nabla_i W_{ij} V_j + \mathbf{g}_i \\ \quad + \left(\alpha h c_0 \frac{\rho_0}{\rho_i} \sum_j \pi_{ij} \nabla_i W_{ij} V_j \right)_{\delta\text{-SPH}}, \\ \Psi_{ij} = 2(\rho_j - \rho_i) \frac{\mathbf{r}_{ji}}{|\mathbf{r}_{ji}|^2} - \left[\langle \nabla \rho \rangle_i^L + \langle \nabla \rho \rangle_j^L \right], \\ \pi_{ij} = \frac{(\mathbf{v}_j - \mathbf{v}_i) \cdot \mathbf{r}_{ji}}{|\mathbf{r}_{ji}|^2}, \end{array} \right. \quad (15)$$

where coefficients δ and α control the diffusion of density and velocity, respectively. $\mathbf{r}_{ij} = |\mathbf{x}_i - \mathbf{x}_j|$, $\langle \nabla \rho \rangle^L$ is the re-normalized density gradient.

However, for the shear flows at high Reynolds numbers, vortical flow evolutions characterized by large negative pressure values and so on, there are still some drawbacks to δ -SPH model. Inspired by the use of particle-shifting techniques (PST) in Refs. [68,69], Sun et al. [70] proposed an improvement of the δ -SPH scheme which is called δ^+ -SPH. In this new scheme, the shifting velocity by Ref. [62] is reformulated and a dependency on the Mach number is introduced. The high Reynolds number viscosity flow is simulated, and the problem of particle clumping in the negative pressure area is solved [71]. Then, Sun et al. [72] proposed a different derivation of the δ^+ -SPH that overcomes the disadvantages of shifting velocity yielding non-physical changes in δ^+ -SPH. Recently, the δ -ALE-SPH model is proposed by Antuono et al. [73] which avoids theoretical inconsistencies of the shifting velocity added in the δ^+ -SPH. As time pass, the scheme based on δ -SPH becomes increasingly perfect.

(2) GSPH method

In recent years, GSPH based on the Riemann model has been applied to fluid dynamics [74]. The Riemann model between a pair of particles i and j in two-dimensional (2D) space is shown in Fig. 3a, \mathbf{e}_{ij} is a unit vector, and the wave

solution of the Riemann solver is shown in Fig. 3b. The contact discontinuity of the Riemann problem is located at $(x_i + x_j)/2$. The physical information on the left state of the discontinuity is

$$(\rho_L, U_L, P_L, c_L) = (\rho_i, \mathbf{v}_i \cdot \mathbf{e}_{ij}, P_i, c_i). \quad (16)$$

The physical information on the right state of the discontinuity is

$$(\rho_R, U_R, P_R, c_R) = (\rho_j, \mathbf{v}_j \cdot \mathbf{e}_{ij}, P_j, c_j). \quad (17)$$

With the solution of the Riemann problem, i.e., U^* and P^* , the discretization of the SPH method is

$$\frac{d\rho_i}{dt} = 2\rho_i \sum_j \frac{m_j}{\rho_j} (\mathbf{v}_i - \mathbf{v}^*) \cdot \nabla_i W_{ij}, \quad (18)$$

$$\frac{d\mathbf{v}_i}{dt} = -2 \sum_j m_j \left(\frac{P^*}{\rho_i \rho_j} \right) \nabla_i W_{ij}, \quad (19)$$

$$\mathbf{v}^* = U^* \mathbf{e}_{ij} + (\nabla_{ij} - U \mathbf{e}_{ij}). \quad (20)$$

This indicates that the inter-particle average velocity and pressure in Eqs. (18) and (19) are simply replaced by the solution of the Riemann problem. A linearised Riemann solver for smooth flows or with only moderately strong shocks can be written as [75]

$$\left\{ \begin{array}{l} U^* = (U_L + U_R) / 2 + \frac{1}{2} \frac{P_L - P_R}{\bar{\rho} c_0}, \\ P^* = (P_L + P_R) / 2 + \frac{1}{2} \bar{\rho} c_0 (U_L - U_R), \end{array} \right. \quad (21)$$

where $\bar{\rho}$ is the average density of the particles i and j . Instead of the explicit artificial viscosity in the traditional SPH, the Riemann-based SPH incorporates an implicit numerical dissipation by solving a Riemann problem between two interactive particles, however, there still exists a shortage in numerical dissipation and computational accuracy. Zhang et al. [75] proposed a low-dissipation SPH method based on a linearized Riemann solver and gave well matched results with the hydrostatic solution without resorting to the computationally elaborate corrections. Following this work, Meng et al. [76] sought a relation between the dissipation and the Reynolds number. Recently, Riemann SPH is more and more widely applied in the SPH method [77-79].

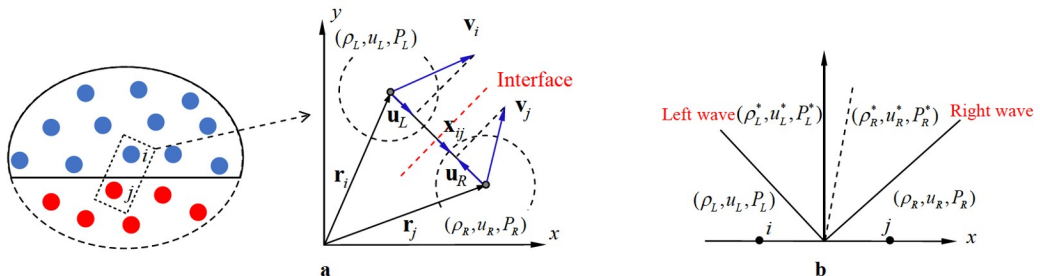


Figure 3 Schematic of **a** the Riemann model between a pair of particles and **b** the wave solution of the Riemann solver.

Some high-order reconstructions of left and right states have been proposed to further eliminate the numerical dissipation and improve the accuracy of calculation in recent years. The MUSCL scheme is first implemented into Riemann-based SPH by Vila [80] using second-order linear reconstructions for the left and right states. The WENO scheme [81] is recently implemented to achieve a high-order Riemann-based SPH scheme. A pioneering study is conducted by Avesani et al. [82], and in this work, high accuracy is achieved using MLS reconstruction for the field variables. Nine stencils, i.e., 1 central stencil and 8 one-sided stencils (shown in Fig. 4), are deployed for the high-order reconstruction in 2D cases. Similar to this study, Avesani et al. [83] combined WENO with Arbitrary DERivatives in space and time (ADER) scheme to achieve a high-order space-time reconstruction. Nogueira et al. [84] deployed a multi-dimensional optimal order detection (MOOD) approach to adaptively reducing the polynomial order for the MLS reconstruction, which increases the stability.

Although 2D reconstruction can increase accuracy, it is usually computationally expensive. Therefore, Zhang et al. [85] considered a fifth-order WENO reconstruction for computing 1D problems. Meng et al. [86] employed the targeted ENO (TENO) scheme [87] to further increase the robustness and better capture shocks. Multi-dimensional WENO reconstruction is first proposed by Avesani et al. [82], and the higher accuracy than linear reconstruction can be achieved by combining the high-order MLS reconstructions. Figure 5 shows the 2D dam-break flow: mechanical energy damping obtained using baseline, WENO-SPH and MUSCL for $Re = 400$. The mechanical energy is better preserved by WENO-SPH [88]. Unfortunately, this multi-dimensional reconstruction exhibits much lower computational efficiency due to a large number of candidate stencils.

2.2.2 Technical methods for the FSI problem

When the solid structure moves or deforms under the interaction with the fluid, the fluid-structure interface can be

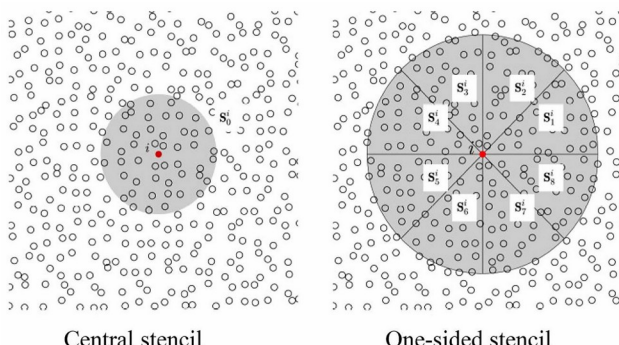


Figure 4 Schematic of the central and one-sided WENO reconstruction stencils for a random particle distribution [82].

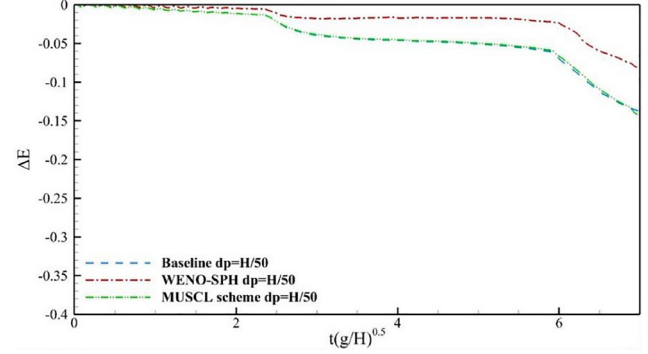


Figure 5 2D dam-break flow: mechanical energy damping obtained using baseline, WENO-SPH and MUSCL for inviscid flow [88].

regarded as a moving boundary. According to the SPH approximation, the fluid particles affect the strain and strain rate of the structure particles, and conversely, the field variables of the fluid are affected by the structural motion [9]. Currently, the repulsive force method (such as the point-surface repulsive force model and point-to-point contact potential model) and virtual particle method (such as the fixed virtual particle method and mirror virtual particle method) are most commonly used [89-91] to address the moving boundary. Most of these contact algorithms are presented from a physical point of view, and a stable and smooth pressure field can be obtained generally.

(1) Repulsive force method. The structure particles explicitly exert a repulsive force on the fluid particles to prevent the fluid particles from penetrating the boundary. Monaghan [7] gave the repulsive force based on the Lennard-Jones (L-J) molecular potential, which is given by

$$F(r_{ij}) = S_1 \left[\left(\frac{r_0}{r_{ij}} \right)^{S_2} - \left(\frac{r_0}{r_{ij}} \right)^{S_3} \right] \frac{\mathbf{r}_{ij}}{r_{ij}^2}, \quad (22)$$

where S_1 , S_2 , and S_3 are the constant parameters, and r_{ij} is the magnitude of the position vector \mathbf{r}_{ij} . r_0 is the cut-off distance. The drawback of this repulsive force is that when the fluid particles flow through the horizontal plane, the normal force cannot be constant and the tangential force cannot be zero. In 2009, Monaghan et al. [92] give the following form of repulsive force:

$$F(r_{ij}) = \begin{cases} \frac{B_{ij}W_{ij}}{\mathbf{r}_{ij}^2}, & \mathbf{r}_{ij} \leq 2h, \\ 0, & \mathbf{r}_{ij} > 2h, \end{cases} \quad (23)$$

where $B_{ij} = 0.02c_i^2 / (m_j + m_i)$. c_i is the sound speed of particle i . This form of repulsive force shows clear parameters and strong applicability.

(2) Virtual particle method. Multiple layers of virtual particles are generated to implicitly represent the solid boundary, and the information on these virtual particles is

interpolated from the flow field [93]. The virtual particle method shows conservation and high precision, while it is time-consuming and difficult to implement for complex boundaries. The following is the interpolation equation of the virtual particle method established on the equilibrium equation at the interface [89].

$$P_w = \frac{\sum_f P_f W_{wf} + (\mathbf{g} - \mathbf{a}_w) \cdot \sum_f \rho_f \mathbf{r}_{wf} W_{wf}}{\sum_f W_{wf}}, \quad (24)$$

where the subscript w represents the wall particle and the subscript f indicates the fluid particle. \mathbf{a}_w is the acceleration of the wall particle, and \mathbf{g} is the gravitational acceleration.

(3) Riemann model contact algorithm. In recent years, the Riemann-based SPH has been applied. Since the solution of the Riemann problem is directly introduced into the SPH governing equation, the force between particles can be determined without other redundant processes.

Zhang et al. [75] established the one-sided Riemann problem to deal with the wall-boundary condition, as shown in Fig. 6. The left state is defined from the fluid particle corresponding to the local boundary normal,

$$(\rho_L, U_L, P_L) = (\rho_f, -\mathbf{n}_w \cdot \mathbf{v}_f, P_f), \quad (25)$$

where the subscript f represents the fluid particles, and \mathbf{n}_w is the local wall-normal direction as shown in Fig. 6.

According to the physical wall boundary condition, the right-state velocity U_R is assumed to be

$$U_R = -U_L + 2\mathbf{v}_w, \quad (26)$$

where \mathbf{v}_w is the wall velocity. Similar to Adami et al. [89], the right-state pressure is assumed as

$$P_R = P_L + \rho_f \mathbf{g} \cdot \mathbf{r}_{fw}, \quad (27)$$

where $\mathbf{r}_{fw} = \mathbf{r}_w - \mathbf{r}_f$, and the right-state density is obtained by

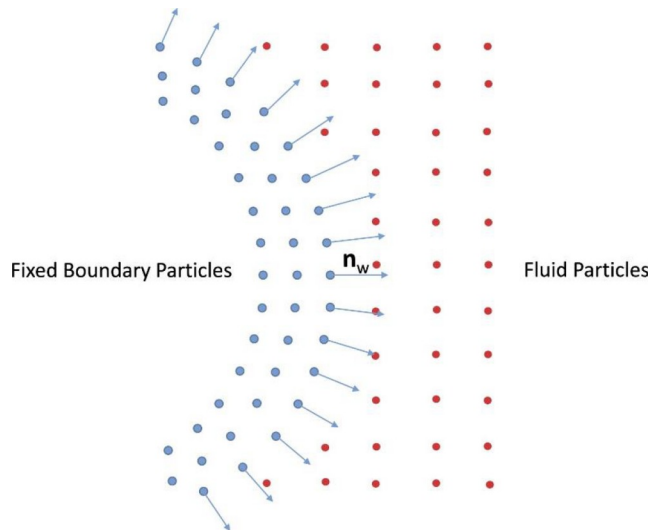


Figure 6 Sketch of fluid particles interacting with fixed wall boundary particles along the wall normal direction through the one-side Riemann problem [75].

applying the artificial equation of state.

Wang et al. [94] solve the Riemann problem between the fluid particle and the elastomer particle to realize the interaction force. The intermediate stress P^* can be obtained by the Riemann solution of the water pressure and elastomer stress, where the deviatoric stress is zero for the fluid particle. If the intermediate stress P^* at intermediate state is obtained by solving the Riemann equation, and then is brought into the momentum equation, the force from particle i to particle j can be achieved. Then the intermediate stress is included in the momentum equation and reflects the force.

2.2.3 Technical methods for solid

The governing equations for the solid are as follows [8]:

$$\begin{cases} \frac{d\rho_i}{dt} = \rho_i \sum_j \frac{m_j}{\rho_j} (\mathbf{v}_i - \mathbf{v}_j) \cdot \nabla_i W_{ij}, \\ \frac{d\mathbf{v}_i}{dt} = \sum_j m_j \left(\frac{\boldsymbol{\sigma}_i}{\rho_i^2} + \frac{\boldsymbol{\sigma}_j}{\rho_j^2} + \Pi_{ij} \right) \nabla_i W_{ij} + \mathbf{F}_B, \\ \frac{d\mathbf{e}_i}{dt} = \frac{1}{2} \sum_{j=1}^N m_j \left(\frac{\boldsymbol{\sigma}_i}{\rho_i^2} + \frac{\boldsymbol{\sigma}_j}{\rho_j^2} + \Pi_{ij} \right) \cdot (\mathbf{v}_i - \mathbf{v}_j) \cdot \nabla_i W_{ij}, \end{cases} \quad (28)$$

where $\boldsymbol{\sigma}$ is the Cauchy stress tensor, Π_{ij} is the artificial viscosity.

The stress tensor $\boldsymbol{\sigma}^{\alpha\beta}$ in the solid can be expressed in terms of pressure P and the deviatoric stress component $\mathbf{S}^{\alpha\beta}$ as follows:

$$\boldsymbol{\sigma}^{\alpha\beta} = -P \delta^{\alpha\beta} + \mathbf{S}^{\alpha\beta}, \quad (29)$$

where the deviatoric stress component $\mathbf{S}^{\alpha\beta}$ is described by introducing the Jaumann rate.

$$\frac{d\mathbf{S}^{\alpha\beta}}{dt} = 2G \left(\dot{\boldsymbol{\epsilon}}^{\alpha\beta} - \frac{1}{3} \delta^{\alpha\beta} \dot{\boldsymbol{\epsilon}}^{\gamma\gamma} \right) + \mathbf{S}^{\alpha\gamma} \mathbf{R}^{\beta\gamma} + \mathbf{R}^{\alpha\gamma} \mathbf{S}^{\gamma\beta}, \quad (30)$$

where G is the shear modulus of the material. $\mathbf{R}^{\alpha\beta}$ is the rotation rate tensor, and $\dot{\boldsymbol{\epsilon}}^{\alpha\beta}$ is the strain rate tensor, which are defined as follows:

$$\dot{\mathbf{R}}^{\alpha\beta} = \frac{1}{2} \left(\frac{\partial \mathbf{v}^\alpha}{\partial \mathbf{x}^\beta} - \frac{\partial \mathbf{v}^\beta}{\partial \mathbf{x}^\alpha} \right), \quad (31)$$

$$\dot{\boldsymbol{\epsilon}}^{\alpha\beta} = \frac{1}{2} \left(\frac{\partial \mathbf{v}^\alpha}{\partial \mathbf{x}^\beta} + \frac{\partial \mathbf{v}^\beta}{\partial \mathbf{x}^\alpha} \right). \quad (32)$$

Similar to fluids, the solids need to be given the relationship between pressure and density. When large density and temperature variations are not involved, the following state equation can be used for solids:

$$P = c_0^2 (\rho - \rho_0). \quad (33)$$

However, in problems involving large changes in density and temperature, such as explosion and HVI, the Mie-Gruenesen equation of state is usually employed for dynamic problems of materials with strength:

$$P(\rho, e) = (1 - S_4\eta)P_H + S_4\rho e, \quad (34)$$

$$P_H = \begin{cases} a_1\eta + a_2\eta^2 + a_3\eta^3, & \eta > 0, \\ a_1\eta, & \eta < 0. \end{cases} \quad (35)$$

In the formula, the subscript H represents the Hugoniot curve, $\eta = \rho / \rho_0 - 1$ is the parameter representing the material compression behavior, and S_4 is the Gruneisen constant. Constants a_1 , a_2 , and a_3 , can be expressed by parameters S_5 and S_6 .

$$\begin{cases} a_1 = \rho_0 S_5^2, \\ a_2 = a_1[1 + 2(S_6 - 1)], \\ a_3 = a_1[2(S_6 - 1) + 3(S_6 - 1)^2]. \end{cases} \quad (36)$$

When the state transformation is not the major component controlling the strength of the material, the elastic-plastic constitutive model is applied to describe the dynamic response of the material. It is required to consider not only the constitutive equation of the structure in the elastic stage, but also to give the constitutive equation of the particles after it reaches the plastic stage.

The stress-strain relation relationship submits Hook's law within the elastic stage, and when the particle reaches the plastic stage, the correction of plasticity should be given. The details are summarized as follows. First, when the material is in elastic stage, the deviatoric stress component \mathbf{S}^{ab} at moment $t + \Delta t$ can be predicted from the deviatoric stress rate tensor at time t . Comparing the equivalent Von Mises stress $\sigma_{t+\Delta t}^{eq}$ at $t + \Delta t$ with the yield stress Y of the material, if the predicted stress is confirmed to yield, then a correction is performed to return it to the yield plane.

When the particle reaches the plastic state, the Von Mises yield criterion should be used to make the correction for the deviatoric stress:

$$\mathbf{S}^{ab} = \mathbf{S}^{ab} \frac{Y}{\sigma_{eq}}. \quad (37)$$

The yield stress in the Johnson-Cook model is calculated as follows:

$$Y = [A + B(\varepsilon_p)^n] \left[1 + C \ln(\dot{\varepsilon}_p / \dot{\varepsilon}_0) \right] \left[1 - \left(\frac{T - T_{room}}{T_{melt} - T_{room}} \right)^m \right], \quad (38)$$

$$T = T_0 + \frac{e - e_0}{C_v}, \quad (39)$$

where ε_p is the equivalent plastic strain, $\dot{\varepsilon}_p$ is the equivalent plastic strain rate, $\dot{\varepsilon}_0$ is the reference value of equivalent plastic strain rate, and A , B , C , n and m are material dependent constants, T_{room} is the room temperature, T_{melt} is melting temperature, T and T_0 are the current temperature and initial temperature, respectively, e and e_0 are the internal energy and initial internal energy respectively, and C_v is the specific heat.

2.2.3.1 The traditional modification of the momentum equation The numerical instability is still an inevitable problem for solid. In 2004, Rabczuk et al. [95] claimed that tensile instability is a severe limitation to the SPH application in solid dynamics. In addition to the above improved algorithms for fluid, many researchers have also proposed a variety of improved methods for the unique characteristics of solid, such as stress point, artificial stress, conservative smoothing method.

(1) Stress point Conventional SPH algorithms often have the hourglass pattern in solid models that result in structures that no longer can resist external force and lose stability. Hence, in 1994, Dyka and Ingel [96] proposed a new approach to addressing tension instability by additionally adding the stress point to the standard SPH method. For motion variables as displacement, velocity and acceleration are calculated and tracked at the original particle of SPH, while the stress, internal energy, and density are calculated and tracked only at the stress point.

For example, the displacement, velocity and stress are approximated as

$$\begin{aligned} \mathbf{x}_i^{SP} &= \sum_j \Phi_{ij}(\mathbf{x}_i^{SP}) \mathbf{x}_j^{SPH}, \\ \mathbf{v}_i^{SP} &= \sum_j \Phi_{ij}(\mathbf{x}_i^{SP}) \mathbf{v}_j^{SPH}, \\ \boldsymbol{\sigma}_i^{SPH} &= \sum_j \Phi_{ij}(\mathbf{x}_i^{SPH}) \boldsymbol{\sigma}_j^{SP}, \end{aligned} \quad (40)$$

where $\Phi_{ij} = \frac{m_j}{\rho_j} W_{ij}$, the superscripts SPH and SP indicate the original particle of SPH and stress point, respectively.

For the 1D case, the acceleration at the original particle of SPH is approximated as

$$\frac{d\mathbf{v}_i}{dt} = \sum_{j=1}^N \sum_{k=a,b} m_{j_k}^{SP} \left[\frac{\boldsymbol{\sigma}_{j_k}^{SP}}{(\rho_{j_k}^{SP})^2} + \frac{\boldsymbol{\sigma}_i^{SPH}}{(\rho_i^{SPH})^2} \right] \nabla_i W_{ij_k}^{SPH}, \quad (41)$$

where the superscripts i and j correspond to the original particle of SPH, k corresponds to the label of stress point a , b for the particle j . One-half the mass of particle j is assigned to each stress point a and b , which has the same displacement, velocity and acceleration as the original particle j . In addition, the stress at original particle i of SPH is given by the equation $\boldsymbol{\sigma}_i \approx \frac{1}{2}(\boldsymbol{\sigma}_{i_a} + \boldsymbol{\sigma}_{i_b})$.

Chalk et al. [97] proposed a new stress-point position updating scheme that solves the tensile instabilities, without the need to adjust non-physical artificial parameters. It is observed that the stress point method can improve, but cannot completely eliminate the tensile instability.

(2) Conservative smoothing method Hicks et al. [98] applied the conservative smoothing approach to controlling the tensile instability in SPH in 1997. The field variables such as velocity, displacement, and density of particles are

obtained through the solution of the conservation equation of continuum mechanics in each time step. Then the field variables of particles are corrected by the conservation smoothing method, which can avoid unexpected changes in field variables, increase the continuity of the field variables, and also assure the stability of the calculation process.

The conservative smoothing formula proposed by Ref. [99] is as follows:

$$Q'_i = Q_i + S_7 \left(\frac{\sum_{j \neq i} m_j Q_j W_{ij} / \rho_j}{\sum_{j \neq i} m_j W_{ij} / \rho_j} - Q_i \right), \quad (42)$$

where Q_i and Q'_i are the field variables of particle i before and after the modification, respectively, and S_7 is the parameter, $0 < S_7 \leq 0.5$. The field variables can be position, velocity, stress, and so on. The physical meaning of the conservative smoothing method is to correct the field variable of particle using the weighted average of the field variables of neighborhood particles excluding particle i itself.

Guenther et al. [100] illustrated that the error of the conservative smoothing method is significantly smaller than that of the artificial viscosity in the shock collision of the ideal gas problem. However, it is noticed that preventing the excessive loss of accuracy by controlling smoothing is very challenging. On this basis, Hicks and Liebrock [101] presented the conservative smoothing procedure using B-spline finite interpolation method to generate the smoothing weights that stabilize SPH in compression as well as in tension.

(3) *Artificial stress* Monaghan [102] proposed the artificial stress method in 2000 to solve the problem of tensile instability in solid. A strong repulsive term (i.e., artificial stress) is introduced into momentum conservation equations to prevent the unphysical piled or scattering of particles, thus leading to the elimination of the tensile instability of SPH.

The corresponding momentum equation is expressed as

$$\frac{d\mathbf{v}_i}{dt} = \sum_{j=1}^N m_j \left(\frac{\boldsymbol{\sigma}_j}{\rho_j^2} + \frac{\boldsymbol{\sigma}_i}{\rho_i^2} + f^n R_{ij} \right) \nabla_i W_{ij}, \quad (43)$$

where f is defined by

$$f = \frac{W(r)}{W(\Delta d)}, \quad (44)$$

where $f^n R_{ij}$ is the artificial stress term, the exponential factor $n = \frac{W(0)}{W(\Delta d)}$, generally is 4, R_{ij} is the artificial stress tensor. In the SPH method, $W(\Delta d)$ is a constant since the smoothing length depends on the particle spacing. f^n makes the artificial repulsion between particles i and j increase rapidly as r decreases. For example, $h = 1.2\Delta d$, $r \rightarrow 0$,

$f^n \approx 11$; as the distance r increases, the artificial repulsion decays dramatically to ensure that the effect of the artificial repulsion is limited to the nearest neighboring particles.

Meanwhile, $R_{ij} = R_i + R_j$, the artificial stress tensor R is calculated by the inverse transformation from the diagonal artificial stress tensor $\bar{R}_i^{\alpha\beta}$, which is obtained according to Eq. (45):

$$\bar{R}_i = \begin{cases} -S_8 \frac{\bar{\sigma}_i}{\rho_i^2}, & \bar{\sigma}_i > 0, \\ 0, & \bar{\sigma}_i \leq 0, \end{cases} \quad (45)$$

where the components $\bar{\sigma}_i$ represent the diagonal stress of the stress tensor σ_i , S_8 is the artificial stress factor in the range $0 < S_8 < 1$, which is used to define the magnitude of the repulsive force. Gray et al. [103] suggest that S_8 be taken as 0.3 in the solid mechanics problem.

Xu et al. [104] proposed a simplified form of artificial stress in 2012, which avoids the inverse transformation of 3D Cartesian coordinate system and is most suitable for the simulations in 3D problems. Hemeda et al. [105] obviously improved the tensile instability by introducing artificial stresses in the application of micro-particle impinging. However, for the artificial stress method, its physical meaning remains to be investigated.

2.2.3.2 Total Lagrangian-SPH

In addition to the above methods, as one of the important algorithms, the TL-SPH method can suppress the tensile instability and increase high-order accuracy, which combined with the Euler SPH method can easily handle the damage problem of the solid [106].

The TL-SPH method has been successfully applied in dynamic problems of the solid. Belytschko and Xiao [107] believed that the Eulerian kernel-based SPH causes tensile instability, which suffers from the stress region distortion. This means that the updated particle position for the kernel function is inconsistent with the material deformation. Fortunately, the Lagrangian kernel does not suffer from this issue. So the Lagrangian frame is applied in the SPH method and called TL-SPH. The governing equations of the solid discretized by the TL-SPH method are as follows:

$$\begin{cases} \rho_i \det(\mathbf{F}_i) - \rho_i^0 = 0, \\ \frac{d\mathbf{v}_i}{dt} = \frac{1}{\rho_i^0} \sum_j V_j^0 (\mathbf{P}_i^{\text{pk}} + \mathbf{P}_j^{\text{pk}} + \Pi_{ij}^0) \nabla^0 W_{ij}, \\ \rho_i^0 e_i \frac{de_i}{dt} = \dot{\mathbf{F}}_i : \mathbf{P}^{\text{pk}}, \end{cases} \quad (46)$$

where ρ_i , \mathbf{v}_i , e_i are the density, the velocity and the internal energy of particle i , respectively. \mathbf{F}_i is the deformation gradient of particle i . ρ_i^0 is the initial density of the particle i . V_j^0 is the initial volume of the neighbour particle j . ∇^0 denotes the divergence or gradient operator for the reference

configuration. \mathbf{P}_i^{pk} and \mathbf{P}_j^{pk} are the first Piola Kirchhoff stress of particle i and particle j , respectively.

In TL-SPH, the computation is based on the reference configuration \mathbf{X}^0 , and the first Piola Kirchhoff stress \mathbf{P}^{pk} is used in the momentum equation. This makes the computation more complex than that in the traditional SPH. The computing procedure of TL-SPH is shown in Table 2.

From the above procedure, the differences between the TL-SPH and traditional SPH can be observed. In TL-SPH, this kind of boundary treatment is only applicable to fixed boundary with no material distortion. To handle moving boundaries and boundaries with material distortion in TL-SPH, a pin-ball contact method [108] is employed. In the TL-SPH, the neighbor list only needs to be reconstructed after updating the configuration. As TL-SPH is based on the reference configuration, theoretically it is free from any tensile instability, whereas SPH has tensile instability and should use a stabilization method. However, TL-SPH needs the updates of the configuration occasionally while modeling the problems with large material distortion.

The TL-SPH method has been successfully applied in the elastic solid [109,110]. Han and Hu [111] utilized TL-SPH to deal with the elastic structure in FSI problems. Hwang et al. [112] developed a fully Lagrangian MPS (moving particle semi-implicit) method to simulate the FSI problems corresponding to elastic structures. To improve the accuracy of the TL-SPH method, Vignjevic et al. [113] recovered the first-order consistency of TL-SPH and provided numerical examples ranging from simple 1D dynamic elasticity to 3D real engineering problems. Chen et al. [44] proposed an improved method of FPM under the TL-Lagrangian framework and verified it by numerical examples, showing that this method can effectively improve the tensile instability.

Although the TL-SPH method can model large deformation with its original form, it is incapable of modeling discrete cracks as it is a continuum based method. Therefore, some algorithms are proposed to overcome this drawback of TL-SPH. These methods include adaptive total Lagrangian-Eulerian SPH [114], the updated Lagrangian Taylor-SPH method [115], and Eulerian-total Lagrangian SPH [106]. Islam and Peng [116] proposed a crack initiation and pro-

Table 2 The computing procedure of TL-SPH

Algorithm: TL-SPH	
Step 1 $\mathbf{v}^n, \mathbf{x}^n, \mathbf{F}^n, e^n, \mathbf{X}^0, \nabla^0 W_{ij}$	Obtain velocity, position in the current configuration, deformation gradient, internal energy at n step, position in the reference configuration, kernel gradient for the reference
Step 2 $\rho = \rho_0/\det(\mathbf{F}^n), \mathbf{F}^n \rightarrow \mathbf{P}^n$	Solve the density by the Jacobian $\det(\mathbf{F}^n)$, update the stress \mathbf{P}^n by the constitutive model
Step 3 $\langle \nabla_0 \cdot \mathbf{P}^n \rangle_i = \sum_j V_j^0 (\mathbf{P}_i^n + \mathbf{P}_j^n) \nabla^0 W_{ij}, \langle \mathbf{P} : \dot{\mathbf{F}} \rangle_i^n = \mathbf{P}_i^n : \sum_j (\mathbf{v}_j^n - \mathbf{v}_i^n) \nabla^0 W_{ij} V_j^0$	Compute the momentum and energy equations
Step 4 $\mathbf{v}_i^{n+1} = \mathbf{v}_i^n + \Delta t \left(\frac{1}{\rho_0} \nabla_0 \cdot \mathbf{P}_i^n + g \right), e^{n+1} = e^n + \frac{1}{\rho_0} \Delta t \langle \mathbf{P} : \dot{\mathbf{F}} \rangle_i^n$	Update the velocity and internal energy
Step 5 $\mathbf{F}^{n+1} = \mathbf{F}^n + \Delta t (\nabla_0 \otimes \mathbf{v}_i^{n+1})^T, \mathbf{x}^{n+1} = \mathbf{x}^n + \Delta t \mathbf{v}^{n+1}$	Update the deformation gradient and the position

pagation model within the TL-SPH framework without any explicit cracking treatments. Serroukh et al. [115] applied the updated Lagrangian Taylor-SPH meshfree method to the numerical analysis of large deformation and failure problems under dynamic conditions. Wang et al. [20] introduced a simplified gradient correction to TL-SPH and proposed the improved TL-SPH method, and implemented a straightforward and robust damage model. It is observed that the TL-SPH method still should be developed to satisfy the simulation of various phenomena of structural response.

2.2.4 SPH algorithms for biomechanics

Recent advances in algorithms of SPH have opened new opportunities to better understand biological processes, owing to the great ability to integrate complex physics into SPH constructions [19]. However, choosing precise governing equations and coupling forces can be very challenging due to the innate complexity of biological systems, such as the integration of multiple processes in dynamic geometries. In this section, the relevant governing equations for biosynthesis describing density changes in root tissue growth are presented to understand how cells grow during organogenesis [117]. The coupled forces of liquid-phase SPH and solid-phase DEM in simple monodisperse suspensions of neutral buoyancy spheres characterizing the effects of flow and mixing on changes in digesta composition are also presented here [118].

Limitations of testing the biophysical hypothesis of self-organization create difficulties in formulating plausible models of plant tissue growth. Building on the SPH method, Mimault et al. [117] linked experimental data to computational modeling to describe the growth of plant tissues at the cellular level by identifying cells as numerical particles. Cell mass increases during tissue growth due to the influx of water and wall thickening through the accumulation of pectin and polysaccharides during the growth process. The framework is modeled as a densification process, which is expressed as a function of the density ρ_i and the growth rate λ_g :

$$\gamma(\rho_i) = \lambda_g \left(\frac{\rho_0}{\rho_i} - 1 \right). \quad (47)$$

Calculating the mass variation during the growth is a two-step process, considering with the mass increase occurs separately from the deformation. The volume is assumed to be constant, thus the particle mass and density are updated with

$$\begin{cases} \gamma_i^n = \gamma(\hat{\rho}_i^n), \\ m_i^{n+1} = m_i^{n-1} \left(1 - 2\Delta t \frac{\gamma_i^n}{\hat{\rho}_i^n} \right), \\ \rho_i^{n+1} = \hat{\rho}_i^n + 2\Delta\gamma^n, \end{cases} \quad (48)$$

where ρ_i and m_i are the density and mass of the particle i . This densification model could account for the relationship that incorporates changes in cell mass due to biological and physical processes. Such an approach of including governing equation can also be applied to various problems such as blood flow through a brain vascular aneurysm [119], transcatheter aortic valve dynamics [120], and *Cae-norhabditis elegans* [121].

Another representative example is simple digesta in the small intestine, which is influenced by the propelling movement pattern of the gut wall. Digestion and elimination of food through the gastrointestinal tract is a necessary physiological function of life. Sinnott et al. [118] denote the simple digesta as a suspension of rigid particles in a viscous Newtonian fluid. The numerical model for peristalsis in the duodenum contains three parts. The intestinal wall is represented as a thin viscoelastic membrane, in detail, the movement of chyme in the intestine is the result of the balance of hydrodynamic and viscoelastic wall forces exerted on it. Discrete regions of the fluid are shown as SPH particles, the motion of which is controlled by local fluid stresses produced by interactions with other particles. The motion of solids' content is estimated by the particle-method DEM. The coupled force exerted by an average continuous solid on the fluid phase is given by Darcy's law:

$$F_{\text{darcy}} = \varepsilon_{\text{DEM}}^2 \mu_f \frac{(\mathbf{v}_f - \mathbf{v}_{\text{DEM}})}{\rho_f K_{\text{DEM}}}, \quad (49)$$

where ε_{DEM} is the porosity of the solid phase, \mathbf{v}_{DEM} is the velocity of DEM solids at that point, K_{DEM} is the permeability of the solid phase porous medium of the solid phase, μ_f is the viscosity coefficient, \mathbf{v}_f is the velocity, ρ_f is the density for SPH fluid particle. The coupling to the DEM is chosen for the SPH because this force on the fluid particles depends only on their state variables and the porosity and velocity values of the porous medium at the location of the SPH particles. This approach can also be applied to a variety of problems, including ultrasound vector flow imaging with coupling SPH and simulator for ultrasound [122] and slurry [123].

SPH provides a natural framework for complex problems in biology, and this method with great compatibility would

bring expansive prospects for new substances and interactions.

3. Engineering applications of the SPH method

With the rapid development of SPH method and its numerical techniques, it has been widely and successfully applied in various fields. Furthermore, SPH has been combined with other methods to handle multiscale complicated problems, such as MD-SPH for modeling reactive energetic materials [124] and SPH-MD-QM models based on the first-principles [125]. Techniques that combine SPH with other particle methods have been studied [126]. In the following, we will introduce the applications of SPH method to fluid, solid and biomechanics, respectively.

3.1 Application of the SPH method in FSI simulations

3.1.1 FSI with rigid body/rigid wall

The fluid interacting with the rigid body/rigid wall are successfully simulated by SPH. In terms of single-phase fluid, Colagrossi et al. [127] conducted to make an in-depth analysis of theoretical structure of SPH regarding the dynamic free-surface boundary condition of liquid sloshing. Oger et al. [128] first used the SPH method to solve the problem of water entry. When the air is considered, there are challenges in the simulation of multiphase flow for the numerical methods. However, the SPH method has certain advantages. As shown in Fig. 7, Yan et al. [129] studied the wedge impacting the water considering the existence of air using SPH, and the phenomenon of air escape is observed. Figure 8 shows the SPH simulation results of the cavity body slamming water involving more complex gas-liquid-solid coupling [130]. And the whole dynamic evolution process of air, such as escaping, merging and gushing, is vividly presented. The presented FSI solver is expected to be further extended for the simulation of fluid interaction with non-linear elastic (e.g., hypo-elastic, hyper-elastic) structures.

3.1.2 FSI with elastomer

In some FSI problems, the deformation of structure is so large that it cannot be ignored. To deal with these problems, a common way is to couple SPH with other methods (e.g., FEM). Siemann et al. [131] addressed an explicit numerical simulation of flexible aircraft ditching using a coupled SPH-FEM approach, in which the impact load by water and the deformation of the fuselage are discussed. The aircraft motion and the deformation of bottom fuselage in ditching are shown in Fig. 9. Xu et al. [132-134] introduced the SPH-FEM method into the field of aircraft tire spray when run-

ning on wet runways, in which the large deformation of tire should be considered. Figure 10 shows the spray patterns and the deformation of tire. With the development of the SPH algorithm for elastomer, the pure particle method for both fluid and structure has gradually been focused. Antoci et al. [135] proposed a new SPH coupling computational model of fluid and elastic structure, in which the interface condition between fluid and solid is enforced by a suitable term obtained by an approximate SPH evaluation of a sur-

face integral of fluid pressure. Wang et al. [136] proposed a new SPH scheme for simulating the water entry of an elastic wedge. The X-direction stress components of the wedge and the hydrostatic pressure of the water are shown in Fig. 11. Besides, the interaction of fluid and flexible structure with large deformation is also common in natural phenomena and industries [137-139]. O'Connor et al. [138] adopted TL-SPH method to describe the interaction of fluid-flexible structure with large nonlinear deformation by the case of a flapping

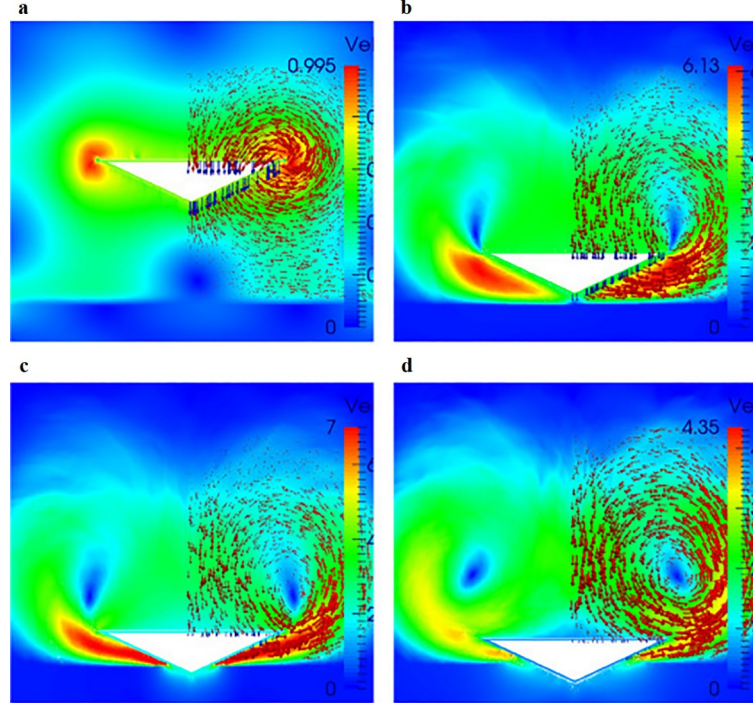


Figure 7 The velocity of water entry of wedge. The arrows indicate the velocity of air [129].

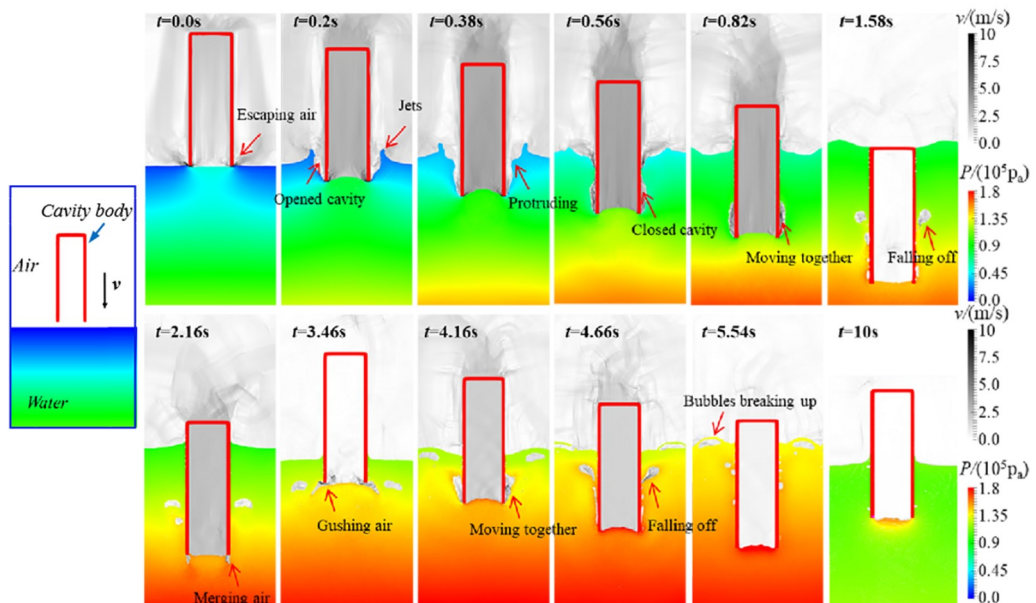


Figure 8 Evolution process of the cavity body slamming water involving gas-liquid-solid coupling [130].

flexible beam and achieved good simulation performance.

3.1.3 Complicated FSI ocean engineering problem

The problem of ocean structures interacting with waves is a

popular research field in ocean engineering, and the SPH method has been widely used in this area [140-143]. The key technical challenge in SPH simulation is the development of wave-generating and wave-absorbing system. An-

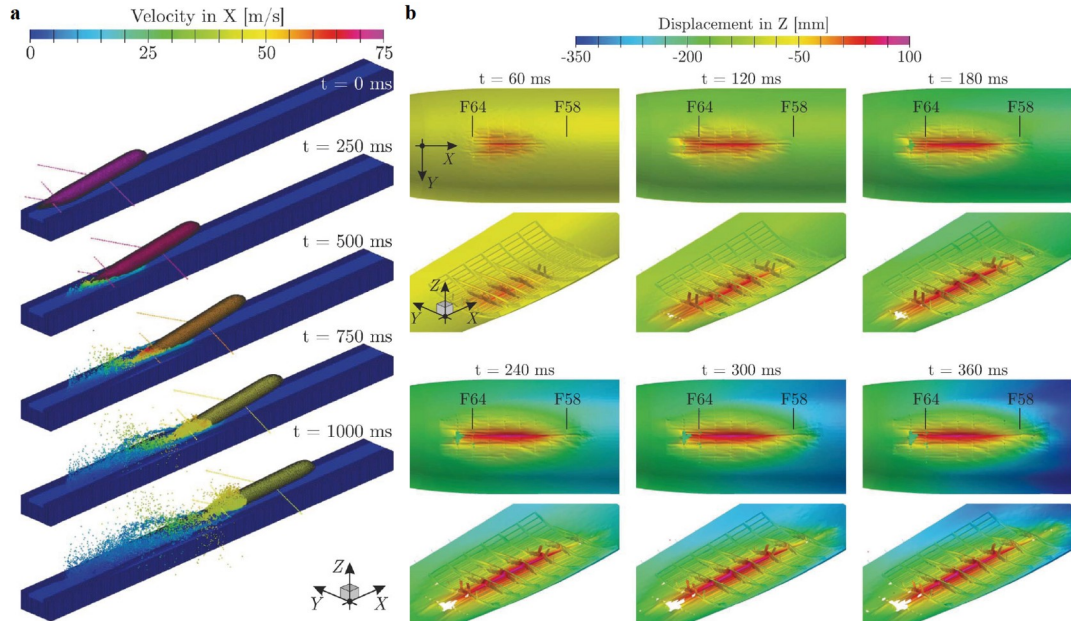


Figure 9 a Aircraft ditching simulation by coupled SPH-FEM method and b the deformation of bottom fuselage [131].

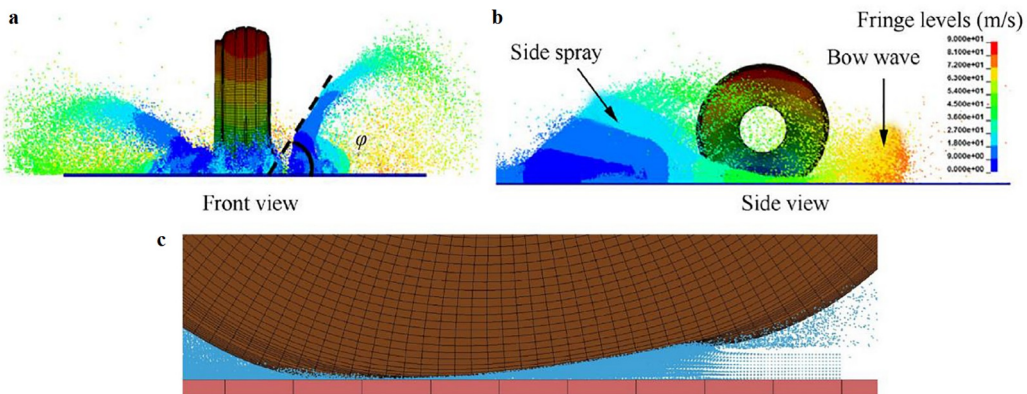


Figure 10 Aircraft tire spray simulation by coupled SPH-FEM method. a, b The spray patterns and c the deformation of tire [133].

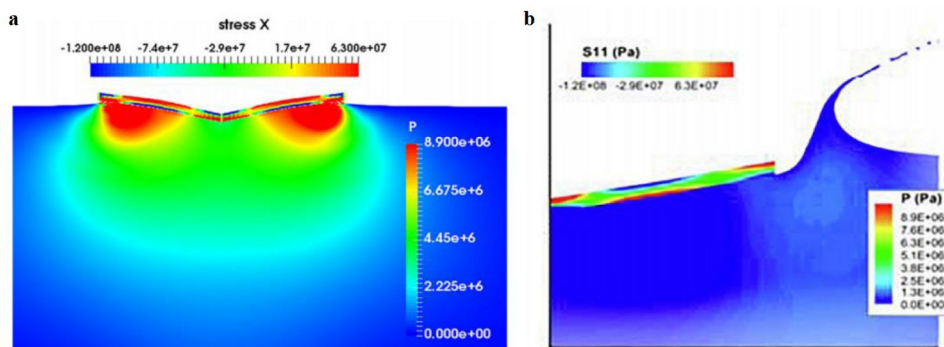


Figure 11 Water entry simulation of an elastic wedge by SPH, a the X-direction stress components of the beam at 2.5 ms and b the hydrostatic pressure of the water at 4.5 ms [136].

tuono et al. [144] adopted the paddle wave maker to generate the standing waves, regular waves and wave packet by the SPH method. More recently, Sun et al. [145] generated waves by paddle motion and absorbed undesirable wave at the end of wave flume by a viscous damping zone, and studied the freak wave impacting on a fixed box-shape structure using the δ^+ -SPH model. Mintu et al. [146] simulated the ship-wave impacting and generated sea spray in complex sea conditions. The spray phenomenon is clearly captured and the results are shown in Fig. 12. In addition, ocean energy receives attention from the scientific and industrial communities in recent years [147,148], which considerably fosters the research of various ocean energy devices. Wei et al. [149] studied wave-flap device interaction, using graphics processor units (GPU) SPH to simulate sea waves and further taking advantage of the physics engine project Chrono to consider the flap device as a rigid body. The bottom foundation is fixed. The flap device is free to move, but it is connected with the bottom foundation through a revolute joint defined by the project Chrono library. Figure 13 illustrates the interaction between the wave and the flap device while the wave is propagating. Moreover, Lyu et al. [150] reviewed the latest development in simulating ocean energy devices based on SPH method. This proves that SPH is advantageous in simulating complicated FSI ocean engineering problems.

3.2 Application of the SPH method in solid with strength

In contrast to computational fluid dynamics and FSI problems, there is a noticeable lag in the development and application of the SPH method in solid mechanics. In recent years, scholars have also made unremitting efforts and promoted the development of SPH methods in the field of solid mechanics. Furthermore, SPH has been applied to

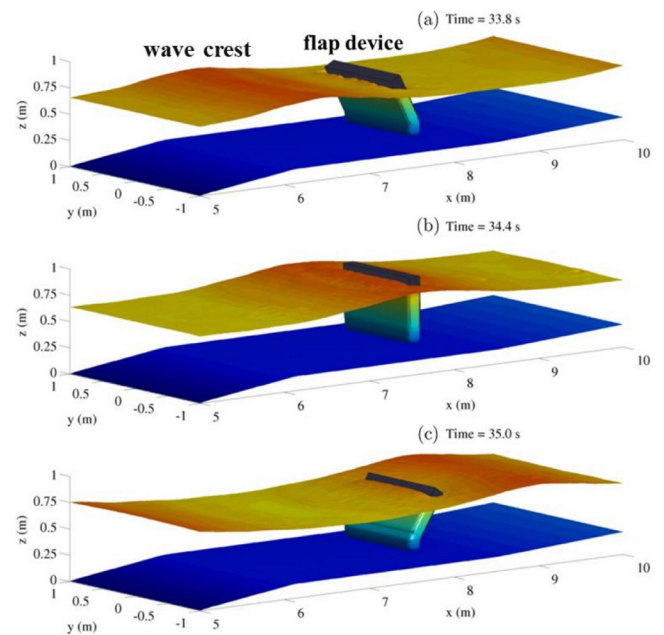


Figure 13 Numerical simulation of wave interaction with oscillating wave surge converter at instants. The wave propagates from the left side to the right side of the plot, and the color indicates the elevation in meters [149].

model complicated manufacturing processes, such as shot peening [151], cutting of materials [152], and water jet abrasion [153]. These applications are classified into four sections, including galaxy, geomechanics, impact dynamics and AM.

3.2.1 Galaxy

Due to the complexity of the fluid-like motion of the nebulas in astrophysics, numerical methods are required to follow their evolution. The SPH method is originally proposed to simulate astrophysical phenomena [154]. Since the SPH method has the merits to be programmed easily and of good robustness, it can be conveniently extended to address more

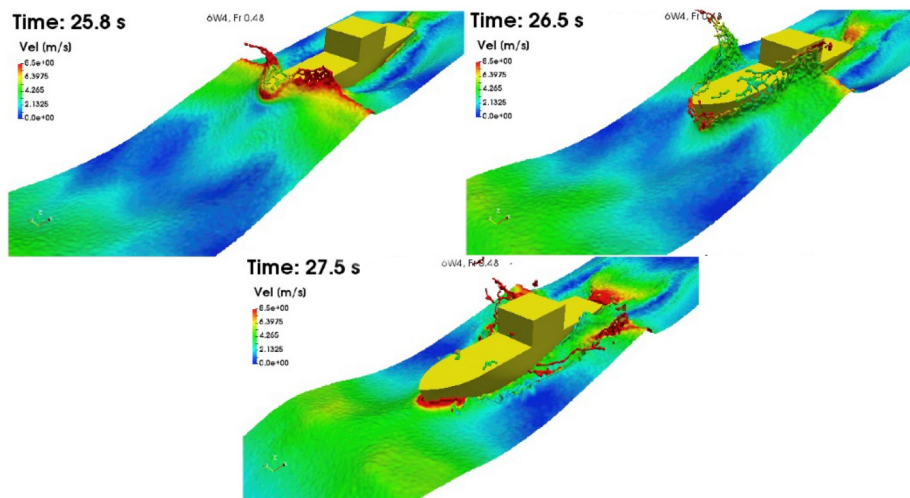


Figure 12 Development of ship-wave impact generated spray [146].

astrophysical problems. To describe the process of conversion of gas material into stars, Berczik [155] modified the standard SPH algorithm of star formation and proposed a new chemo-dynamical SPH (CD-SPH) code to describe the dynamical and chemical evolution of triaxial disk-like galaxies. In addition, the SPH method has been used to model the formation and merging of galaxies [156]. In 2012, Pakmor et al. [157] proposed the SPH code GADGET-2 to simulate the inspiration of the binary system, implemented the stellar equation of state and nuclear reaction networks, and applied it to solve the merger of white dwarfs. A white dwarf star may increase its mass by absorbing He-rich material from a companion star, eventually causing the explosion of supernova Ia. In 2013, Liu et al. [158] used the SPH method to represent the impact simulations of the supernova Ia explosion on the companion star. Figure 14 shows the density evolution of the explosion ejecta and companion star material and illustrates the stripping of He-rich material from the companion star and the propagation process of shock wave. Interest in using SPH for modeling the electrostatic transport of charged lunar dust on the moon's surface has also been reported [159].

3.2.2 Geotechnical mechanics

Geotechnical materials, including rock and soil, are significantly different from other metallic materials. Over the last

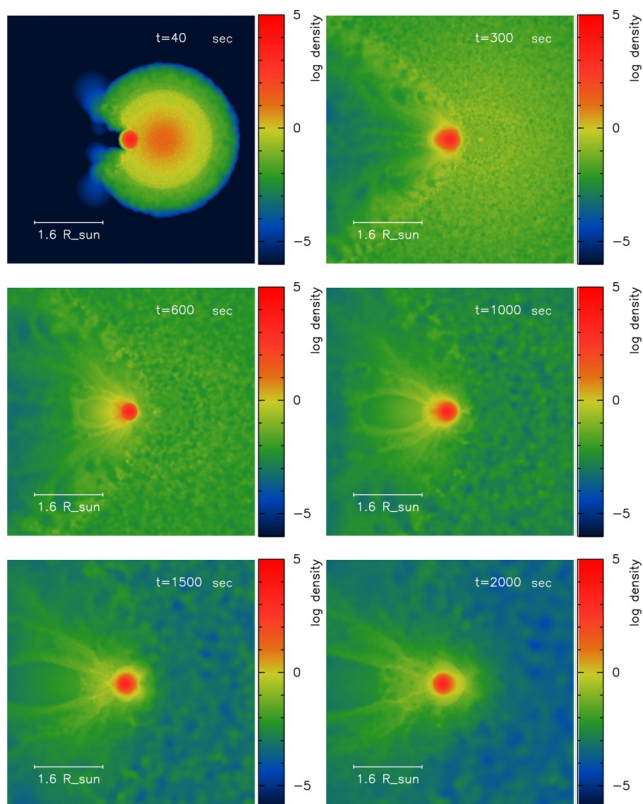


Figure 14 Variation of the density structure of explosion ejecta and companion material with time in impact simulations [158].

few years, SPH has also found important applications in the modeling of natural disasters, for example, landslides [160,161] or general problems in geotechnical engineering [162].

Soil is a common geological type in geotechnical, in which there are a large number of discrete solid particles with special mechanical properties and deformation behavior. Granular flow is prevalent in a large number of natural and industrial processes. Thus, understanding the mechanisms of granular flows plays an important role in reducing natural hazards (e.g., landslides, snow avalanches and soil liquefaction). In recent years, SPH methods have been found to provide superior ability to capture the deformation and damage of granular flows [163]. For the problem of modeling granular flows using the SPH method, the constitutive equations and yield criterion are of vital importance to accurately capture essential characteristics of granular flow.

In 2006, for non-cohesion granular soil, the elastic-perfectly plastic model is used to describe the relationship between stress and strain, and the plastic response of the material was captured by the Mohr-Coulomb failure criterion [164]. For the visco-plastic granular soil, Jop et al. [165] originally proposed the $\mu(I)$ -rheological constitutive model, which can provide a clear description of the material motion under shear. To precisely describe the hardening and softening effects, Bui and Nguyen [3] proposed the general elasto-plastic constitutive model. The hardening and softening behavior is controlled by a stress tensor related yield function and the plastic response of the material is captured by the Drucker-Prager yield criterion. Considering the effect of material dilatancy for sandy soils, the elasto-plastic soil constitutive model for sandy soils based on the Drucker Prager model with a non-associated flow law is applied to describe the plastic behavior of soil. The non-associated flow accurately simulates the real behavior of the soil under external loading through the dilatancy angle. Similar to tensile instability, the phenomenon of tension cracking may occur during large deformation of the soil, which can be solved by the artificial stress method. These results provide constructive suggestions for a continuum description of the mechanical behavior of granular flows and would be of considerable help in predicting natural geophysical hazards. Figure 15 shows the progressive failure process of the embankment under the seepage flow with the embedded failure surface observed in the experiment (i.e., dashed line) [166]. Before the seepage reaches the foot of the downstream slope, the deformation of the embankment is negligible (Fig. 15a). When the seepage reaches the foot of the downstream slope, the soil in this region loses shear strength and triggers embankment damage. The failure process begins with a dramatic change in plastic strain and void ratio at the foot of downstream slope as well as a slight settlement at the top of the downstream of the embankment (Fig. 15b). Subsequently, from the foot of the downstream slope, the first

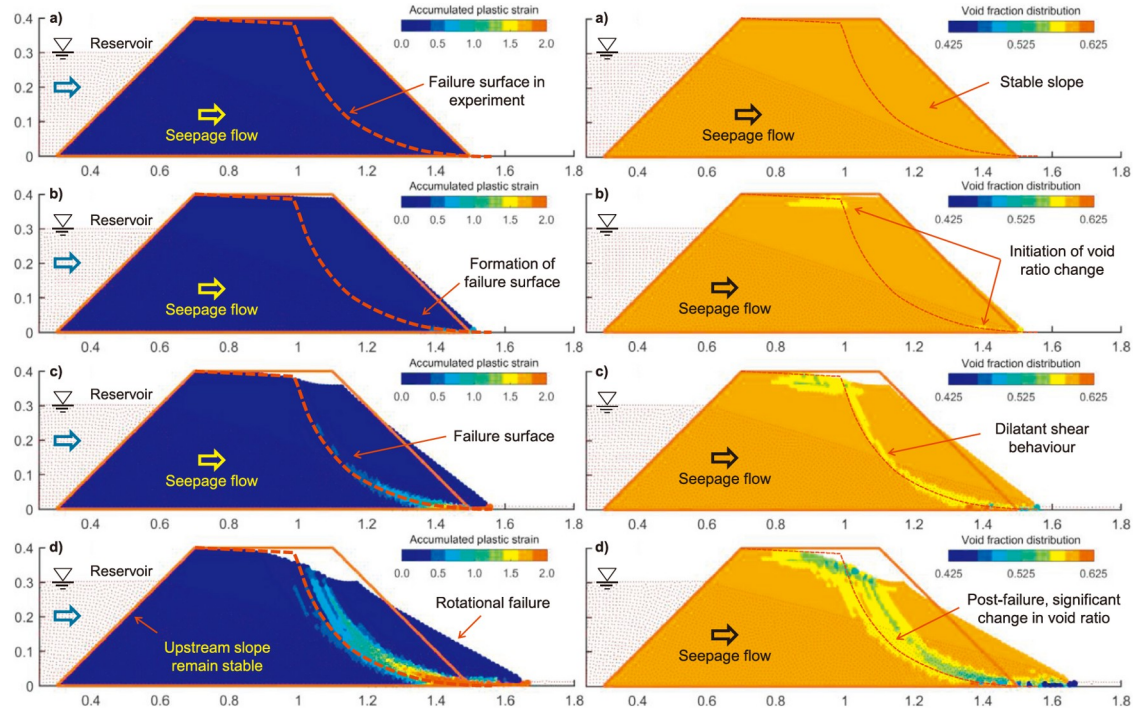


Figure 15 Progressive failure of the embankment predicted by SPH [166]. Left side is the accumulated plastic strain. Right side is the void fraction distribution in the embankment during the post-failure process.

shear zone presented by the high plastic strain concentration gradually progresses upward along the major failure surface observed in the experiment to the top of the embankment. This localisation failure band corresponds to the area of loose soil formed due to the dilation behaviour of the soil subjected to shearing. In particular, a large amount of plastic volume change occurs between the soil particles along the shear band during the post-failure regime, resulting in void fraction of the soil to reduce. Corresponding to the generation of this localisation band, the downstream soil begins to slope along this major potential sliding surface (Fig. 15c). As the flow continues, the downstream slope fails completely in the tilting mode, as shown in Fig. 15d, where the large shear zone divides the soil into two parts on the left and the right side (Fig. 15d).

The rocks play an important role in natural and industrial, which often lead to geological disasters. The breakage of rocks is a typical problem that is usually combined with the formation of crucial fractures and fragmentation. The failure of rocks can be divided into brittle failure and ductile failure according to the deformation during failure. Das and Cleary [167] employed the SPH method and a continuum damage model to simulate the fragmentation of rocks under impact. The literature simulates the unconfined compressive strength test, which can be useful in determining the response of the material to the load and predicting the compressive strength of the material. Figure 16 shows the comparison of the fracture pattern predicted by the SPH method with the experimental results by Kahraman and

Alber [168]. The fracture pattern and the size of the fragments obtained from the simulation are in good agreement with the experiment. The primary fracture starts at the corners and expands along the diagonals. This indicates that SPH is able to simulate the typical damage patterns of rock specimens observed in unconfined compressive strength test.

3.2.3 Explosion and impact

The SPH method can not only deal with large deformation problems, but also track particles well. Great advancements in the SPH method in various fields, such as underwater explosion [169] and detonation [170], have been made in recent years. In previous applications of simulating the detonation process of explosives by the SPH method, detonation is usually regarded as steady-state detonation, and the reaction rate of explosives is ignored. Yang et al. [171] applied the SPH method to simulate the detonation of condensed explosives with reaction rate and introduced the ignition and growth model to represent the reaction of condensed explosives. Figure 17 shows the cylindrical divergent detonation process simulated by the SPH method. Comparing the results of the numerical simulation with the experiments, the evolution of the detonation wave is in good agreement [171]. Underwater explosions and the destruction of structures in the water involve complex physical processes, which bring great challenges to theoretical analysis and numerical techniques. Recently, the SPH method has been further extended to the application of underwater ex-

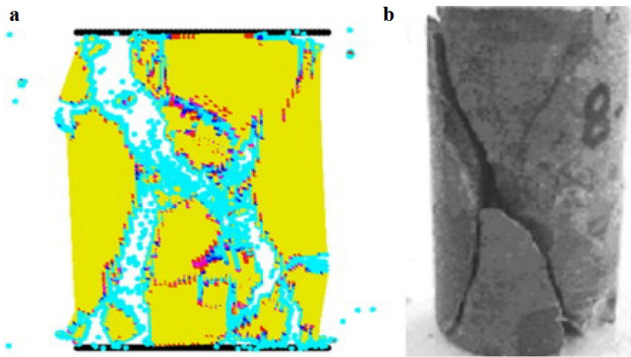


Figure 16 Comparison of the SPH simulation with a typical experimental fracture pattern [167].

plosions. Zhang et al. [172] adopted a fully meshless approach, i.e., the load is solved by the SPH method and the structural response is solved by the RKPM method. Figure 18 shows the damage effects simulation of cabins subjected to contact underwater explosion based on the coupled SPH-RKPM method. This provides a new approach to the numerical simulation of underwater explosion. Moreover, advances in the past decade have been on multiple fronts. SPH has been extended for very complicated problems, such as modeling of ignition, growth, reaction, and afterburning of aluminized explosives [173,174].

SPH models have also been developed for simulating surface erosion caused by the impacts of foreign particles

[175-178]. Moreover, as another typical problem of solid dynamics, the response of the structure under impact load is complex and uncertain. To investigate the real deformation process of the structure with strength under impact loading, the introduction of the physical fracture criterion is essentially required to accurately describe the damage behavior of the material. However, the fracture caused by the loss of particle interaction in the domain is a natural phenomenon in the SPH simulation, which we call numerical fracture. It is observed that when simulating the response of material under dynamic loading, the numerical fracture often occurred before the physical material reached the damage criterion, as shown in Fig. 19a [179]. The improved algorithms mentioned above for the problem of tensile instability in solid improve the numerical fracture phenomenon to a certain extent, but do not solve the problem in essence.

To prevent the numerical fractures, instead of the improved algorithm for tension instability in solid, a more direct approach of the particle splitting algorithm with the generation of new particles is used to improve the local resolution and adjust the particle distribution. Kitsionas and Whitworth [180] have implemented a particle-splitting method for the first time in astrophysics. Xu et al. [181-183] proposed a simple particle addition method to prevent numerical fracture in the SPH method, which can be easily used in both 2D and 3D regular and irregular particle models. The particle splitting algorithm can effectively

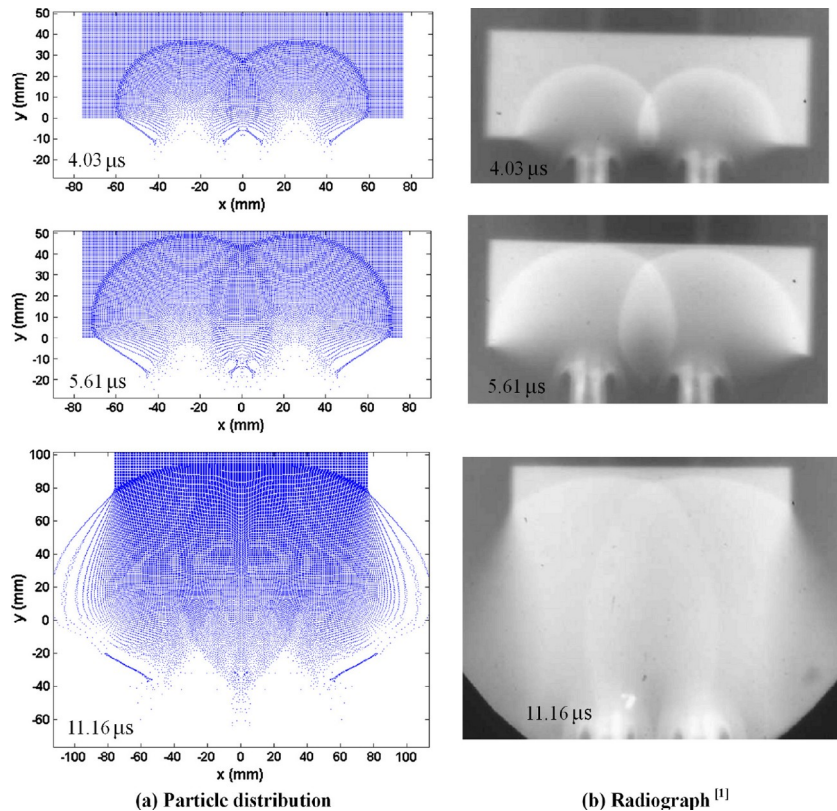


Figure 17 Particle distribution and radiograph in cylindrically divergent detonation process [171].

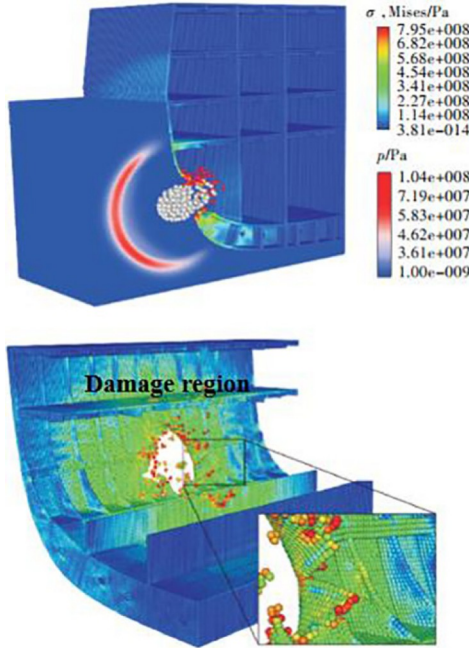


Figure 18 Damage effects simulation of cabins subjected to contact underwater explosion based on coupled SPH-RKPM method [172].

improve the numerical fracture problem through the local refinement of particles. Later Shintate et al. [179] adopted new particle generation techniques in the simulation of high-speed collision problems of the composite materials. In the fracture analysis, Johnson-Cook fracture model is used as the criterion, as shown in Fig. 19b. Compared with Fig. 19a, the result observed after eliminating the numerical fracture is shown.

Another alternative to solve the numerical fracture phenomenon is the variable smoothing length method [184]. Gingold et al. [185] are the first to propose algorithms in which the particles have different smoothing lengths, with the assumption that the smoothing length is related to the density. However, it is indicated that the inconsistency of

smoothing length affects the differential approximation, which causes great errors in the simulation results. Qiang et al. [186] developed a fully variable smoothing length method, which fundamentally corrects the calculation error caused by the traditional variable smoothing length method. In the SPH simulation of most problems, the usual smoothing length is 1.0–1.5 times the initial particle spacing. The method has a great advantage for problems with violent changes in density and smoothing length such as large deformation and large twisting. In recent years, scholars have conducted many researches on the variable smoothing length method and expanded the application of the method to numerical simulations of large deformations, such as the penetration [187], water entry simulation [188] and detonation [170].

The selection of physical fracture criterion is crucial to describe the failure behavior of materials under impact loading, except for numerical fracture phenomena. For different materials under different loading conditions, the physical fracture criterion varies. In 2018, Zhu et al. [189] adopted the cumulative-damage failure criterion to analyze the development of cracks and spalling of Al_2O_3 ceramic plate in impact loading. The accumulated incremental effective plastic strain is used to determine the damage. The morphological characteristics of the elliptical fragment cloud are also depicted. Zhang et al. [190] employed the Grady failure model to analyze the motion of debris clouds. According to the maximum stress criterion, the debris cloud structure and the fragment distribution outside the main structure of debris cloud are well obtained, as shown in Fig. 20.

Generally, in the TL-SPH method, the particle interactions are calculated based on the initial configuration, and the connectivity between particles is fixed, so the material is treated as a continuum, and the cracking and fragmentation of the material during failure analysis cannot be described. Islam and Peng [116] proposed a pseudo-spring analogy method to simulate cracks and damage in solid material. The

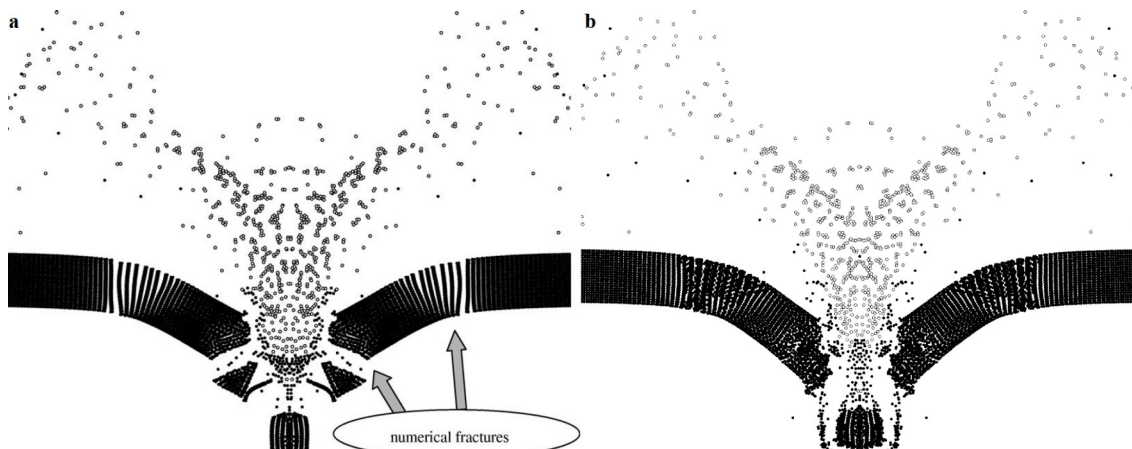


Figure 19 HVI response simulated by **a** conventional SPH method and **b** improved SPH method [179].

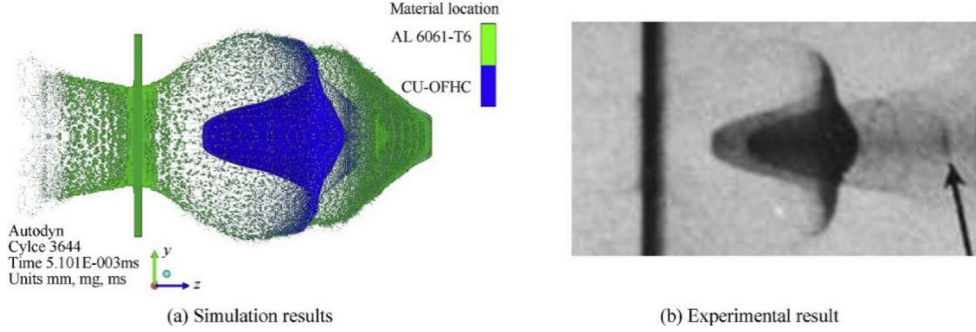


Figure 20 Comparison of numerical simulation and experimental result at 5.1 μ s of the disk projectile impacting the thin plate at a velocity of 6.39 km/s [190].

interaction between particle i and neighboring particle j is elucidated by the interaction coefficient f_{ij} and the damage factor D_{ij} . As the damage factor increases, the interaction between particles gradually disappears. Then the pseudo-spring method is used to describe the discontinuous crack surface of the material. The crack initiation, propagation and failure of notched beams under impact can be simulated by this method, which does not need cracking treatments to clarify the damage and failure process of material.

The recognition of crack-tip is a fundamental problem in dealing with solid fractures by the meshless method. Here, we introduce three commonly used criteria to identify the crack discontinuity field: the visibility criterion, diffraction criterion and transmission criterion. The visibility criterion is the simplest method, and if the connection between a point and the field node in the support domain is intercepted by a discontinuous interface (crack), the field node is excluded from the support domain. Unlike the visibility criterion, in the diffraction criterion, the support domain of the node can bypass the crack tip. The transparency criterion is that at the crack tip, the crack is regarded as completely transparent, and as the distance from the crack tip increases, the transmission of the crack decreases until it disappears [191].

3.2.4 Additive manufacturing

AM is one of the most popular processes in the manufacturing industry nowadays [192]. As a 3D printing technique, AM allows materials to be stacked point by point or layer by layer to form 3D solids. The AM of metal includes four main types: powder bed fusion, material jetting, binder injection and direct energy deposition [193]. As proper process parameters influence the quality of the product directly, it is crucial to select appropriate process parameters, such as laser power, scan speed, scan spacing, and powder delivery rate. With the development of numerical simulation in recent years [194], the SPH method has been found to have great potential in simulating the free surface melting, flow, re-solidification and large deformation of the AM process. In this section, we will focus on two types of AM

techniques simulated using the SPH approach.

Selective laser melting (SLM) is an important technique for powder bed fusion. In recent years, there have been many numerical works to simulate laser-related manufacturing processes while considering thermodynamic problems [195-197]. In the simulations, solid powders are generally treated as immobile rigid bodies, while the motion of liquid metal in the molten pool is described by the Navier-Stokes equation. Under the action of laser energy, the solid powders transformed into the liquid phase and formed a melt pool. This physical process is simulated for the first time using the SPH method in the numerical attempts of laser welding [195,198]. On the basis of the classical formula, Shah and Volkov [199] combined the SPH method with the classical ray-tracing method to predict the propagation and radiation of laser during SLM absorption. Furthermore, how to describe the phase transition in SLM presents a new challenge for the numerical method. Hence, Meier et al. [200] addressed the thermo-capillary phase transition problem of solid, liquid and gas phases in the SLM process, and proposed a new scheme of interface stabilization to achieve a stable and smooth gas-liquid interface. This provides a comprehensive insight into the birth of gas inclusion. For a 3D line melting problem with more complex and realistic geometries, the melt pool shape and final topology of solidified surface as well as the temperature field are shown in Fig. 21 [200].

More contents and details about phase transition in SLM can be found in Refs. [200-202]. Here, we introduce a simple model of phase transition [202]. In which, the rate of change of the stored internal energy, \dot{e} , is obtained from the conservation equation (50), where $E = \frac{1}{2}[\nabla \mathbf{v} - (\nabla \mathbf{v})^T]$ is the symmetric component of the velocity gradient, q_{cond} is the conductive flux vector, and q_{laser} is the laser energy. The internal energy and temperature are assumed to be linearly related, $\rho \dot{e} = pc\dot{T}$. Its special feature is the introduction of a phase transition temperature bandwidth of size δT . The heat capacity in different material states is shown in Eq. (51), where c_s and c_L are the solid and liquid heat capacities re-

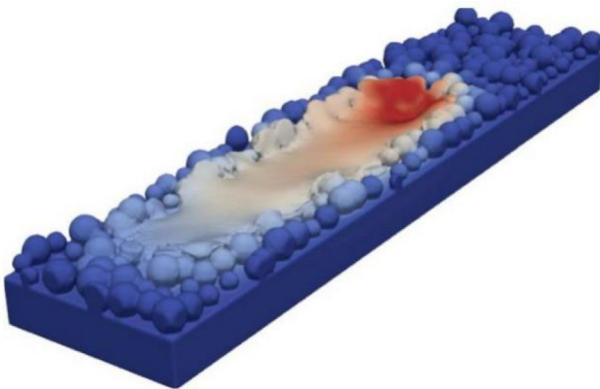


Figure 21 The melt pool shape and final topology of the solidified surface in the 3D line melting problem [200].

spectively, T_M is the melting temperature, and L is the latent heat of melting. The phase of the SPH particle is tracked by a state variable S , where $S = 1$ indicates the liquid state, $S = 0$ for solid, and $0 < S < 1$ for solid-liquid ratio fraction.

$$\rho \dot{e} = \sigma : E - \nabla \cdot q_{\text{cond}} + q_{\text{laser}}, \quad (50)$$

$$c = \begin{cases} c_S, \\ \frac{c_S + c_L}{2} + \frac{L}{\delta T}, \\ c_L, \end{cases} \quad (51)$$

$$S = \begin{cases} 0, & T < T_M - \frac{\delta T}{2}, \\ \frac{T - (T_M - \delta T/2)}{\delta T}, & T_M - \frac{\delta T}{2} < T < T_M + \frac{\delta T}{2}, \\ 1, & T_M + \frac{\delta T}{2} < T. \end{cases}$$

Cold spraying is also a popular AM technology nowadays. Since the deposition of cold spraying particles takes place at a temperature below the melting point, the original properties of the material are retained. In this way, the coatings or products may possess low residual stress and great bond strength. Moreover, SPH has been applied to simulate AM processes using cold spray [203].

Initially, Yin et al. [204] adopted the commercial software LS-DYNA to establish an SPH particle model to simulate cold spraying particle impacting the substrate, and then they extended the single-particle model to multi-particle simulation. It is found that good agreements are achieved with experimental results. Subsequently, the researchers began to develop their own SPH code. Manap et al. [205] incorporated the interface force using the cohesive zone model to accurately describe the interaction between particles and substrate. Gnanasekaran et al. [203] established 2D and 3D single and multi-particle self-made models, and analyzed the deformation behavior of materials at interfaces with different angles and speeds. Figure 22 illustrates the temperature

distribution of a multi-particle impact. Hemed et al. [105] further considered the effect of the oxide layers on the spray or the substrate by applying the modified Johnson-Holmquist model.

With other types of metal AM, the simulation of material jetting and binder bonding processes may involve fluid dynamics processes such as liquid solidification and viscous fluid flow [206,207], which indicates the wide application of the SPH method in AM simulations in the near future.

In the simulation of AM, phase transition occurs when the heat reaches certain conditions, so it is crucial to accurately characterize heat transfer in phase change problems. Cleary et al. [208] constructed a set of rules of isothermal boundaries to ensure continuity of heat flux across discontinuities in density, specific heat, and conductivity and when there are significant continuous spatial variations in material properties. Based on this, an increasing number of solid-liquid phase change problems have been simulated by the SPH method, such as soil freezing [209], lava flow [210], super-cooled large droplet freezing [211] and landslides [212].

3.3 Application of the SPH method in biomechanics

The SPH applications described above have spanned many fields of science and engineering. In this section, a range of cutting-edge examples of SPH application to biomechanics, covering three aspects of FSI, solid, and others will be reviewed [10]. Many biomechanical problems require FSI analysis [18], and we choose several areas: hemodynamically, gut health, and human water sports.

The blood flows dynamic is one of the notable implementations of FSI in biomedical applications [119,122,213-215]. Thrombosis plays a crucial role in atherosclerosis and hemostasis. When a blood vessel is injured, platelets adhere or aggregate on the surface of the damaged area of the blood vessel. For numerical simulation of platelet movement, the method based on a penalty or spring force mechanism is employed to simulate the adhesion and aggregation process of platelets in blood flow [216]. Figure 23a depicts the formation of a thrombus at 0.2 s and 0.6 s at a blood flow velocity of 500 μm/s given in

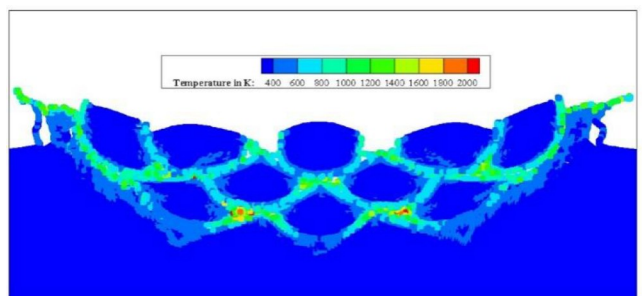


Figure 22 Contours of temperature distribution for multi-particle impact and the morphology of the substrate at the velocity of 500 m/s [203].

the study of Al-Saad et al. [214]. At 0.2 s, it can be observed that when the platelets are within a distance from the damaged area, due to the existence of adhesion force, platelets are activated in the damaged area and form a primary thrombus (in the area of the black circle). Platelets adhering to the wall are activated and attract other platelets within a certain distance from them because of the aggregation forces between platelets. The process described above can be seen more clearly in the enlarged white area. At 0.6 s, the entire damaged area is covered with multiple layers of platelets. Additionally, when the thrombus reaches a certain volume, a portion of the thrombus breaks off and re-enters the bloodstream for downstream transport.

The mechanical and chemical breakdown of food occurs in the gastrointestinal tract. A comprehensive understanding of the effects of periodic muscle contractions and relaxations of the intestinal wall on agitating, mixing, and pushing the multiphase digesta along the gut is one of the topics of interest in improving digestive health. Sinnott et al. [118] investigated the differences in transport and mixing of contents caused by different solid concentrations. Figure 23b shows the overall movement of the contents during the first peristaltic wave passing along the length of the duodenum for 3.0 s. The wave travels from the left to the right, and two-phase suspensions with different solids contents of 2% and 20% are mixed by pulling along the axial direction. In the figure, the fluid phase is colored by axial velocity, and

the solid phase is colored by initial position. It can be observed that the axial elongation of the relaxation zone is small and spherical, and the internal flow field is symmetrically distributed, while the reverse jet phenomenon exists in the contraction zone. The expanding wall with 20% solids has a slightly steeper trailing edge gradient near the constriction, while the reverse jet is narrower and more concentrated. This suggests that the peristaltic movement pattern does not guarantee the homogeneity of multiphase digesta throughout the gut.

Platform diving is an Olympic sport. Considering the fluid forces exerted on the body during and after diving, the geometry of the athlete, and the underwater motion or deformation, Harrison et al. [217] developed a coupled biomechanical-SPH model to reveal the links between water entry techniques, underwater trajectory, and loading on the body. Figure 23c shows the surface splash and flow domains around the athlete with an entry pitch angle of $+10^\circ$ and 0° . The arm and head are observed to enter the water at 0.03 s. For the entry pitch angle of $+10^\circ$, the body and water chamber are aligned so that only hands are in contact with the water. For the entry pitch angle of 0° , the body is aligned in the cavity for water contact with the head and hands. After 0.28 s, for the entry pitch angle of $+10^\circ$, the pitch continues in the positive direction and the body is now almost level. For the entry pitch angle of 0° , the body leans only moderately in the positive direction, and all but the rear

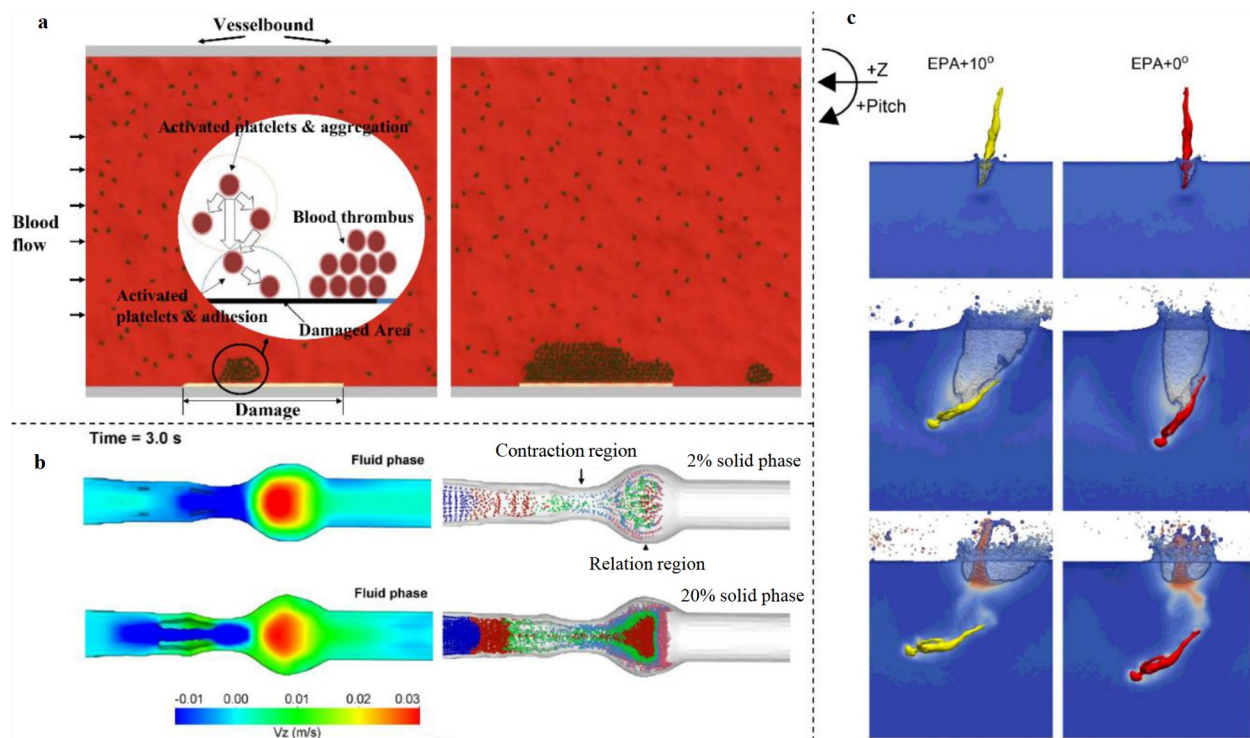


Figure 23 The schematic diagram for the biomechanical application of FSI. **a** Snapshots of thrombus formation and separation at a flow rate of $500 \mu\text{m/s}$ of blood at times 0.2 s and 0.6 s [214]. **b** The bulk motion of contents with the two-phase suspension of 2% and 20% volume solids at 3.0 s [118]. **c** The flow around the athlete and surface splash after entering the water with entry pitch angle $+10^\circ$ and 0° [217].

of the legs are submerged. Once the cavity behind the athlete begins to collapse, the converging free-surface structures collide at high speed, resulting in a pronounced vertical jet structure extending beyond the length of the athlete's body, vertically into the air. At 0.42 s, the cavity is almost completely collapsed, and the body position and the shape of the splash are different due to the different pitch angles of the water inlet. For an entry pitch angle of $+10^\circ$, a larger cavity is created due to the larger cross-sectional area exposed to the water, resulting in a larger perimeter of the splash area. Differences in these splashes and jets affect scoring in games.

The application of the SPH method in solids is also explored, including the construction of complex biological tissues, and the exploration of material properties under large deformation conditions. Typical examples include red blood cells [218], soft tissue [219], *Caenorhabditis elegans* [121], and cardiac function with network [220] are given below.

Healthy human red blood cells have a disc-like biconcave shape at rest. Red blood cells exhibit different types of movement and deformation as blood flows through capillaries. Gallage et al. [218] combined a 3D spring network model with the SPH concept to simulate the movement and deformation of individual red blood cells in a narrow capillary, as shown in Fig. 24a. The plasma particles start to

move due to the pressure applied at the inlet, and this movement puts additional pressure on the red blood cells, so the red blood cells flow with the plasma and gradually deform as they pass through the capillaries. A bullet-like shape is observed as it passes through the narrowest part of the capillary, while a typical parachute shape is observed before and after the narrow part.

Investigating high-speed microparticle impact responses to soft tissue is critical for technological applications, such as transdermal delivery in the medical field, which involves microscopic-scale permeation phenomena. Ballistic gelatin is a common human tissue substitute. Meng et al. [219] investigated the penetrations of a silica particle with a diameter of $7.38 \mu\text{m}$ in 10wt% gelatin with various elastic modulus at initial velocity of 1290 m/s , and the extent of tissue damage following projectile penetration can be determined, as shown in Fig. 24b. The cavity is shaped like an elongated cone that expands in both radial and longitudinal directions over time. When the gelatin has a larger Young's modulus, the cavity tends to collapse more quickly after expanding to its maximum dimension, due to the recovery of elastic deformation.

How the nervous system controls the movement of organisms has been studied by Palyanov and his research partners [121]. Motor neurons convert signals from the nervous system into the activation patterns of muscles,

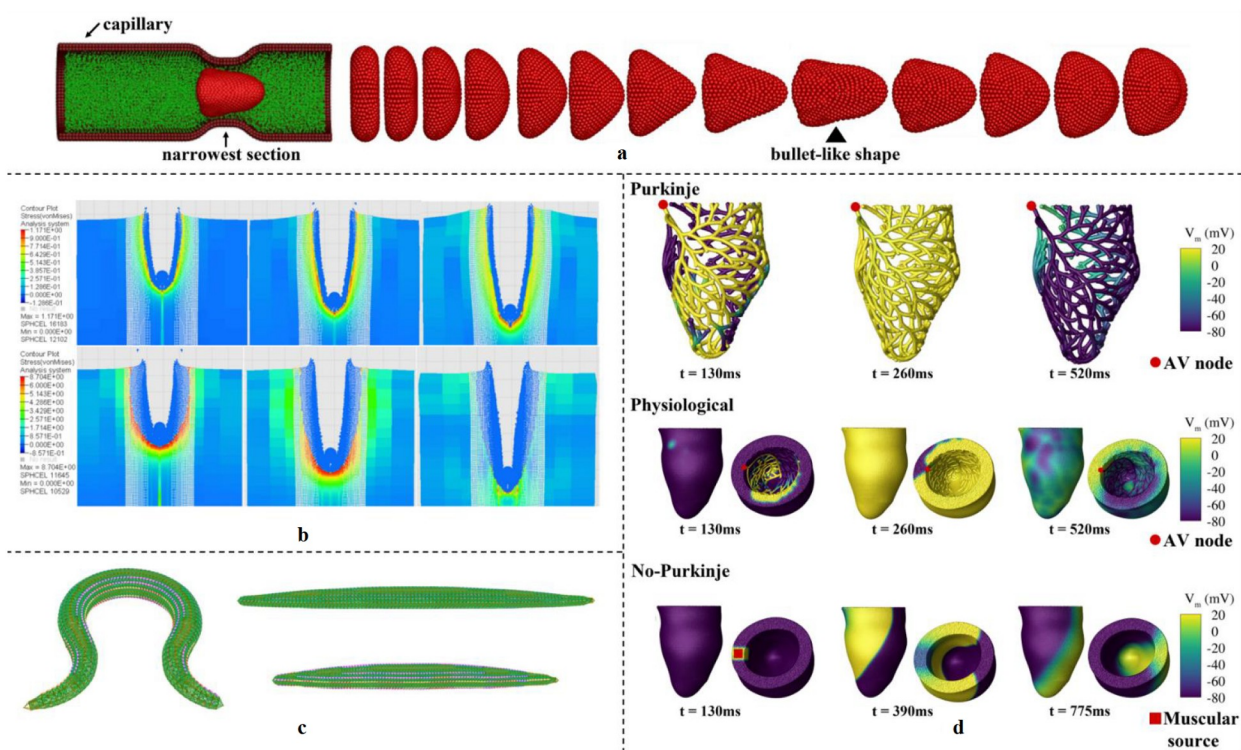


Figure 24 The schematic diagram for the biomechanical application of solid. **a** Deformed morphology of red blood cells passing through narrowed capillaries [218]. **b** The dynamic process of gelatin samples with elastic moduli of 1 MPa and 40 MPa impacted at a velocity of 1290 m/s [219]. **c** The dynamic process of gelatin samples with elastic moduli of 1 MPa and 40 MPa impacted by the silica sphere at a velocity of 1290 m/s [121]. **d** Consequences of activation of the ventricle within a Purkinje or no-Purkinje network at various times [220].

which in turn generate physical forces on the body and move them around the environment. This means exploring the possibility space of how different muscle activation patterns affect behavior, which in turn allows exploring how different nervous system activity patterns affect behavior. Biophysical measurements of *Caenorhabditis elegans* worm bodies are the most comprehensive for any animal in the field of biology. They built a 3D computational biomechanical model of the *Caenorhabditis elegans* body based on real anatomy through a Sibernet engine. This model includes an elastic wall cuticle under hydrostatic pressure, driven by contracting and relaxing body wall muscle cells. Figure 24c shows the basic behavior of a complete *Caenorhabditis elegans* body model including omega-turn posture and shortening, which is achieved by controlling muscles on the right and left sides of the model's body or equal activation force to all muscles between the tail and the head.

The development and exploration of whole-heart simulators are of great help for clinical applications, in which the Purkinje network is considered to be the basis for the accurate description of the electrical activation of the left and right ventricles. Zhang et al. [220] addressed for the first time the problems of network generation on arbitrarily complex surfaces, electrical activation in Purkinje networks, propagation coupling properties resulting from the interaction of Purkinje networks with the myocardium, and electromechanical coupling of the myocardium. Figure 24d reports the activation of the left ventricular transmembrane potential with and without the Purkinje network at different

times. Under physiologically healthy conditions with a Purkinje network, starting from the atrioventricular (AV) node, the left ventricle is rapidly activated by a free-pulse pattern that enters the myocardium and excites a transmembrane potential at the apex of the left ventricle, allowing the wavefront to expand unsmoothly. In the absence of the Purkinje network, the left ventricle is activated by the slow and steady diffusion of a transmembrane potential that starts from a muscle source located in the region of the AV node and propagates from the base to the apex.

The application of the SPH method to the simulation of FSI and solid problems has been discussed previously. Emerging fields such as human breathing [221], plant developmental biology [117] and cell migration [222] are also discussed below.

At the end of 2019, corona-virus disease 19 began to spread around the world, the virus is widely accepted to be transmitted through the air, and many health organizations and governments began to recommend the use of face masks to reduce transmission. English et al. [221] simulated the effect of face coverings on the spread of breathing type flows. As shown in Fig. 25a, the particles are colored according to their distance from the entrance. Comparing the simulation results for times of 1.0 s and 2.0 s with and without a mask, there is a significant difference in the distance that exhaled particles can travel, and when a mask is used, the particles stay in a more localized area of the entrance.

A major challenge in plant developmental biology is to understand how cells grow during organ formation. Mimault

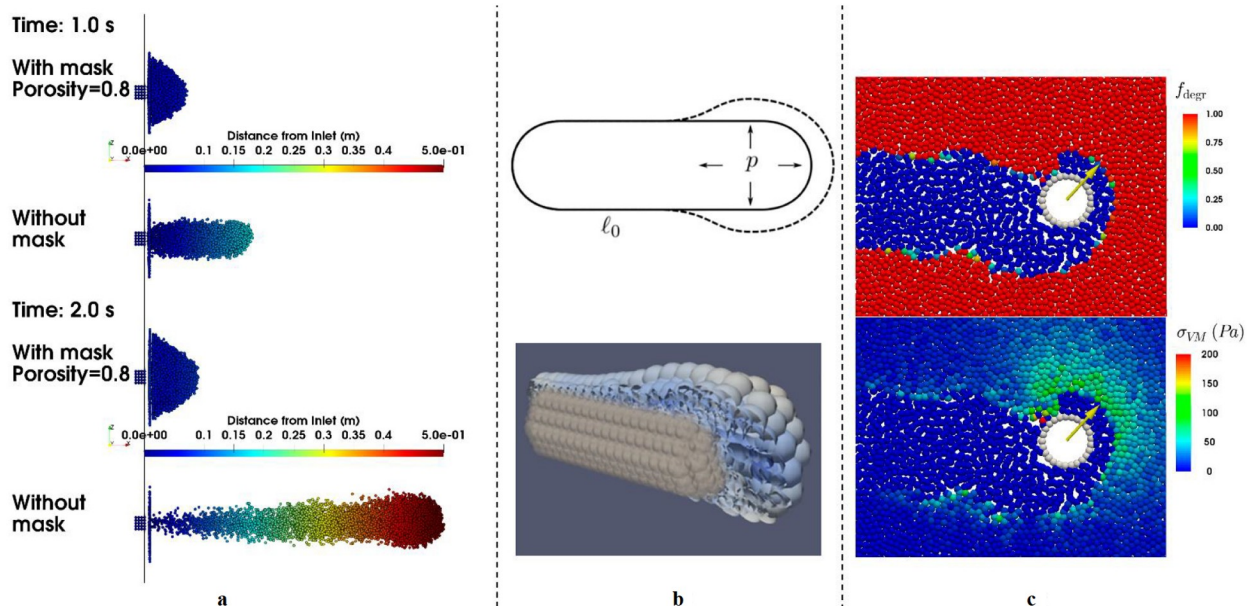


Figure 25 The schematic diagram for the biomechanical application of others. **a** The spread of exhaled SPH particles within or without a mask [221]. **b** Schematic for simulating isotropic growth and particle distribution for 60 s [117]. **c** Degradation factor f_{degr} and von Mises stress distribution (bottom) in the degradable viscoelastic extracellular matrix around a migrating cell [222].

et al. [117] based on the SPH method considered the growth processes of plant tissues at different scales with the turgor pressure, cell wall anisotropy, cell wall biosynthesis, and cell division. Figure 25b shows the formation of an isotropic product, and the particle distribution at time 60 s is given. The outgrowth is generated from a cylindrical domain sample with non-zero pressure in half of the rod holes and zero elsewhere. The increase in expansion pressure leads to isotropic growth, which gradually forms a spherical bulge. This is because the growth will not preferentially expand in any direction, so the shape of the cells will approximate a sphere. This result helps to understand primordium formation in meristems or the response to disease during tumor formation.

The extracellular matrix is an organized molecular network secreted by cells that provides structural support for tissues and is critical to the ability of cells to sense their environment and migrate. Heck et al. [222] demonstrated by simulating a rigid, circular self-propelling object (representing a cell) that locally degrades the extracellular matrix by fluidizing it to allow migration, providing new insights into cell-extracellular matrix interactions. Degradation is implemented by introducing a degradation factor f_{degr} , where 1 is for intact viscoelastic solids and 0 for fully degraded materials. Arrows point to the direction of migration. Through the extracellular matrix, the cell has migrated leaving behind a trail of degraded matrix with low Von Mises stress caused by the local degradation, as shown in Fig. 25c.

Considering the potential applications in bioengineering and biomechanics, coupled with the great advantages of meshless and particle methods, we believe this area of research will continue to help improve human health through its novel and insightful contributions.

4. Development of the SPH program

4.1 Computational efficiency

In engineering applications, the most challenging problem is the dramatic increase in the number of particles and the extremely limited computational efficiency based on CPU conditions, which restricts the applications of the SPH in large-scale or multi-scale problems. To overcome this problem, we focus on three efficient methods: the multiscale adaptive resolution, the parallel algorithm and the automated mesh generation.

4.1.1 Multiscale adaptive resolution

To maintain the resolution with lower computational cost, it is necessary to introduce an effective variable resolution scheme to the framework of SPH.

To save computer time and memory, the adaptive particle refinement is first applied to astrophysical problems [223] based on a density criterion for particle resolution changes, which offers a stable and economic way to increase the local resolution of an SPH simulation of self-gravitating collapse. Recently, Feldman et al. [224] proposed a new particle refinement technique in which one mother particle is split into several daughter particles to improve the computing efficiency and enlarge the computing scale, which makes SPH a perfect candidate for solution refinement and dynamic variable resolution simulations. To reduce the kernel gradient error, Reyes López et al. [225] improved Feldman et al. [224] method by enforcing conservation of the rate of change of density during the refined process, which provides a good trade-off between the accuracy and the cost of the simulation. A simpler method is proposed by Omidvar et al. [226] for large-scale free-surface and FSI problem, which leads to a computer run speed of nearly 200%.

Earlier, a new particle refinement technique is proposed by Barcarolo et al. [227], which introduced automatic particle refinement/derefinement algorithms and led to more efficient and faster SPH simulations than before [166]. Figure 26 shows the result of jet impacting a flat plate with 4 refinement levels. In order to improve the pressure field oscillation at coarse/fine interfaces, Chiron et al. [228] introduced a smoothed particle disordering procedure into the refinement approach and proposed a genuine adaptive particle refinement from the adaptive mesh refinement. Sun et al. [229] combined Chiron's method with δ^+ -SPH and tensile instability control, and successfully applied it to 3D water-entry problems (Fig. 27). The overall computational cost is significantly reduced and the results obtained are encouraging. Recently, Liu et al. [230] proposed a different ancient particle-refinement scheme with a hybrid particle interacting technique for multi-resolution SPH that avoids direct interactions of coarse and fine particles. Using this adaptive particle refinement in SPH, the calculation efficiency is improved without reducing the calculation accuracy, which provides technical support for the numerical study of large-scale engineering problems.

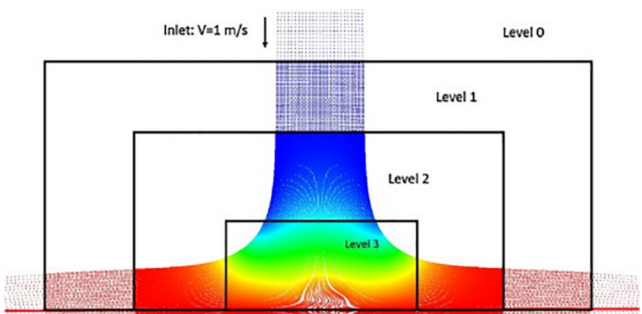


Figure 26 Simulation of jet impacting a flat plate with several refinement zones [227].

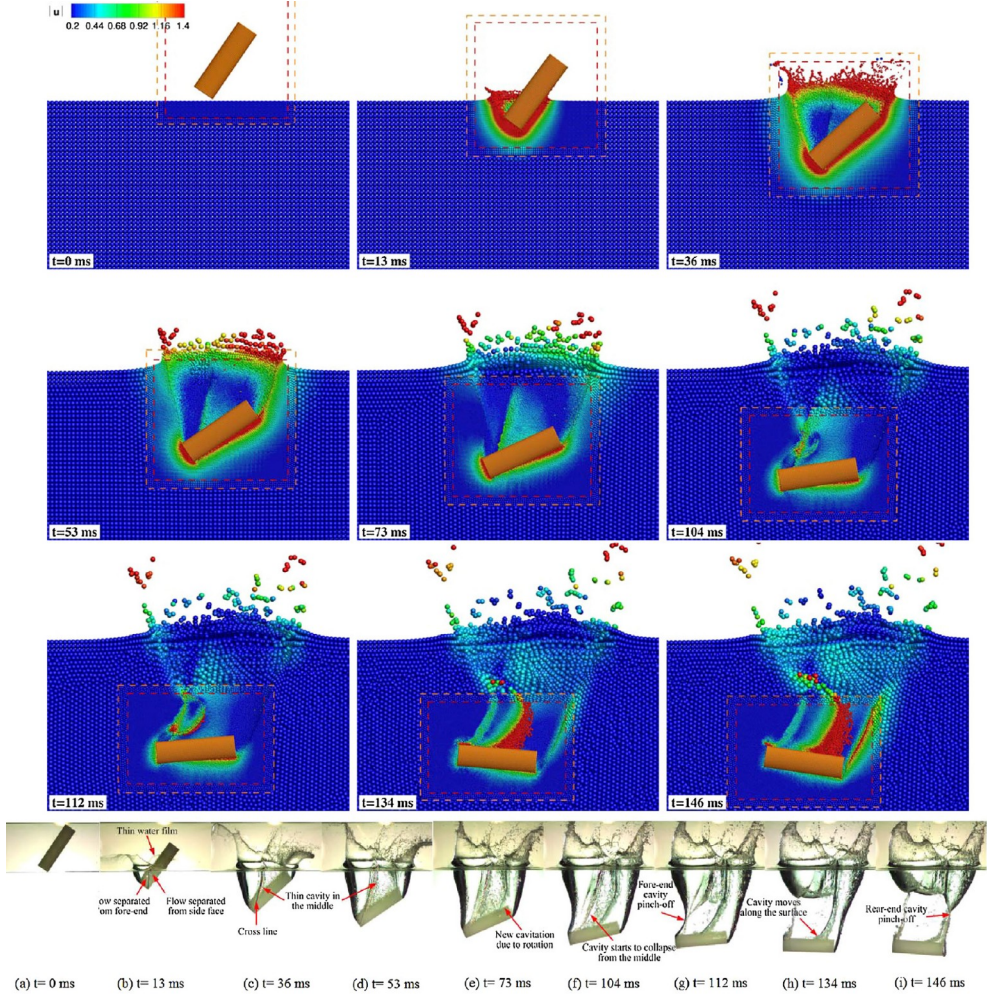


Figure 27 Water entry of 3D cylinder with based on multi-resolution [229].

He et al. [231] proposed a time-space adaptive SPH method, which is implemented in the case of two plate collision and significantly reduced the computational time and improved the calculation efficiency. Zhang et al. [232] proposed a multi-resolution SPH method to increase the computational efficiency, where the fluid and solid equations are discretized by different spatial-temporal resolutions. Figure 28 presents the velocity- and position-based Verlet schemes for the different spatial-temporal resolutions.

4.1.2 Research on parallel algorithm

An alternative solution to solve the problem of the large computation quantity and the low efficiency is parallel computation of the SPH method. There are a large number of relevant studies in this field, including the traditional coarse-grained parallel based on multiple CPU (central processing unit), the fine-grained parallel based on GPU and the coarse-fine-grained parallel based on connecting multiple GPUs by MPI (message passing interface).

In the field of CPU parallel work, Davé et al. [233] developed an SPH solver named parallel tree SPH in 1997,

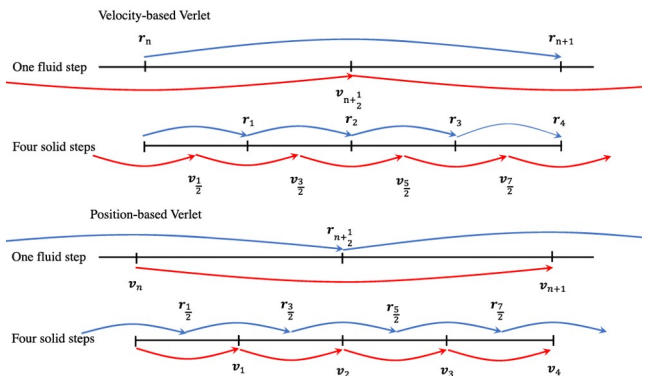


Figure 28 Sketch of velocity- and position-based Verlet schemes for the different spatial-temporal resolutions [232].

which is used to simulate the movement evolution of celestial objects in the universe. Moulinec et al. [234] developed Spartacus-3D, which is based on MPI. Ferrari et al. [235] developed a 3D parallel SPH code based on MPI, using the strategies of splitting the problem and load balancing to improve the computational efficiency. Lia et al. [236] developed a parallel SPH code for the study of galaxy

formation, which calculated 20000 particles on 1, 2, 4, 8, 16, 32 and 64 processors, and the speed-up ratio is close to 90%. Marrone et al. [237] developed an MPI-OpenMP hybrid parallel program, where the communication between computing nodes is implemented by MPI, and the communication within one node is implemented by OpenMP. Almost linear scalability is obtained using 256 cores for a simulation with 40 million particles. However, the development of CPU parallel work has entered a bottleneck period now because of the limitations of CPU performance. The CPU is mostly used for logical judgment and caching, and the capacity improvement mainly depends on the increase in the number of main frequencies and cores, which is limited by the manufacturing technology.

The GPU is a new architecture that is available for large-scale parallel computing and has great advantages over traditional CPU computing. GPU is originally developed as a graphics computing processor in games and video displays, but with the development of technology, especially the implementation of floating-point operations on GPU and the release of CUDA (compute unified device architecture), GPU computing is increasingly used in large-scale scientific computation. Compared with CPU, the advantage of GPU lies in the design of the architecture, which has more computing units. A single GPU usually has hundreds of computing cores, which is more suitable for data-intensive calculations such as the particle SPH method. From the perspective of the processor performance comparison in recent years (Fig. 29), we can see that the computing performance of GPU has grown rapidly, and has greatly exceeded that of CPU.

There have been many research results on GPU parallel SPH algorithms in recent years. In 2012, researchers from several universities jointly developed an open-source SPH parallel program, DualSPHysics [238], which is based on a single GPU. This program adopts several optimization strategies to improve parallel efficiency, including maximizing GPU program occupancy, reducing global memory calls, and simplifying the neighborhood particle search method. Then Valdez-Balderas et al. [239] extended this

program to the multi-GPU parallel. They assigned different computational domains to different GPUs by physically and statically dividing the problem. Domínguez et al. [240] implemented the dynamic load balancing of the multi-GPU parallel SPH approach, and also researched the asynchronous execution to mask the communication time. This program successfully simulates 1 billion particles using 64 GPUs (telsa m2090) in the Barcelona Supercomputing Center, and the total timestep is 237342 with the computational time of 91.9 h. Ji et al. [241] proposed a new SPH parallel framework, which improved the communication strategy. With the improvement of the GPU hardware, a new technology named NVLink is developed, which can make the GPUs communicate with each other directly without passing through the CPU. In 2021, O'Connor et al. [242] performed SPH calculations using the NVLink 2.0 interconnects. The performance showed an approximately 92%-94% weak scaling efficiency in both 2D and 3D on up to four GPUs.

4.1.3 Research on automated mesh generation

In the parallel work of the SPH method, the topic of automated parallel mesh generation is critical for capturing complex physical phenomena in various areas, especially when involving the technique of adaptive particle refinement. Developing scalable, stable and high-quality parallel mesh generation methods is important in reducing simulation cost and achieving high-accuracy for the underlying numerical methods. To fully exploit the potential of distributed memory system, the parallel mesh generator needs to resolve various difficulties, e.g., the data dependency, the load balancing and the irregular behavior of the mesh refinement.

In 2017, Fu et al. [243] proposed a centroidal Voronoi particle (CVP) method for dynamic load balancing in particle-based simulations, in which the load balance target is achieved by solving a Voronoi particle (VP) evolution model equation. Then they integrated the CVP method as dynamic partitioner and developed a new multi-resolution parallel framework for the SPH method [244]. In 2019, Ji et

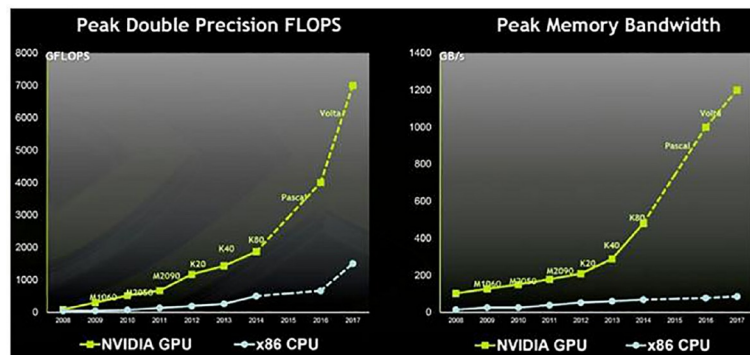


Figure 29 Peak double precision FLOPS (left) and peak memory bandwidth (right) comparison between CPU and GPU (From NVIDIA).

al. [245] developed a Lagrangian inertial CVP (LICVP) method to extend the original CVP method. In 2020, a feature-aware SPH for isotropic unstructured mesh generation is developed [246,247], in which two additional objectives are achieved. First, a feature boundary correction term is introduced to address the issue of incomplete kernel support at the boundary vicinity. The mesh generation of feature curves, feature surfaces and volumes can be handled concurrently without explicitly following a dimensional sequence. Second, a two-phase model is proposed to characterize the mesh-generation procedure by a feature-size-adaptation phase and a mesh-quality-optimization phase.

4.2 Software development

At present, the SPH code is developing continuously. In 1989, the TreeSPH code is developed [248], and it is successfully applied to various cosmological simulations. Later, the GADGET-2 [249] code is developed based on the main structure of TreeSPH. (Dual)SPHysics (<https://dual.sphysics.org/>) is a platform of SPH codes for studying complex flow problems in the fields of hydraulic and coastal engineering [250]. With powerful parallel computing capabilities, it can simulate practical engineering problems with high resolution in a reasonable time, which has been developed to version V5.0. As an open source multi-physics and multi-resolution library based on the SPH method, SPHinXsys [251] is developed by Pro. Hu's research group and provides a C++ API for accurate simulations including fluids, solids, multibody dynamics, etc. to model and optimize coupled industrial dynamic systems through the SPH method. The Developer's repository link: <https://github.com/Xiangyu-Hu/SPHinXsys>. Altair-nanoFluidX [252] is a program developed based on the particle method for fluids that undergo severe deformation during simulation, such as sloshing, violent multiphase fluid motion, or fast motion through complex geometries. OpenFPM [253] (<http://openfpm.mpi-cbg.de/>) is a set of extensible and open C++ programs on CPU and GPU with SPH, MD, and particle mesh methods, which are available with scalable parallel performance. SPHERA is an SPH computational fluid dynamics code developed by Amicarelli et al. [254]. It is mainly used in floods, rapid landslides, wave motion, removal of sediments from water bodies, fuel sloshing tanks, etc. The developer's repository link: <https://github.com/AndreaAmicarelliRSE/SPHERA>.

The most useful numerical tool for solid structures is FEM, which is proposed in the 1950s and great improvement in the parallel calculation developed rapidly during the 1990s. The SPH methodology and application from complex fluid to solid have been developed for nearly half a century since 1977. With the massive improvements in the numerical algorithm and the growing demand for complex en-

gineering applications, there is an urgent need for high computational efficiency with parallel simulation for excellent SPH programs and software.

5. Conclusion

This paper provides an overview of the SPH methodology, from fundamental principles with kernel function, the high-accuracy algorithms of numerical consistency to different applications in various fields, FSI program with interaction forces, solid mechanics with numerical fracture, and bioengineering with the SPH compatibility. In particular, the high-order reconstruction scheme has been fully discussed. The advantages of the SPH method in dealing with extremely large deformation problems of geomechanics, solid mechanics and biomechanics are elaborated in detail, together with the state-of-the-art in SPH program.

A series of higher-order SPH algorithms, such as the higher-order reconstruction method, discontinuity algorithm, and TL-SPH algorithm, is summarized by constructing a new calculation scheme, thus contributing to the improvement of the accuracy of simulation calculation. For the problem of nonphysical fluctuations of pressure field present in the simulations of fluid, δ -SPH and GSPH method based on the Riemann model are able to solve it successfully, thus making the numerical simulation structure closer to the experimental phenomenon. In the FSI problem, three commonly used contact algorithms between fluid and solid structures are summarized, which are able to obtain stable and smooth pressure fields and accurately describe the interaction between fluid and solid structure. When simulating large deformation of solid under impact or explosion loading, the traditional improved algorithms, namely the stress point method, conservative smoothing method, artificial stress method, TL-SPH algorithm and particle splitting algorithm, etc., are elaborated for the defects of tensile instability that are present, making outstanding contributions to the accurate description of the damage fracture and crack extension processes of solid materials under loading. In the field of biomechanics, this paper elucidates the unique biomechanical advantages of the SPH method from the relevant governing equations of root tissue growth to the cells that grow during organogenesis. The application progress of SPH methods in biological fields such as hemodynamically, gut health, and human water sports is detailed. In addition, for the high-efficiency and large-scale requirements of engineering applications for computational simulation, the paper discusses multiscale adaptive resolution and the GPU parallel algorithm, which can effectively improve computational efficiency. The features and recent advances in computing software are also summarized.

More efforts are needed to expand the application of the

SPH method to model materials in solid dynamics. The SPH method in further work should still pay many attentions like:

(1) The tensile instability present in solids is still a matter of concern and needs to be urgently resolved in the follow-up problems related to elastic and brittle materials.

(2) The balance between the accuracy and efficiency of multi-resolution technology is the eternal pursuit of computational simulation. Although some effective resolutions have been proposed to improve computational efficiency, it is still a tremendous challenge for the SPH method.

(3) To investigate the deformation and damage mechanism of solid materials by the SPH method in further work, the most challenging task is to describe the fracture behavior of target materials under various loads. For different materials, especially advanced and complex materials, it is vital to develop proper constitutive models and select appropriate fracture criteria for the kind of particle methods.

(4) The prediction of the characteristics of rock breakage by the SPH method can contribute to the understanding of the basic principles of rock damage. However, unlike landslides, explosions and other macroscopic natural disasters, the initiation and propagation of rock cracks can be significantly influenced by microstructural properties. Therefore, the establishment of multi-scale coupled SPH model will be the focus of future engineering research.

(5) Recently, a new meshfree framework based on deep learning and the neural network has been developed rapidly [255] and may become a hot topic in the field of computational mechanics in the future. However, the application of deep learning technology in solid dynamics remains to be explored. We are confident that the SPH method, a fascinating research approach, will make a novel and insightful contribution to the scientific and technological development of various engineering fields and to the progress of human society in the future.

Author contributions Fei Xu was responsible for methodology, writing review & editing, organization, supervision, funding acquisition and resources; Jiayi Wang contributed to the original draft and writes the technical methods for solid and solid application. Yang Yang summarized the development of high-accuracy SPH algorithms. Lu Wang reviewed the technical methods for fluid and applications. Zhen Dai wrote the advancement in application of additive manufacturing. Ruiqi Han was assigned to write the section on the application of the SPH method in biomechanics.

Acknowledgements This work was supported by the National Natural Science Foundation of China (Grant No. 11972309), and Overseas Expertise Introduction Project for Discipline Innovation (the 111 Project) (Grant No. BP0719007). We also thank Professor Guirong Liu from the University of Cincinnati, Professor Lin Fu and Tianrun Gao from the Hong Kong University of Science and Technology for their helpful comments and support. The contributions of Xianpeng Zhang, Zhe Ji and Fupei Xie from Northwestern Polytechnical University, Jingyu Wang from Technische Universität München and Qiuju Yang from Taiyuan University of Technology in this review are also acknowledged.

1 J. J. Monaghan, Smoothed particle hydrodynamics, *Rep. Prog. Phys.*

- 68, 1703 (2005).
- 2 M. B. Liu, and G. R. Liu, Smoothed particle hydrodynamics (SPH): An overview and recent developments, *Arch Comput. Methods Eng.* 17, 25 (2010).
- 3 H. H. Bui, and G. D. Nguyen, Smoothed particle hydrodynamics (SPH) and its applications in geomechanics: From solid fracture to granular behaviour and multiphase flows in porous media, *Comput. Geotech.* 138, 104315 (2021).
- 4 S. Meng, L. Taddei, N. Lebaal, and S. Roth, Advances in ballistic penetrating impact simulations on thin structures using smooth particles hydrodynamics: A state of the art, *Thin-Walled Struct.* 159, 107206 (2021).
- 5 S. R. Jeske, M. S. Simon, O. Semenov, J. Kruska, O. Mokrov, R. Sharma, U. Reisgen, and J. Bender, Quantitative evaluation of SPH in TIG spot welding, *Comp. Part. Mech.* (2022).
- 6 H. Shen, E. Brousseau, and S. Kulasegaram, Assessment and validation of SPH modeling for nano-indentation, *Comp. Part. Mech.* (2022).
- 7 J. J. Monaghan, Simulating free surface flows with SPH, *J. Comput. Phys.* 110, 399 (1994).
- 8 G. R. Liu, and M. B. Liu, Smoothed Particle Hydrodynamics: A Meshfree Particle Method (World Scientific, Singapore, 2003).
- 9 M. Liu, and Z. Zhang, Smoothed particle hydrodynamics (SPH) for modeling fluid-structure interactions, *Sci. China-Phys. Mech. Astron.* 62, 984701 (2019).
- 10 T. Ye, D. Pan, C. Huang, and M. Liu, Smoothed particle hydrodynamics (SPH) for complex fluid flows: Recent developments in methodology and applications, *Phys. Fluids* 31, 011301 (2019).
- 11 L. D. Libersky, and A. G. Petschek, Smooth Particle Hydrodynamics with Strength of Materials (Springer, Berlin, Heidelberg, 1991), pp. 248-257.
- 12 H. T. Tran, Y. Wang, G. D. Nguyen, J. Kodikara, M. Sanchez, and H. H. Bui, Modelling 3D desiccation cracking in clayey soils using a size-dependent SPH computational approach, *Comput. Geotech.* 116, 103209 (2019).
- 13 W. Jiao, and X. Chen, Review on long-rod penetration at hypervelocity, *Adv. Mech.* 49, 201904 (2019).
- 14 Y. Wu, and X. Chen, A numerical simulation method for long rods penetrating into ceramic targets, *Expl. Shock Waves* 40, 053301 (2020).
- 15 M. K. Rausch, G. E. Karniadakis, and J. D. Humphrey, Modeling soft tissue damage and failure using a combined particle/continuum approach, *Biomech. Model. Mechanobiol.* 16, 249 (2017).
- 16 Y. Huang, and Z. Dai, Large deformation and failure simulations for geo-disasters using smoothed particle hydrodynamics method, *Eng. Geol.* 168, 86 (2014).
- 17 M. Kojić, N. Filipović, B. Stojanović, and N. Kojić, Computer Modeling in Bioengineering: Theoretical Background, Examples and Software (Wiley, Chichester, 2008).
- 18 M. Toma, R. Chan-Akeley, J. Arias, G. D. Kurgansky, and W. Mao, Fluid-structure interaction analyses of biological systems using smoothed-particle hydrodynamics, *Biology* 10, 185 (2021).
- 19 L. W. Zhang, A. S. Ademiloye, and K. M. Liew, Meshfree and particle methods in biomechanics: Prospects and challenges, *Arch. Computat. Methods Eng.* 26, 1547 (2018).
- 20 L. Wang, F. Xu, and Y. Yang, An improved total Lagrangian SPH method for modeling solid deformation and damage, *Eng. Anal. Bound. Elem.* 133, 286 (2021).
- 21 J. W. Swegle, D. L. Hicks, and S. W. Attaway, Smoothed particle hydrodynamics stability analysis, *J. Comput. Phys.* 116, 123 (1995).
- 22 J. P. Morris, Analysis of smoothed particle hydrodynamics with applications (1996).
- 23 P. Lancaster, and K. Salkauskas, Surfaces generated by moving least squares methods, *Math. Comp.* 37, 141 (1981).
- 24 G. A. Dilts, Moving-least-squares-particle hydrodynamics? I. Consistency and stability, *Int. J. Numer. Meth. Eng.* 44, 1115 (1999).
- 25 G. A. Dilts, Moving least-squares particle hydrodynamics II:

- Conservation and boundaries, *Int. J. Numer. Meth. Eng.* **48**, 1503 (2000).
- 26 W. K. Liu, S. Jun, and Y. F. Zhang, Reproducing kernel particle methods, *Int. J. Numer. Meth. Fluids* **20**, 1081 (1995).
- 27 W. K. Liu, S. Jun, S. Li, J. Adee, and T. Belytschko, Reproducing kernel particle methods for structural dynamics, *Int. J. Numer. Meth. Eng.* **38**, 1655 (1995).
- 28 W. K. Liu, S. Jun, D. T. Sihling, Y. Chen, and W. Hao, Multi-resolution reproducing kernel particle method for computational fluid dynamics, *Int. J. Numer. Meth. Fluids* **24**, 1391 (1997).
- 29 C. T. Sun, P. C. Guan, J. H. Jiang, and O. L. A. Kwok, The weighted reconstruction of reproducing kernel particle method for one-dimensional shock wave problems, *Ocean Eng.* **149**, 325 (2018).
- 30 Z. Liu, H. Gao, G. Wei, and Z. Wang, The meshfree analysis of elasticity problem utilizing radial basis reproducing kernel particle method, *Results Phys.* **17**, 103037 (2020).
- 31 J. Ma, H. Gao, G. Wei, and J. Qiao, The meshless analysis of wave propagation based on the Hermite-type RRKPM, *Soil Dyn. Earthquake Eng.* **134**, 106154 (2020).
- 32 P. P. Peng, and Y. M. Cheng, Analyzing three-dimensional transient heat conduction problems with the dimension splitting reproducing kernel particle method, *Eng. Anal. Bound. Elem.* **121**, 180 (2020).
- 33 Z. Liu, G. Wei, and Z. Wang, The radial basis reproducing kernel particle method for geometrically nonlinear problem of functionally graded materials, *Appl. Math. Model.* **85**, 244 (2020).
- 34 R. Kiran, N. Nguyen-Thanh, J. Huang, and K. Zhou, Buckling analysis of cracked orthotropic 3D plates and shells via an isogeometric-reproducing kernel particle method, *Theor. Appl. Fract. Mech.* **114**, 102993 (2021).
- 35 J. K. Chen, J. E. Beraun, and T. C. Carney, A corrective smoothed particle method for boundary value problems in heat conduction, *Int. J. Numer. Meth. Eng.* **46**, 231 (1999).
- 36 M. B. Liu, G. R. Liu, and K. Y. Lam, A one-dimensional meshfree particle formulation for simulating shock waves, *Shock Waves* **13**, 201 (2003).
- 37 F. Xu, Y. Zhao, R. Yan, and T. Furukawa, Multidimensional discontinuous SPH method and its application to metal penetration analysis, *Int. J. Numer. Meth. Eng.* **93**, 1125 (2013).
- 38 G. M. Zhang, and R. C. Batra, Modified smoothed particle hydrodynamics method and its application to transient problems, *Comput. Mech.* **34**, 137 (2004).
- 39 M. B. Liu, W. P. Xie, and G. R. Liu, Modeling incompressible flows using a finite particle method, *Appl. Math. Model.* **29**, 1252 (2005).
- 40 Y. Yang, F. Xu, M. Zhang, and L. Wang, An effective improved algorithm for finite particle method, *Int. J. Comput. Methods* **13**, 1641009 (2016).
- 41 L. Wang, Y. Yang, and F. Xu, An improved finite particle method considering interfacial discontinuities, *Expl. Shock Waves* **39**, 121 (2019).
- 42 L. Wang, F. Xu, and Y. Yang, An improved specified finite particle method and its application to transient heat conduction, *Int. J. Comput. Methods* **14**, 1750050 (2017).
- 43 R. Yan, and F. Xu, Research and improvement on the accuracy of discontinuous smoothed particle hydrodynamics (DSPH) method, *Comput. Mater. Continua* **47**, 179 (2015).
- 44 D. Chen, W. Huang, and S. W. Sloan, An alternative updated Lagrangian formulation for finite particle method, *Comput. Methods Appl. Mech. Eng.* **343**, 490 (2019).
- 45 D. Asprone, F. Auricchio, G. Manfredi, A. Prota, A. Reali, and G. Sangalli, Particle methods for a 1D elastic model problem: Error analysis and development of a second-order accurate formulation, *Comput. Model. Eng. Sci.* **62**, 1 (2010).
- 46 D. Asprone, F. Auricchio, and A. Reali, Novel finite particle formulations based on projection methodologies, *Int. J. Numer. Meth. Fluids* **65**, 1376 (2011).
- 47 A. M. A. Nasar, G. Fournakas, S. J. Lind, J. R. C. King, B. D. Rogers, and P. K. Stansby, High-order consistent SPH with the pressure projection method in 2-D and 3-D, *J. Comput. Phys.* **444**, 110563 (2021).
- 48 Z. L. Zhang, and M. B. Liu, A decoupled finite particle method for modeling incompressible flows with free surfaces, *Appl. Math. Model.* **60**, 606 (2018).
- 49 C. V. Achim, R. E. Rozas, and P. G. Toledo, Semi-decoupled first-order correction for smoothed particle hydrodynamics, *Appl. Math. Model.* **93**, 314 (2021).
- 50 F. Liu, Y. Yu, Q. Wang, and Y. Luo, A coupled smoothed particle hydrodynamic and finite particle method: An efficient approach for fluid-solid interaction problems involving free-surface flow and solid failure, *Eng. Anal. Bound. Elem.* **118**, 143 (2020).
- 51 C. Huang, D. H. Zhang, Y. L. Si, Y. X. Shi, and Y. G. Lin, Coupled finite particle method for simulations of wave and structure interaction, *Coast. Eng.* **140**, 147 (2018).
- 52 C. Huang, T. Long, and M. B. Liu, Coupling finite difference method with finite particle method for modeling viscous incompressible flows, *Int. J. Numer. Meth. Fluids* **90**, 564 (2019).
- 53 Z. L. Zhang, T. Long, J. Z. Chang, and M. B. Liu, A smoothed particle element method (SPEM) for modeling fluid-structure interaction problems with large fluid deformations, *Comput. Methods Appl. Mech. Eng.* **356**, 261 (2019).
- 54 Z. Mao, G. R. Liu, and X. Dong, A comprehensive study on the parameters setting in smoothed particle hydrodynamics (SPH) method applied to hydrodynamics problems, *Comput. Geotech.* **92**, 77 (2017).
- 55 J. Yang, X. Zhang, G. R. Liu, and W. Zhang, A compact perfectly matched layer algorithm for acoustic simulations in the time domain with smoothed particle hydrodynamic method, *J. Acoust. Soc. Am.* **145**, 204 (2019).
- 56 J. Yang, X. Zhang, G. R. Liu, Z. Mao, and W. Zhang, Perfectly matched layer absorbing boundary conditions for Euler equations with oblique mean flows modeled with smoothed particle hydrodynamics, *J. Acoust. Soc. Am.* **147**, 1311 (2020).
- 57 Y. Lin, G. R. Liu, and G. Wang, A particle-based free surface detection method and its application to the surface tension effects simulation in smoothed particle hydrodynamics (SPH), *J. Comput. Phys.* **383**, 196 (2019).
- 58 M. Hu, G. Wang, G. Liu, and Q. Peng, The application of godunov SPH in the simulation of energetic materials, *Int. J. Comput. Methods* **17**, 1950028 (2020).
- 59 A. Colagrossi, and M. Landrini, Numerical simulation of interfacial flows by smoothed particle hydrodynamics, *J. Comput. Phys.* **191**, 448 (2003).
- 60 S. Shao, and E. Y. M. Lo, Incompressible SPH method for simulating Newtonian and non-Newtonian flows with a free surface, *Adv. Water Resour.* **26**, 787 (2003).
- 61 R. Xu, P. Stansby, and D. Laurence, Accuracy and stability in incompressible SPH (ISPH) based on the projection method and a new approach, *J. Comput. Phys.* **228**, 6703 (2009).
- 62 S. J. Lind, R. Xu, P. K. Stansby, and B. D. Rogers, Incompressible smoothed particle hydrodynamics for free-surface flows: A generalised diffusion-based algorithm for stability and validations for impulsive flows and propagating waves, *J. Comput. Phys.* **231**, 1499 (2012).
- 63 S. Adami, X. Y. Hu, and N. A. Adams, A transport-velocity formulation for smoothed particle hydrodynamics, *J. Comput. Phys.* **241**, 292 (2013).
- 64 S. Marrone, M. Antuono, A. Colagrossi, G. Colicchio, D. Le Touzé, and G. Graziani, δ-SPH model for simulating violent impact flows, *Comput. Methods Appl. Mech. Eng.* **200**, 1526 (2011).
- 65 S. De Chowdhury, and S. A. Sannasiraj, Numerical simulation of 2D sloshing waves using SPH with diffusive terms, *Appl. Ocean Res.* **47**, 219 (2014).
- 66 A. Valizadeh, and J. J. Monaghan, A study of solid wall models for weakly compressible SPH, *J. Comput. Phys.* **300**, 5 (2015).
- 67 R. Vacondio, B. D. Rogers, P. K. Stansby, and P. Mignosa, Variable

- resolution for SPH in three dimensions: Towards optimal splitting and coalescing for dynamic adaptivity, *Comput. Methods Appl. Mech. Eng.* **300**, 442 (2016).
- 68 G. Oger, S. Marrone, D. Le Touzé, and M. de Leffe, SPH accuracy improvement through the combination of a quasi-Lagrangian shifting transport velocity and consistent ALE formalisms, *J. Comput. Phys.* **313**, 76 (2016).
- 69 X. Yang, Z. Zhang, G. Zhang, S. Feng, and Z. Sun, Simulating multi-phase sloshing flows with the SPH method, *Appl. Ocean Res.* **118**, 102989 (2022).
- 70 P. N. Sun, A. Colagrossi, S. Marrone, and A. M. Zhang, The δ -plus-SPH model: Simple procedures for a further improvement of the SPH scheme, *Comput. Methods Appl. Mech. Eng.* **315**, 25 (2017).
- 71 P. N. Sun, A. Colagrossi, and A. M. Zhang, Numerical simulation of the self-propulsive motion of a fishlike swimming foil using the δ -SPH model, *Theor. Appl. Mech. Lett.* **8**, 115 (2018).
- 72 P. N. Sun, A. Colagrossi, S. Marrone, M. Antuono, and A. M. Zhang, A consistent approach to particle shifting in the δ -plus-SPH model, *Comput. Methods Appl. Mech. Eng.* **348**, 912 (2019).
- 73 M. Antuono, P. N. Sun, S. Marrone, and A. Colagrossi, The δ -ALE-SPH model: An arbitrary Lagrangian-Eulerian framework for the δ -SPH model with particle shifting technique, *Comput. Fluids* **216**, 104806 (2021).
- 74 X. L. Fang, A. Colagrossi, P. P. Wang, and A. M. Zhang, An accurate and robust axisymmetric SPH method based on Riemann solver with applications in ocean engineering, *Ocean Eng.* **244**, 110369 (2022).
- 75 C. Zhang, X. Y. Hu, and N. A. Adams, A weakly compressible SPH method based on a low-dissipation Riemann solver, *J. Comput. Phys.* **335**, 605 (2017).
- 76 Z. F. Meng, P. P. Wang, A. M. Zhang, F. R. Ming, and P. N. Sun, A multiphase SPH model based on Roe's approximate Riemann solver for hydraulic flows with complex interface, *Comput. Methods Appl. Mech. Eng.* **365**, 112999 (2020).
- 77 Z. F. Meng, A. M. Zhang, P. P. Wang, and F. R. Ming, A shock-capturing scheme with a novel limiter for compressible flows solved by smoothed particle hydrodynamics, *Comput. Methods Appl. Mech. Eng.* **386**, 114082 (2021).
- 78 Z. F. Meng, F. R. Ming, P. P. Wang, and A. M. Zhang, Numerical simulation of water entry problems considering air effect using a multiphase Riemann-SPH model, *Adv. Aerodyn.* **3**, 13 (2021).
- 79 Z. F. Meng, A. M. Zhang, J. L. Yan, P. P. Wang, and A. Khayyer, A hydroelastic fluid-structure interaction solver based on the Riemann-SPH method, *Comput. Methods Appl. Mech. Eng.* **390**, 114522 (2022).
- 80 J. P. Vila, SPH renormalized hybrid methods for conservation laws: Applications to free surface flows, edited by M. Griebel, and M. A. Schweitzer, *Meshfree Methods for Partial Differential Equations II* (Springer, Berlin, Heidelberg, 2005), pp. 207-229.
- 81 G. S. Jiang, and C. W. Shu, Efficient implementation of weighted ENO schemes, *J. Comput. Phys.* **126**, 202 (1996).
- 82 D. Avesani, M. Dumbser, and A. Bellin, A new class of Moving-Least-Squares WENO-SPH schemes, *J. Comput. Phys.* **270**, 278 (2014).
- 83 D. Avesani, M. Dumbser, R. Vacondio, and M. Righetti, An alternative SPH formulation: ADER-WENO-SPH, *Comput. Methods Appl. Mech. Eng.* **382**, 113871 (2021).
- 84 X. Nogueira, L. Ramírez, S. Clain, R. Loubère, L. Cueto-Felgueroso, and I. Colominas, High-accurate SPH method with multi-dimensional optimal order detection limiting, *Comput. Methods Appl. Mech. Eng.* **310**, 134 (2016).
- 85 X. Zhang, H. Tian, L. Kuo, and W. Chen, A contact SPH method with high-order limiters for simulation of inviscid compressible flows, *Commun. Comput. Phys.* **14**, 425 (2013).
- 86 Z. F. Meng, A. M. Zhang, P. P. Wang, F. R. Ming, and B. C. Khoo, A targeted essentially non-oscillatory (TENO) SPH method and its applications in hydrodynamics, *Ocean Eng.* **243**, 110100 (2022).
- 87 L. Fu, X. Y. Hu, and N. A. Adams, A family of high-order targeted ENO schemes for compressible-fluid simulations, *J. Comput. Phys.* **305**, 333 (2016).
- 88 C. Zhang, G. M. Xiang, B. Wang, X. Y. Hu, and N. A. Adams, A weakly compressible SPH method with WENO reconstruction, *J. Comput. Phys.* **392**, 1 (2019).
- 89 S. Adami, X. Y. Hu, and N. A. Adams, A generalized wall boundary condition for smoothed particle hydrodynamics, *J. Comput. Phys.* **231**, 7057 (2012).
- 90 Z. L. Zhang, K. Walayat, J. Z. Chang, and M. B. Liu, Meshfree modeling of a fluid-particle two-phase flow with an improved SPH method, *Int. J. Numer. Methods Eng.* **116**, 530 (2018).
- 91 C. Chen, A. M. Zhang, J. Q. Chen, and Y. M. Shen, SPH simulations of water entry problems using an improved boundary treatment, *Ocean Eng.* **238**, 109679 (2021).
- 92 J. J. Monaghan, and J. B. Kajtar, SPH particle boundary forces for arbitrary boundaries, *Comput. Phys. Commun.* **180**, 1811 (2009).
- 93 Z. J. Wei, D. Yu, and C. H. Zhou, SPH Simulation of dam break flow impacting plunge pool, *Water Resour. Power* **39**, 41 (2021).
- 94 L. Wang, F. Xu, and Y. Yang, Research on water entry problems of gas-structure-liquid coupling based on SPH method, *Ocean Eng.* **257**, 111623 (2022).
- 95 T. Rabczuk, T. Belytschko, and S. P. Xiao, Stable particle methods based on Lagrangian kernels, *Comput. Methods Appl. Mech. Eng.* **193**, 1035 (2004).
- 96 C. T. Dyka, and R. P. Ingel, An approach for tension instability in smoothed particle hydrodynamics (SPH), *Comput. Struct.* **57**, 573 (1995).
- 97 C. M. Chalk, M. Pastor, J. Peakall, D. J. Borman, P. A. Sleigh, W. Murphy, and R. Fuentes, Stress-particle smoothed particle hydrodynamics: An application to the failure and post-failure behaviour of slopes, *Comput. Methods Appl. Mech. Eng.* **366**, 113034 (2020).
- 98 D. L. Hicks, J. W. Swegle, and S. W. Attaway, Conservative smoothing stabilizes discrete-numerical instabilities in SPH material dynamics computations, *Appl. Math. Comput.* **85**, 209 (1997).
- 99 P. W. Randles, and L. D. Libersky, Smoothed particle hydrodynamics: Some recent improvements and applications, *Comput. Methods Appl. Mech. Eng.* **139**, 375 (1996).
- 100 C. Guenther, D. Hicks, and J. Swegle, Conservative smoothing versus artificial viscosity, NASA STI/Recon Technical Report N (Sandia National Lab, Albuquerque, 1994), pp. 94-1853.
- 101 D. L. Hicks, and L. M. Liebrock, Conservative smoothing with B-splines stabilizes SPH material dynamics in both tension and compression, *Appl. Math. Comput.* **150**, 213 (2004).
- 102 J. J. Monaghan, SPH without a tensile instability, *J. Comput. Phys.* **159**, 290 (2000).
- 103 J. P. Gray, J. J. Monaghan, and R. P. Swift, SPH elastic dynamics, *Comput. Methods Appl. Mech. Eng.* **190**, 6641 (2001).
- 104 X. Xu, J. Ouyang, T. Jiang, and Q. Li, Numerical simulation of 3D-unsteady viscoelastic free surface flows by improved smoothed particle hydrodynamics method, *J. Non-Newtonian Fluid Mech.* **177-178**, 109 (2012).
- 105 A. A. Hemeda, C. Zhang, X. Y. Hu, D. Fukuda, D. Cote, I. M. Nault, A. Nardi, V. K. Champagne, Y. Ma, and J. W. Palko, Particle-based simulation of cold spray: Influence of oxide layer on impact process, *Addit. Manuf.* **37**, 101517 (2021).
- 106 M. R. I. Islam, A. Bansal, and C. Peng, Numerical simulation of metal machining process with Eulerian and total Lagrangian SPH, *Eng. Anal. Bound. Elem.* **117**, 269 (2020).
- 107 T. Belytschko, and S. Xiao, Stability analysis of particle methods with corrected derivatives, *Comput. Math. Appl.* **43**, 329 (2002).
- 108 J. Campbell, R. Vignjevic, and L. Libersky, A contact algorithm for smoothed particle hydrodynamics, *Comput. Methods Appl. Mech. Eng.* **184**, 49 (2000).
- 109 A. M. Salehizadeh, and A. R. Shafeie, A coupled ISPH-TLSPH method for simulating fluid-elastic structure interaction problems, *J.*

- Mar. Sci. Appl.** **21**, 15 (2022).
- 110 D. S. Morikawa, and M. Asai, Coupling total Lagrangian SPH-EISPH for fluid-structure interaction with large deformed hyper-elastic solid bodies, *Comput. Methods Appl. Mech. Eng.* **381**, 113832 (2021).
- 111 L. Han, and X. Hu, SPH modeling of fluid-structure interaction, *J. Hydodyn.* **30**, 62 (2018).
- 112 S. C. Hwang, A. Khayyer, H. Gotoh, and J. C. Park, Development of a fully Lagrangian MPS-based coupled method for simulation of fluid-structure interaction problems, *J. Fluids Struct.* **50**, 497 (2014).
- 113 R. Vignjevic, J. R. Reveles, and J. Campbell, SPH in a total Lagrangian formalism, *Comput. Model. Eng. Sci.* **14**, 181 (2006).
- 114 J. Young, F. Teixeira-Dias, A. Azevedo, and F. Mill, Adaptive total Lagrangian Eulerian SPH for high-velocity impacts, *Int. J. Mech. Sci.* **192**, 106108 (2021).
- 115 H. K. Serroukh, M. Mabssout, and M. I. Herreros, Updated Lagrangian Taylor-SPH method for large deformation in dynamic problems, *Appl. Math. Model.* **80**, 238 (2020).
- 116 M. R. I. Islam, and C. Peng, A total Lagrangian SPH method for modelling damage and failure in solids, *Int. J. Mech. Sci.* **157-158**, 498 (2019).
- 117 M. Mimault, M. Ptashnyk, G. W. Bassel, and L. X. Dupuy, Smoothed particle hydrodynamics for root growth mechanics, *Eng. Anal. Bound. Elem.* **105**, 20 (2019).
- 118 M. D. Sinnott, P. W. Cleary, and S. M. Harrison, Peristaltic transport of a particulate suspension in the small intestine, *Appl. Math. Model.* **44**, 143 (2017).
- 119 L. D. G. Sigalotti, J. Klapp, K. Pedroza, E. Nathal, and C. E. Alvarado-Rodríguez, Numerical simulation of the blood flow through a brain vascular aneurysm with an artificial stent using the SPH method, *Engineering* **10**, 891 (2018).
- 120 W. Mao, K. Li, and W. Sun, Fluid-structure interaction study of transcatheter aortic valve dynamics using smoothed particle hydrodynamics, *Cardiovasc. Eng. Tech.* **7**, 374 (2016).
- 121 A. Palyanov, S. Khayrulin, and S. D. Larson, Three-dimensional simulation of the *Caenorhabditis elegans* body and muscle cells in liquid and gel environments for behavioural analysis, *Phil. Trans. R. Soc. B* **373**, 20170376 (2018).
- 122 S. Shahriari, and D. Garcia, Meshfree simulations of ultrasound vector flow imaging using smoothed particle hydrodynamics, *Phys. Med. Biol.* **63**, 205011 (2018).
- 123 P. W. Cleary, Prediction of coupled particle and fluid flows using DEM and SPH, *Miner. Eng.* **73**, 85 (2015).
- 124 G. R. Liu, G. Y. Wang, Q. Peng, and S. De, A micro-macro coupling approach of MD-SPH method for reactive energetic materials, AIP Conf. Proc. **1793**, 050006 (2017).
- 125 Q. Peng, Q. Rahul, G. Wang, G. R. Liu, S. Grimme, and S. De, Predicting elastic properties of β -HMX from first-principles calculations, *J. Phys. Chem. B* **119**, 5896 (2015).
- 126 M. B. Liu, and G. R. Liu, Particle Methods for Multi-Scale and Multi-Physics (World Scientific, Singapore, 2016).
- 127 A. Colagrossi, M. Antuono, and D. Le Touzé, Theoretical considerations on the free-surface role in the smoothed-particle-hydrodynamics model, *Phys. Rev. E* **79**, 056701 (2009).
- 128 G. Oger, B. Alessandrini, and P. Ferrant, in Capture of air cushion effects in a wedge water entry SPH simulation: Proceedings of the 15th International Offshore and Polar Engineering Conference, Seoul, 2005.
- 129 R. Yan, J. J. Monaghan, A. Valizadeh, and F. Xu, The effect of air on solid body impact with water in two dimensions, *J. Fluids Struct.* **59**, 146 (2015).
- 130 Q. Yang, F. Xu, Y. Yang, J. Wang, A. Wang, and C. Ma, Numerical study on the dynamic characteristics of water entry of cavity body using two-phase SPH method, *Acta Mech. Sin.* **37**, 1072 (2021).
- 131 M. H. Siemann, D. B. Schwinn, J. Scherer, and D. Kohlgrüber, Advances in numerical ditching simulation of flexible aircraft models, *Int. J. Crashworthiness* **23**, 236 (2018).
- 132 F. Xu, X. Ren, X. Zhang, X. Gao, and J. Liu, Decreasing effectiveness of chine tire on contaminated runway at high taxiing speed, *J. Aircraft* **57**, 198 (2020).
- 133 X. Zhang, F. Xu, X. Ren, X. Gao, and R. Cao, Consideration on aircraft tire spray when running on wet runways, *Chin. J. Aeronaut.* **33**, 520 (2020).
- 134 X. Guan, F. Xu, M. Hu, X. Ren, and X. Zhang, Numerical simulation of water spray generated by aircraft multi-wheels, *Int. J. Comput. Fluid Dyn.* **35**, 93 (2021).
- 135 C. Antoci, M. Gallati, and S. Sibilla, Numerical simulation of fluid-structure interaction by SPH, *Comput. Struct.* **85**, 879 (2007).
- 136 L. Wang, F. Xu, and Y. Yang, SPH scheme for simulating the water entry of an elastomer, *Ocean Eng.* **178**, 233 (2019).
- 137 X. Yang, M. Liu, S. Peng, and C. Huang, Numerical modeling of dam-break flow impacting on flexible structures using an improved SPH-EBG method, *Coast. Eng.* **108**, 56 (2016).
- 138 J. O'Connor, and B. D. Rogers, A fluid-structure interaction model for free-surface flows and flexible structures using smoothed particle hydrodynamics on a GPU, *J. Fluids Struct.* **104**, 103312 (2021).
- 139 A. M. A. Nasar, B. D. Rogers, A. Revell, and P. K. Stansby, Flexible slender body fluid interaction: Vector-based discrete element method with Eulerian smoothed particle hydrodynamics, *Comput. Fluids* **179**, 563 (2019).
- 140 A. Skillen, S. Lind, P. K. Stansby, and B. D. Rogers, Incompressible smoothed particle hydrodynamics (SPH) with reduced temporal noise and generalised Fickian smoothing applied to body-water slam and efficient wave-body interaction, *Comput. Methods Appl. Mech. Eng.* **265**, 163 (2013).
- 141 M. B. Liu, J. R. Shao, and H. Q. Li, An SPH model for free surface flows with moving rigid objects, *Int. J. Numer. Meth. Fluids* **74**, 684 (2014).
- 142 P. Sun, F. Ming, and A. Zhang, Numerical simulation of interactions between free surface and rigid body using a robust SPH method, *Ocean Eng.* **98**, 32 (2015).
- 143 K. Pan, R. H. A. IJzermans, B. D. Jones, A. Thyagarajan, B. W. H. van Beest, and J. R. Williams, Application of the SPH method to solitary wave impact on an offshore platform, *Comp. Part. Mech.* **3**, 155 (2016).
- 144 M. Antuono, A. Colagrossi, S. Marrone, and C. Lugni, Propagation of gravity waves through an SPH scheme with numerical diffusive terms, *Comput. Phys. Commun.* **182**, 866 (2011).
- 145 P. N. Sun, M. Luo, D. Le Touzé, and A. M. Zhang, The suction effect during freak wave slamming on a fixed platform deck: Smoothed particle hydrodynamics simulation and experimental study, *Phys. Fluids* **31**, 117108 (2019).
- 146 S. Mintu, D. Molyneux, and B. Colbourne, Full-scale SPH simulations of ship-wave impact generated sea spray, *Ocean Eng.* **241**, 110077 (2021).
- 147 S. Marrone, A. Colagrossi, V. Baudry, and D. Le Touzé, Extreme wave impacts on a wave energy converter: Load prediction through a SPH model, *Coast. Eng. J.* **61**, 63 (2019).
- 148 G. Zhu, D. Graham, S. Zheng, J. Hughes, and D. Greaves, Hydrodynamics of onshore oscillating water column devices: A numerical study using smoothed particle hydrodynamics, *Ocean Eng.* **218**, 108226 (2020).
- 149 Z. Wei, B. L. Edge, R. A. Dalrymple, and A. Héault, Modeling of wave energy converters by GPUSPH and Project Chrono, *Ocean Eng.* **183**, 332 (2019).
- 150 H. G. Lyu, P. N. Sun, X. T. Huang, S. Y. Zhong, Y. X. Peng, T. Jiang, and C. N. Ji, A review of SPH techniques for hydrodynamic simulations of ocean energy devices, *Energies* **15**, 502 (2022).
- 151 X. Dong, G. R. Liu, Z. Li, and W. Zeng, Smoothed particle hydrodynamics (SPH) modeling of shot peening process, *J. Clin. Med.* **17**, 799 (2017).
- 152 W. Niu, R. Mo, G. R. Liu, H. Sun, X. Dong, and G. Wang, Modeling of orthogonal cutting process of A2024-T351 with an improved SPH method, *Int. J. Adv. Manuf. Technol.* **95**, 905 (2018).

- 153 L. Feng, X. Dong, Z. Li, G. Liu, and Z. Sun, Modeling of waterjet abrasion in mining processes based on the smoothed particle hydrodynamics (SPH) method, *Int. J. Comput. Methods* **17**, 1950075 (2020).
- 154 R. A. Gingold, and J. J. Monaghan, Smoothed particle hydrodynamics: Theory and application to non-spherical stars, *Mon. Not. R. Astron. Soc.* **181**, 375 (1977).
- 155 P. Berczik, Modeling the star formation in galaxies using the chemodynamical SPH code, *Astrophys. Space Sci.* **271**, 103 (2000).
- 156 J. J. Monaghan, Modelling the universe, *Publ. Astron. Soc. Aust.* **8**, 233 (1990).
- 157 R. Pakmor, P. Edelmann, F. K. Röpke, and W. Hillebrandt, Stellar GADGET: A smoothed particle hydrodynamics code for stellar astrophysics and its application to Type Ia supernovae from white dwarf mergers, *Mon. Not. R. Astron. Soc.* **424**, 2222 (2012).
- 158 Z. W. Liu, R. Pakmor, I. R. Seitzenzahl, W. Hillebrandt, M. Kromer, F. K. Röpke, P. Edelmann, S. Taubenberger, K. Maeda, B. Wang, and Z. W. Han, The impact of Type Ia supernova explosions on helium companions in the Chandrasekhar-mass explosion scenario, *Astrophys. J.* **774**, 37 (2013).
- 159 Z. Mao, and G. R. Liu, A smoothed particle hydrodynamics model for electrostatic transport of charged lunar dust on the moon surface, *Comp. Part. Mech.* **5**, 539 (2018).
- 160 Y. Bao, Y. Huang, G. R. Liu, and G. Wang, SPH simulation of high-volume rapid landslides triggered by earthquakes based on a unified constitutive model. Part I: Initiation process and slope failure, *Int. J. Comput. Methods* **17**, 1850150 (2018).
- 161 Y. Bao, Y. Huang, G. R. Liu, and W. Zeng, SPH simulation of high-volume rapid landslides triggered by earthquakes based on a unified constitutive model. Part II: Solid-liquid-like phase transition and flow-like landslides, *Int. J. Comput. Methods* **17**, 1850149 (2018).
- 162 G. R. Liu, Z. Mao, and Y. Huang, SPH modeling for soil mechanics with application to landslides, edited by P. Samui, S. Kumari, V. Makarov, P. Kurup, Modeling in Geotechnical Engineering (Academic Press, 2021), pp. 257-289.
- 163 C. T. Nguyen, C. T. Nguyen, H. H. Bui, G. D. Nguyen, and R. Fukagawa, A new SPH-based approach to simulation of granular flows using viscous damping and stress regularisation, *Landslides* **14**, 69 (2016).
- 164 H. H. Bui, K. Sako, R. Fukagawa, and J. Guan, in Non-cohesion material flows in rotating drum: Smoothed particle hydrodynamics (SPH) and discrete element method (DEM): Proceedings of the 41st Japan National Conference on Geotechnical Engineering (JNCGS), 2006.
- 165 P. Jop, Y. Forterre, and O. Pouliquen, A constitutive law for dense granular flows, *Nature* **441**, 727 (2006).
- 166 H. H. Bui, and G. D. Nguyen, A coupled fluid-solid SPH approach to modelling flow through deformable porous media, *Int. J. Solids Struct.* **125**, 244 (2017).
- 167 R. Das, and P. W. Cleary, Effect of rock shapes on brittle fracture using Smoothed Particle Hydrodynamics, *Theor. Appl. Fract. Mech.* **53**, 47 (2010).
- 168 S. Kahraman, and M. Alber, Estimating unconfined compressive strength and elastic modulus of a fault breccia mixture of weak blocks and strong matrix, *Int. J. Rock Mech. Min. Sci.* **43**, 1277 (2006).
- 169 F. R. Ming, A. M. Zhang, and W. S. Yang, Three-dimensional simulations on explosive load characteristics of underwater explosion near free surface, *Expl. Shock Waves* **32**, 508 (2012).
- 170 H. F. Qiang, S. J. Fan, F. Chen, and H. Liu, Numerical simulation on penetration of concrete target by shaped charge jet with SPH method, *Expl. Shock Waves* **36**, 516 (2016).
- 171 G. Yang, Y. Fu, D. Hu, and X. Han, Feasibility analysis of SPH method in the simulation of condensed explosives detonation with ignition and growth model, *Comput. Fluids* **88**, 51 (2013).
- 172 A. Zhang, S. Wang, Y. Peng, F. Ming, and Y. Liu, Research progress in underwater explosion and its damage to ship structures, *Chin. J. Ship Res.* **14**, 1 (2019).
- 173 G. Wang, G. Liu, Q. Peng, and S. De, A SPH implementation with ignition and growth and afterburning models for aluminized explosives, *Int. J. Comput. Methods* **14**, 1750046 (2017).
- 174 G. Wang, G. Liu, Q. Peng, S. De, D. Feng, and M. Liu, A 3D smoothed particle hydrodynamics method with reactive flow model for the simulation of ANFO, *Propellants Explosives Pyrotechnics* **40**, 566 (2015).
- 175 X. W. Dong, G. R. Liu, Z. Li, and W. Zeng, A smoothed particle hydrodynamics (SPH) model for simulating surface erosion by impacts of foreign particles, *Tribol. Int.* **95**, 267 (2016).
- 176 X. Dong, Z. Li, Q. Zhang, W. Zeng, and G. R. Liu, Analysis of surface-erosion mechanism due to impacts of freely rotating angular particles using smoothed particle hydrodynamics erosion model, *Proc. Inst. Mech. Engineers Part J-J. Eng. Tribol.* **231**, 1537 (2017).
- 177 X. Dong, Z. Li, G. Liu, L. Zhao, and X. Zhang, Numerical study of impact behaviors of angular particles on metallic surface using smoothed particle hydrodynamics, *Tribol. Trans.* **60**, 693 (2017).
- 178 L. Feng, G. R. Liu, Z. Li, X. Dong, and M. Du, Study on the effects of abrasive particle shape on the cutting performance of Ti-6Al-4V materials based on the SPH method, *Int. J. Adv. Manuf. Technol.* **101**, 3167 (2019).
- 179 K. Shintate, and H. Sekine, Numerical simulation of hypervelocity impacts of a projectile on laminated composite plate targets by means of improved SPH method, *Compos. Part A-Appl. Sci. Manuf.* **35**, 683 (2004).
- 180 S. Kitsionas, and A. P. Whitworth, Smoothed Particle Hydrodynamics with particle splitting, applied to self-gravitating collapse, *Mon. Not. R. Astron. Soc.* **330**, 129 (2002).
- 181 F. Xu, Y. Zhao, Y. Li, and M. Kikuchi, Study of numerical and physical fracture with SPH method, *Acta Mech. Solid Sin.* **23**, 49 (2010).
- 182 Y. Zhao, F. Xu, and Y. Li, A method of preventing SPH numerical fracture for irregular particle models, *Acta Aeronau. Astronaut. Sin.* **30**, 2100 (2009).
- 183 Y. Zhao, F. Xu, Y. Li, and L.-D. Chen, An improved SPH method for preventing numerical fractures, *Expl. Shock Waves* **29**, 503 (2009).
- 184 W. Benz, Smooth particle hydrodynamics: A review, edited by J. R. Buchler, *The Numerical Modelling of Nonlinear Stellar Pulsations: Problems and Prospects* (Springer Netherlands, Dordrecht, 1990).
- 185 R. A. Gingold, and J. J. Monaghan, Kernel estimates as a basis for general particle methods in hydrodynamics, *J. Comput. Phys.* **46**, 429 (1982).
- 186 H. F. Qiang, K. P. Wang, and W. R. Gao, Numerical simulation of high explosive detonation process using SPH method with fully variable smoothing lengths, *Energ. Mater.* **17**, 27 (2009).
- 187 Z. Zhang, H. Qiang, and W. Gao, Application of SPH-FEM contact algorithm in impact dynamics simulation, *Acta Mech. Solida Sin.* **32**, 319 (2011).
- 188 Y. Shen, W. Shi, J. Chen, and K. He, Application of SPH method with space-based variable smoothing length to water entry simulation, *J. Ship Mech.* **24**, 323 (2020).
- 189 Y. Zhu, G. R. Liu, Y. Wen, C. Xu, W. Niu, and G. Wang, Back-spalling process of an Al_2O_3 ceramic plate subjected to an impact of steel ball, *Int. J. Impact Eng.* **122**, 451 (2018).
- 190 C. Zhang, D. Di, X. Chen, and K. Wen, Characteristics structure analysis on debris cloud in the hypervelocity impact of disk projectile on thin plate, *Defence Tech.* **16**, 299 (2020).
- 191 D. Organ, M. Fleming, T. Terry, and T. Belytschko, Continuous meshless approximations for nonconvex bodies by diffraction and transparency, *Comput. Mech.* **18**, 225 (1996).
- 192 W. J. Sames, F. A. List, S. Pannala, R. R. Dehoff, and S. S. Babu, The metallurgy and processing science of metal additive manufacturing, *Int. Mater. Rev.* **61**, 1 (2016).
- 193 W. E. Frazier, Metal additive manufacturing: A review, *J. Materi Eng Perform* **23**, 1917 (2014).
- 194 A. Otto, H. Koch, K. H. Leitz, and M. Schmidt, Numerical simula-

- tions—A versatile approach for better understanding dynamics in laser material processing, *Phys. Procedia* **12**, 11 (2011).
- 195 M. Tong, and D. J. Browne, Smoothed particle hydrodynamics modelling of the fluid flow and heat transfer in the weld pool during laser spot welding, *IOP Conf. Ser.-Mater. Sci. Eng.* **27**, 012080 (2012).
- 196 A. Farrokhpahan, M. Bussmann, and J. Mostaghimi, New smoothed particle hydrodynamics (SPH) formulation for modeling heat conduction with solidification and melting, *Numer. Heat Transfer Part B-Fundamentals* **71**, 299 (2016).
- 197 R. Das, and P. W. Cleary, Three-dimensional modelling of coupled flow dynamics, heat transfer and residual stress generation in arc welding processes using the mesh-free SPH method, *J. Comput. Sci.* **16**, 200 (2016).
- 198 H. Hu, F. Fetzer, P. Berger, and P. Eberhard, Simulation of laser welding using advanced particle methods, *GAMM-Mitteilungen* **39**, 149 (2016).
- 199 D. Shah, and A. N. Volkov, in combined smoothed particle hydrodynamics-ray tracing method for simulations of keyhole formation in laser melting of bulk and powder metal targets: Proceedings of International Mechanical Engineering Congress and Exposition, Salt Lake City, 2019.
- 200 C. Meier, S. L. Fuchs, A. J. Hart, and W. A. Wall, A novel smoothed particle hydrodynamics formulation for thermo-capillary phase change problems with focus on metal additive manufacturing melt pool modeling, *Comput. Methods Appl. Mech. Eng.* **381**, 113812 (2021).
- 201 Y. Qiu, X. Niu, T. Song, M. Shen, W. Li, and W. Xu, Three-dimensional numerical simulation of selective laser melting process based on SPH method, *J. Manuf. Process.* **71**, 224 (2021).
- 202 M. A. Russell, A. Souto-Iglesias, and T. I. Zohdi, Numerical simulation of laser fusion additive Manufacturing processes using the SPH method, *Comput. Methods Appl. Mech. Eng.* **341**, 163 (2018).
- 203 B. Gnanasekaran, G. R. Liu, Y. Fu, G. Wang, W. Niu, and T. Lin, A Smoothed Particle Hydrodynamics (SPH) procedure for simulating cold spray process—A study using particles, *Surf. Coatings Tech.* **377**, 124812 (2019).
- 204 S. Yin, X. F. Wang, B. P. Xu, and W. Y. Li, Examination on the calculation method for modeling the multi-particle impact process in cold spraying, *J. Therm. Spray Tech.* **19**, 1032 (2010).
- 205 A. Manap, K. Ogawa, and T. Okabe, Numerical analysis of interfacial bonding of Al-Si particle and mild steel substrate by cold spray technique using the SPH method, *J. Solid Mech. Mater. Eng.* **6**, 241 (2012).
- 206 S. Tyagi, A. Yadav, and S. Deshmukh, Review on mechanical characterization of 3D printed parts created using material jetting process, *Mater. Today-Proc.* **51**, 1012 (2022).
- 207 H. Deng, Y. Huang, S. Wu, and Y. Yang, Binder jetting additive manufacturing: Three-dimensional simulation of micro-meter droplet impact and penetration into powder bed, *J. Manuf. Process.* **74**, 365 (2022).
- 208 P. W. Cleary, and J. J. Monaghan, Conduction modelling using smoothed particle hydrodynamics, *J. Comput. Phys.* **148**, 227 (1999).
- 209 P. Chen, G. Yang, and N. Wu, Meshless numerical analysis of phase change problems in artificial freezing technology applied in geo-media, *Int. J. Comput. Methods* **18**, 2150023 (2021).
- 210 A. Héault, G. Bilotta, A. Vicari, E. Rustico, and C. D. Negro, Numerical simulation of lava flow using a GPU SPH model, *Ann. Geophys.* **54**, 600 (2011).
- 211 X. Cui, W. G. Habashi, and V. Casseau, Multiphase SPH modelling of supercooled large droplets freezing on aircraft surfaces, *Int. J. Comput. Fluid Dyn.* **35**, 79 (2021).
- 212 D. S. Morikawa, and M. Asai, A phase-change approach to landslide simulations: Coupling finite strain elastoplastic TLSRH with non-Newtonian IISPH, *Comput. Geotech.* **148**, 104815 (2022).
- 213 S. M. Mousavi J. S., D. Faghihi, K. Sommer, M. M. S. Bhurwani, T. R. Patel, B. Santo, M. Waqas, C. Ionita, E. I. Levy, A. H. Siddiqui, and V. M. Tutino, Realistic computer modelling of stent retriever thrombectomy: A hybrid finite-element analysis-smoothed particle hydrodynamics model, *J. R. Soc. Interface* **18**, 20210583 (2021).
- 214 M. Al-Saad, C. A. Suarez, A. Obeidat, S. P. A. Bordas, and S. Kulasegaram, Application of smooth particle hydrodynamics method for modelling blood flow with thrombus formation, *Comput. Model. Eng. Sci.* **122**, 831 (2020).
- 215 F. Wang, S. Xu, D. Jiang, B. Zhao, X. Dong, T. Zhou, and X. Luo, Particle hydrodynamic simulation of thrombus formation using velocity decay factor, *Comput. Methods Programs Biomed.* **207**, 106173 (2021).
- 216 H. Kamada, K. Tsubota, M. Nakamura, S. Wada, T. Ishikawa, and T. Yamaguchi, A three-dimensional particle simulation of the formation and collapse of a primary thrombus, *Int. J. Numer. Meth. Biomed. Eng.* **26**, 488 (2010).
- 217 S. M. Harrison, R. C. Z. Cohen, P. W. Cleary, S. Barris, and G. Rose, A coupled biomechanical-smoothed particle hydrodynamics model for predicting the loading on the body during elite platform diving, *Appl. Math. Model.* **40**, 3812 (2016).
- 218 H. N. P. Gallage, S. C. Saha, and Y. T. Gu, in Deformation of a three-dimensional red blood cell in a stenosed micro-capillary: Proceedings of 8th Australasian Congress on Applied Mechanics, ACAM 7, Melbourne, 2014.
- 219 S. Meng, L. Taddei, N. Lebaal, D. Veysset, and S. Roth, Modeling micro-particles impacts into ballistic gelatine using smoothed particles hydrodynamics method, *Extreme Mech. Lett.* **39**, 100852 (2020).
- 220 C. Zhang, X. Hu, and H. Gao, in An integrative SPH for cardiac function with network: Proceedings of the 16th SPHERIC International Workshop (Istituto Nazionale di Geofisica e Vulcanologia, Catania, 2022).
- 221 A. English, B. D. R., G. Fourtakas, S. J. Lind, and P. K. Stansby, in SPH model of human breathing with and without face coverings: Proceedings of the 16th SPHERIC International Workshop (Istituto Nazionale di Geofisica e Vulcanologia, Catania, 2022).
- 222 T. Heck, B. Smeets, S. Vanmaercke, P. Bhattacharya, T. Odenthal, H. Ramon, H. Van Oosterwyck, and P. Van Liedekerke, Modeling extracellular matrix viscoelasticity using smoothed particle hydrodynamics with improved boundary treatment, *Comput. Methods Appl. Mech. Eng.* **322**, 515 (2017).
- 223 M. R. Bate, I. A. Bonnell, and N. M. Price, Modelling accretion in protoplanetary systems, *Mon. Not. R. Astron. Soc.* **277**, 362 (1995).
- 224 J. Feldman, and J. Bonet, Dynamic refinement and boundary contact forces in SPH with applications in fluid flow problems, *Int. J. Numer. Meth. Eng.* **72**, 295 (2007).
- 225 Y. Reyes López, D. Roose, and C. Recarey Morfa, Dynamic particle refinement in SPH: Application to free surface flow and non-cohesive soil simulations, *Comput. Mech.* **51**, 731 (2013).
- 226 P. Omidvar, P. K. Stansby, and B. D. Rogers, Wave body interaction in 2D using smoothed particle hydrodynamics (SPH) with variable particle mass, *Int. J. Numer. Meth. Fluids* **68**, 686 (2012).
- 227 D. A. Barcarolo, D. Le Touzé, G. Oger, and F. de Vuyst, Adaptive particle refinement and derefinement applied to the smoothed particle hydrodynamics method, *J. Comput. Phys.* **273**, 640 (2014).
- 228 L. Chiron, G. Oger, M. de Leffe, and D. Le Touzé, Analysis and improvements of Adaptive Particle Refinement (APR) through CPU time, accuracy and robustness considerations, *J. Comput. Phys.* **354**, 552 (2018).
- 229 P. Sun, A. M. Zhang, S. Marrone, and F. Ming, An accurate and efficient SPH modeling of the water entry of circular cylinders, *Appl. Ocean Res.* **72**, 60 (2018).
- 230 H. Liu, H. F. Qiang, F. Z. Chen, and C. Shi, A particle refinement scheme with hybrid particle interacting technique for multi-resolution SPH, *Eng. Anal. Bound. Elem.* **118**, 108 (2020).
- 231 L. He, S. Liu, Y. Gan, M. Seaid, and C. Niu, Development of time-space adaptive smoothed particle hydrodynamics method with

- Runge-Kutta Chebyshev scheme, *Eng. Anal. Bound. Elem.* **126**, 55 (2021).
- 232 C. Zhang, M. Rezavand, and X. Hu, A multi-resolution SPH method for fluid-structure interactions, *J. Comput. Phys.* **429**, 110028 (2021).
- 233 R. Davé, J. Dubinski, and L. Hernquist, Parallel TreeSPH, *New Astron.* **2**, 277 (1997).
- 234 C. Moulinec, R. Issa, J.-C. Marongiu, and D. Violeau, Parallel 3-D SPH simulations, *Comput. Model. Eng. Sci.* **25**, 133 (2008).
- 235 A. Ferrari, M. Dumbser, E. F. Toro, and A. Armanini, A new 3D parallel SPH scheme for free surface flows, *Comput. Fluids* **38**, 1203 (2009).
- 236 C. Lia, and G. Carraro, A parallel TreeSPH code for galaxy formation, *Mon. Not. R. Astron. Soc.* **314**, 145 (2000).
- 237 S. Marrone, B. Bouscasse, A. Colagrossi, and M. Antuono, Study of ship wave breaking patterns using 3D parallel SPH simulations, *Comput. Fluids* **69**, 54 (2012).
- 238 A. J. C. Crespo, J. M. Domínguez, B. D. Rogers, M. Gómez-Gesteira, S. Longshaw, R. Canelas, R. Vacondio, A. Barreiro, and O. García-Feal, DualSPHysics: Open-source parallel CFD solver based on smoothed particle hydrodynamics (SPH), *Comput. Phys. Commun.* **187**, 204 (2015).
- 239 D. Valdez-Balderas, J. M. Domínguez, B. D. Rogers, and A. J. C. Crespo, Towards accelerating smoothed particle hydrodynamics simulations for free-surface flows on multi-GPU clusters, *J. Parallel Distributed Computing* **73**, 1483 (2013).
- 240 J. M. Domínguez, A. J. C. Crespo, D. Valdez-Balderas, B. D. Rogers, and M. Gómez-Gesteira, New multi-GPU implementation for smoothed particle hydrodynamics on heterogeneous clusters, *Comput. Phys. Commun.* **184**, 1848 (2013).
- 241 Z. Ji, F. Xu, A. Takahashi, and Y. Sun, Large scale water entry simulation with smoothed particle hydrodynamics on single- and multi-GPU systems, *Comput. Phys. Commun.* **209**, 1 (2016).
- 242 J. O'Connor, J. M. Domínguez, B. D. Rogers, S. J. Lind, and P. K. Stansby, Eulerian incompressible smoothed particle hydrodynamics on multiple GPUs, *Comput. Phys. Commun.* **273**, 108263 (2022).
- 243 L. Fu, X. Y. Hu, and N. A. Adams, A physics-motivated Centroidal Voronoi Particle domain decomposition method, *J. Comput. Phys.* **335**, 718 (2017).
- 244 Z. Ji, L. Fu, X. Y. Hu, and N. A. Adams, A new multi-resolution parallel framework for SPH, *Comput. Methods Appl. Mech. Eng.* **346**, 1156 (2019).
- 245 Z. Ji, L. Fu, X. Y. Hu, and N. A. Adams, A Lagrangian Inertial Centroidal Voronoi Particle method for dynamic load balancing in particle-based simulations, *Comput. Phys. Commun.* **239**, 53 (2019).
- 246 Z. Ji, L. Fu, X. Hu, and N. Adams, A consistent parallel isotropic unstructured mesh generation method based on multi-phase SPH, *Comput. Methods Appl. Mech. Eng.* **363**, 112881 (2020).
- 247 Z. Ji, L. Fu, X. Hu, and N. Adams, A feature-aware SPH for isotropic unstructured mesh generation, *Comput. Methods Appl. Mech. Eng.* **375**, 113634 (2021).
- 248 L. Hernquist, and N. Katz, TreeSPH—A unification of SPH with the hierarchical tree method, *Astrophys. J. Suppl. Ser.* **70**, 419 (1989).
- 249 V. Springel, The cosmological simulation code GADGET-2, *Mon. Not. R. Astron. Soc.* **364**, 1105 (2005).
- 250 A. Mokos, B. D. Rogers, and P. K. Stansby, A multi-phase particle shifting algorithm for SPH simulations of violent hydrodynamics with a large number of particles, *J. Hydraulic Res.* **55**, 143 (2017).
- 251 C. Zhang, M. Rezavand, Y. Zhu, Y. Yu, D. Wu, W. Zhang, J. Wang, and X. Hu, SPHinXsys: An open-source multi-physics and multi-resolution library based on smoothed particle hydrodynamics, *Comput. Phys. Commun.* **267**, 108066 (2021).
- 252 Z. Ji, M. Stanic, E. A. Hartono, and V. Chernoray, Numerical simulations of oil flow inside a gearbox by Smoothed Particle Hydrodynamics (SPH) method, *Tribol. Int.* **127**, 47 (2018).
- 253 P. Incardona, A. Leo, Y. Zaluzhnyi, R. Ramaswamy, and I. F. Sbalzarini, OpenFPM: A scalable open framework for particle and particle-mesh codes on parallel computers, *Comput. Phys. Commun.* **241**, 155 (2019).
- 254 A. Amicarelli, S. Manenti, R. Albano, G. Agate, M. Paggi, L. Longoni, D. Mirauda, L. Ziane, G. Viccione, S. Todeschini, A. Sole, L. M. Baldini, D. Brambilla, M. Papini, M. C. Khellaf, B. Tagliaferro, L. Sarno, and G. Pirovano, SPHERA v.9.0.0: A computational fluid dynamics research code, based on the smoothed particle hydrodynamics mesh-less method, *Comput. Phys. Commun.* **250**, 107157 (2020).
- 255 H. Wessels, C. Weißenfels, and P. Wriggers, The neural particle method—An updated Lagrangian physics informed neural network for computational fluid dynamics, *Comput. Methods Appl. Mech. Eng.* **368**, 113127 (2020).

光滑粒子流体力学方法在流体、固体和生物力学中的应用

徐绯, 王佳怡, 杨扬, 王璐, 代震, 汉芮岐

摘要 光滑粒子流体力学(smoothed particle hydrodynamics, SPH)作为最早发展的无网格粒子方法之一,对于模拟爆炸、冲击等涉及大变形问题,具有广阔的发展前景。本文对SPH方法在流体、固体和生物力学领域的改进算法和工程应用进行了全面介绍。阐述了SPH的基本理论和高精度SPH改进算法,分析了流体、固体和生物力学领域的改进技术。在模拟流体问题时,采用 δ -SPH和GSPH方法解决了流体不稳定性的这些问题,并且讨论了流固耦合中的界面接触方法。针对固体的数值模拟,总结了三种传统改进方法(如应力点法、守恒光滑法、人工应力法)和Total Lagrangian SPH方法,改善了拉伸不稳定性问题;在生物力学方面,阐述了SPH控制方程和相互作用力的计算方法。本文综述了近年来SPH方法的应用进展,包括复杂海洋工程中的流固耦合问题,固体领域的天体、岩土力学、爆炸冲击以及增材制造等工程应用和生物力学中血流动力学、肠道健康和植物生长等典型应用;并分析了国内外SPH软件的发展,介绍了多尺度自适应分辨率方法、并行计算方法和网格自动生成技术来克服数值模拟方法在计算效率和计算规模上的限制。最后对目前存在的问题进行总结与展望,包括提高SPH算法的数值精度、如何精确描述固体的损伤与断裂问题和计算精度与效率之间的平衡等。在未来研究中,建立多尺度耦合SPH模型和深度学习将是进一步拓宽SPH方法应用的重要方向。